SRI International

Final Summary Report • February 1996

NIF TARGET AREA DESIGN SUPPORT

R. E. Tokheim, Senior Physicist and Project Leader
L. Seaman, Senior Research Engineer
D. R. Curran, Scientific Director
Poulter Laboratory

SRI Project PYU-7463

Prepared for:

University of California
Lawrence Livermore National Laboratory
P.O. Box 808
Livermore, CA 94551

Attn: Mike Tobin, L-481
Sara Kassahun, L-443

Contract No. B319742

333 Ravenswood Avenue • Menlo Park, CA 94025-3493 • (415) 326-6200 • FAX: (415) 326-5512 • Telex 334486

DISCLAIMER

DISCLAIMER

Final Summary Report • February 1996

NIF TARGET AREA DESIGN SUPPORT

R. E. Tokheim, Senior Physicist and Project Leader
L. Seaman, Senior Research Engineer
D. R. Curran, Scientific Director
Poulter Laboratory

SRI Project PYU-7463

Prepared for:

University of California
Lawrence Livermore National Laboratory
P.O. Box 808
Livermore, CA 94551

Attn: Mike Tobin, L-481
Sara Kassahun, L-443

Contract No. B319742

Approved:

James D. Colton
Laboratory Director
Poulter Laboratory

David M. Golden
Senior Vice President
Science and Technology Group

SRI International 333 Ravenswood Avenue • Menlo Park, CA 94025-3493 • (415) 326-6200 • FAX: (415) 326-5512 • Telex: 334486

CONTENTS

SUMMARY

SRI International continued support work for the National Ignition Facility, Chamber Dynamics Group at Lawrence Livermore National Laboratory (LLNL). The work entailed computational modeling of shrapnel and debris generation from copper shine shields, hohlraum, and stainless steel cryogenic support tubes for 1.8 MJ and 1.0 MJ no-yield and 20 MJ yield shots. Also, we addressed the effects of shrapnel at the first wall. Computations for 1.8 MJ showed an ionized gold hohlraum, but about half solid and half ionized copper shine shields, when material cell phase boundaries were maintained. This debris generation represents a potential threat to the first wall and debris shields. Further work is required to translate these results into particle size distributions based on computed strain rates.

We used simple algorithms for x-ray loading of frost layers protecting the target support to compute peak stress attenuation. These results are in agreement with LLNL experiments and prior calculations. We also made recommendations for passive and active Phebus and Nova experiments. Further computations will be needed to interpret experimental results.

We developed algorithmic formulas for predicting damage in candidate first wall materials and we found damage algorithms for fused-silica debris shield material. We estimated worse case impacts (150 μm at 400 m/s) and made recommendations for minimum, first wall, material thicknesses. We recommend beebee gun experiments to verify the algorithm for actual, first wall, candidate materials.

We obtained very preliminary computational results at 20 MJ for predicting shrapnel mass and particle density at the first wall in spherical polar coordinate space with the hohlraum axis as the polar direction. The results indicate a complicated array of overlapping distributions of solid, melted, and vaporized material. Melt and vapor material are somewhat directional; solid shrapnel tends to be more uniformly dispersed. Further verification is needed, as well as computations for different masses and particle sizes.

ACKNOWLEDGMENTS

The work presented in this report was performed for the National Ignition Facility, Chamber Dynamics Group at Lawrence Livermore National Laboratory. We are especially indebted to Mike Tobin for his guidance of this work. Special thanks go to Bonita Lew and Thomas Cooper from SRI for performing the computations.

INTRODUCTION

SRI International continued support work for the National Ignition Facility (NIF), Chamber Dynamics Group at Lawrence Livermore National Laboratory (LLNL). This report summarizes our activities over the reporting period 12 July 1995 to 31 January 1996.

During the project, frequent review meetings were held, at which SRI presented results in both written and viewfoil formats. In addition, teleconferences were held regularly (often weekly) to review the progress made by all participants of the Chamber Dynamics team. Major review meetings included one at LLNL on 13 September 1995, and one at Y-12 in Oak Ridge, TN, on 5-6 December 1995. We also met at SRI on 8 and 22 September 1995, to review project status with Mike Tobin. We attended a Final Optics Design Review meeting at LLNL on 29 January 1996, where we discussed future program activities. A summary of our discussions is given in the Reported Progress section, which ends with an update on our most recent progress. Copies of write-ups and presentations (in chronological order) are attached as appendices.

REPORTED PROGRESS

"Update on SRI NIF Support" (13 September 1995)

We met at LLNL with the Chamber Dynamics group. We presented an update on our project work: (1) Our approach to making shrapnel computations for the 1.8 MJ (3ω) no-yield shot with hohlraum and copper shine shields (including the effects of 1ω, 2ω, x rays, and debris), (2) A description of the fused-silica, hypervelocity, impact data from National Aeronautics and Space Administration (NASA) (Karen Edelstein), (3) A description of an algorithmic tool (McNIF) that could be used to integrate the target chamber design work and could eventually be useful for NIF operations and experiment designs. Appendix I gives details.

"Possible McNIF Frost Algorithms" (13 September 1995)

In this presentation, we described the frost-layer computations for protecting the target support from x-ray loading. Early in the program, LLNL and University of California at Berkeley (Per Peterson) asked us to undertake some computations of stress attenuation of x-ray loading on frost layers at the target support. We used simple design algorithms to estimate stress attenuation of frost for a worst case, 590 J/cm^2, 50 eV blackbody, 20 ns x-ray loading at 10 cm from the 0.74 MJ point source [Nova hohlraum for Nuclear Weapons Effects Testing (NWET)]. The results show that simplified algorithms appear practical, and that about a 1 cm layer of frost will be required to protect the target positioner cone in the worst case, noncryogenic environment. More comparisons with detailed hydrocode calculations are needed to confirm the above conclusion. Prior experiments and detailed calculations by LLNL are consistent with our conclusions. Appendix II gives details.

"Possible Phebus or Nova Experiments" (19 October 1995)

We prepared a requested wish list of experiments that could be performed on Phebus or Nova. Included was a description of possible Phebus/Nova experiments using an all-purpose experimental fixture we proposed. Appendix III gives details.

"Minimum Required Thicknesses for NIF Chamber First Wall Coating" (7 November 1995)

We decided B_4C looks good as a first wall material, but it needs an aluminum backing to be a good armor to stop potential cracking and spall. We combined available data and simple theory to estimate the minimum required thicknesses of ceramic, first wall materials and plastic, debris shield, coating materials to afford reliable protection against debris and shrapnel in 20 MJ yield shots. Appendix IV gives details.

"Shrapnel and Debris Generation in NIF Chamber from Cryo Tubes and Hohlraum" (5-6 December 1995)

We completed computations for the 1.8 MJ (3ω) and 1.0 MJ no-yield cases with hohlraum and Cu shine shields (1ω and 2ω). We computed the mass and momentum distribution at the wall. Results showed only ionized material remaining. However, the computations included much rezoning, and minimum cell energies were averaged to higher values. Because the code run did not allow for thermal diffusion or radiation transport, which are likely to be significant, the results will at least, represent an upper bound. Ongoing calculations were made for the 1.8 MJ case with material phase-boundary energies maintained.

Our analysis also showed results for a 20 MJ shot in tracing shrapnel/debris to the first wall, indicating a complicated pattern of overlapping areas of shrapnel mass distribution. Further work is needed. We concluded our shrapnel/debris calculations for the hohlraum, shine shields, and cryogenic tubes and made estimates of the worst case threats, described below. Appendix V gives details.

"NIF Chamber First Wall, Debris Shield, and Beam Dump Hardening Issues" (5-6 December 1995)

We summarized our analysis on the minimum thicknesses required for the NIF chamber first wall and debris coating materials, to counter the expected, worst case, shrapnel threat. We concluded that the minimum first wall thicknesses are larger than desired (5 mm instead of 1 mm), primarily because of possible extensive, subcrater fracturing. A 2 mm thickness might work because of the low probability of a second impact at the same location. The worst case impact appears to be 150 μm steel shrapnel particles impacting at about 400 m/s. Therefore, initial "certification testing" should focus on reproducing these conditions. Because these estimated first wall thicknesses may or may not be practical, impact testing should be done soon to resolve the issue. Appendix VI gives details.

LLNL Workshop at Oak Ridge (5-6 December 1995)

At the LLNL workshop, the Chamber Dynamics contractor team met with Roland Seals and the Y-12 thermal spray and research facility team to explore the feasibility of plasma-spraying the first wall of the NIF target chamber. This issue was addressed after presentations of the latest research results were made by Mike Tobin, Bob Peterson (University of Wisconsin), Bob Tokheim (SRI International), Roland Seals, and many of his team members. We also discussed key issues and specific ideas for the Phebus experiments.

Three key issues arose from the meeting. First, Mike showed results of observations made recently on Nova experiments regarding pop-off of material particles on both sprayed and sintered samples of B_4C; the material removed is much greater than that expected from vaporization or melting alone. Machining the specimens probably contributed to the significant pop-off. Sprayed samples made by Los Alamos National Laboratory were not machined, and no pop-off phenomenon was reported by those performing the Helen experiments. In any case, further investigation of pop-off is needed to understand the mechanisms involved.

A second key issue Mike reported was severe outgassing in sprayed materials. This appears to be associated with the amount of porosity, but could be related to boride chemistry. In fact, the low porosity, sintered B_4C passed the outgassing test. Further investigation is needed.

A third key issue (which was initially the main issue was how best to fabricate the wall plates. Sintered material can be made many millimeters thick, but is probably too expensive, although further investigation is needed to determine this. Spraying would be the easiest, but so far Y-12 has not sprayed a boron or boride thicker than 0.5 mm. Y-12 states that the sprayed particle size, type and conditions of spraying, and environment for spraying have not yet been optimized. However, they have been able to spray alumina to several millimeters in thickness without difficulty. Another option is to accept the damage the shrapnel will do to the thinner layer and plan to provide thicker layers later with improved technology. Another alternative is to spray a graded layering of B_4C over alumina. Experiments and computations are needed to investigate impedance mismatch effects and delamination of bonds.

"Update on Recent Hohlraum and Shrapnel Results" (31 January 1996)

We completed the computation for the 1.8 MJ shot with the shine shield while maintaining cell material phase-boundary separation in the computational mesh (to avoid averaging out lower energy cells). We found that, although only ionized Au (from the hohlraum) appears, equal masses of ionized and solid Cu (from the shine shields) occur, with a considerably lesser amount of vaporized Cu, and no appreciable melted Cu. These results represent a lower limit on solid

debris, because radiation diffusion is not included in the two-dimensional part of the computation (the initial part used HYADES, which does include effects of radiation diffusion). Further work based on these computations is needed to estimate from knowledge of material strain rates, velocities, and momentum, damage at the first wall.

We have very preliminary computational results for shrapnel from the cryo tubes for a 20 MJ shot. The results show mass and particle densities at the first wall for a single cryo tube pair. Mass coming from different sections and sectors of cryo tubes overlaps at the first wall in a complicated array. Melt and vapor materials are somewhat directional, whereas solid shrapnel tends to be more uniformly dispersed. Further work is needed to verify the results obtained and to compute additional, selected, mass and particle size distributions at the first wall and at debris shields. Then damage can be computed based on algorithms we have and expect to improve through beebee gun experiments. Appendix VII gives details.

Appendix I

UPDATE ON SRI NIF SUPPORT

UPDATE ON SRI NIF SUPPORT

R. E. Tokheim and D. R. Curran
SRI INTERNATIONAL

13 September 1995
Chamber Dynamics Meeting
ICF Applications Group
LLNL

OUTLINE

- "Shrapnel" Computations for 1.8 MJ No-yield Case with Shine Shields
  - Configuration
  - Approach
  - Results
- Fused-Silica Impact Data from NASA
- McNIF
  - Menu
  - Demonstration

Configuration for 1.8 MJ, no-yield case:

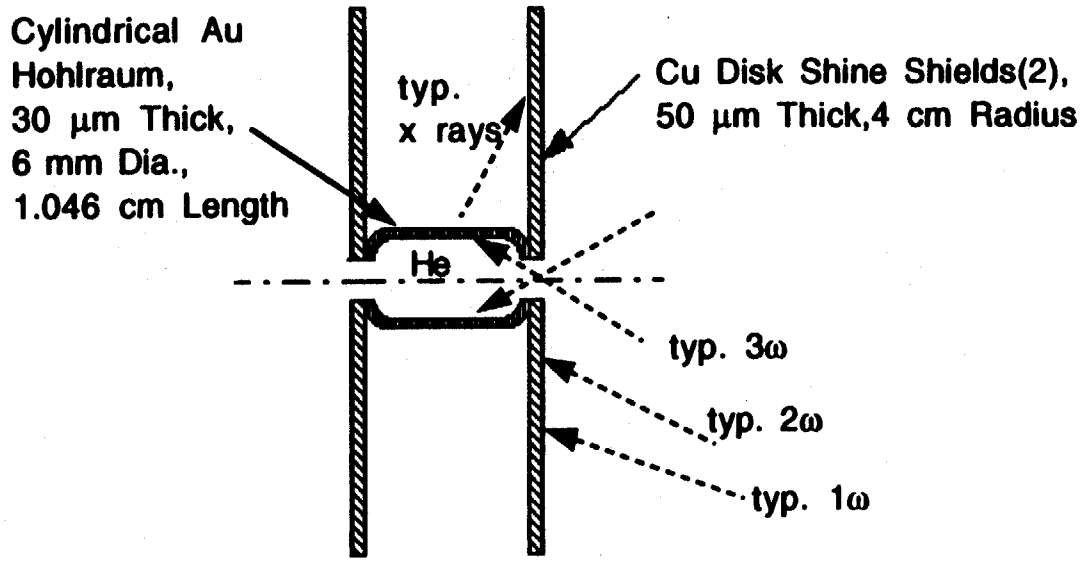

Approach:

- LLNL computations of $1\omega/2\omega$ intensity onto Cu shine shields
- Plot of typical intensity variation on shine shields
- Use of HYADES runs at certain locations for initialization of shine-shield L2D computations
- Modified use of previous L2D Au hohlraum computations
- Energy deposition of mixed-blackbody x rays through hohlraum to inside of shine shields during L2D run

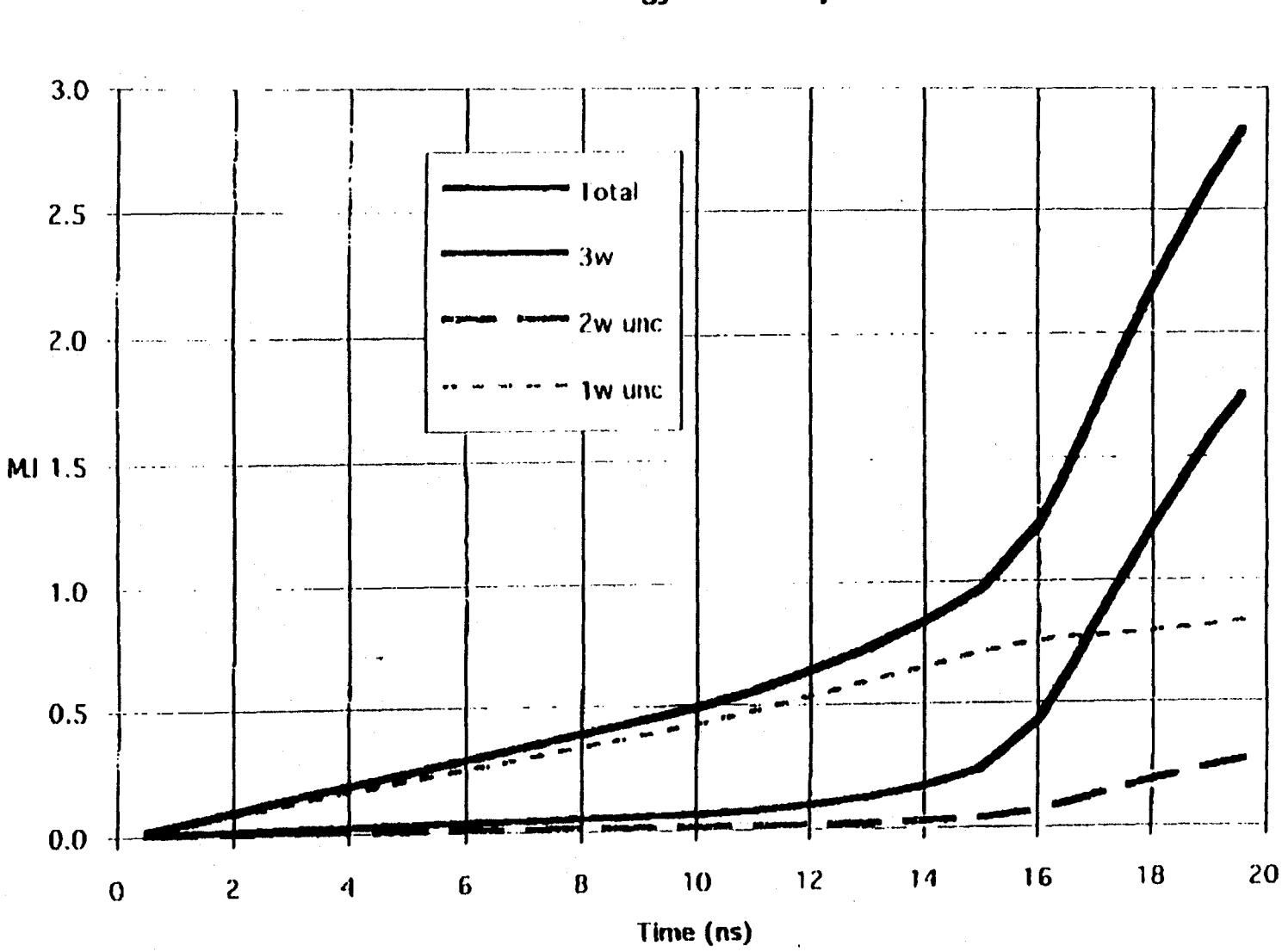

Figure 1: Integrated energies in total laser input, 3ω light, and unconverted light in 2ω and 1ω

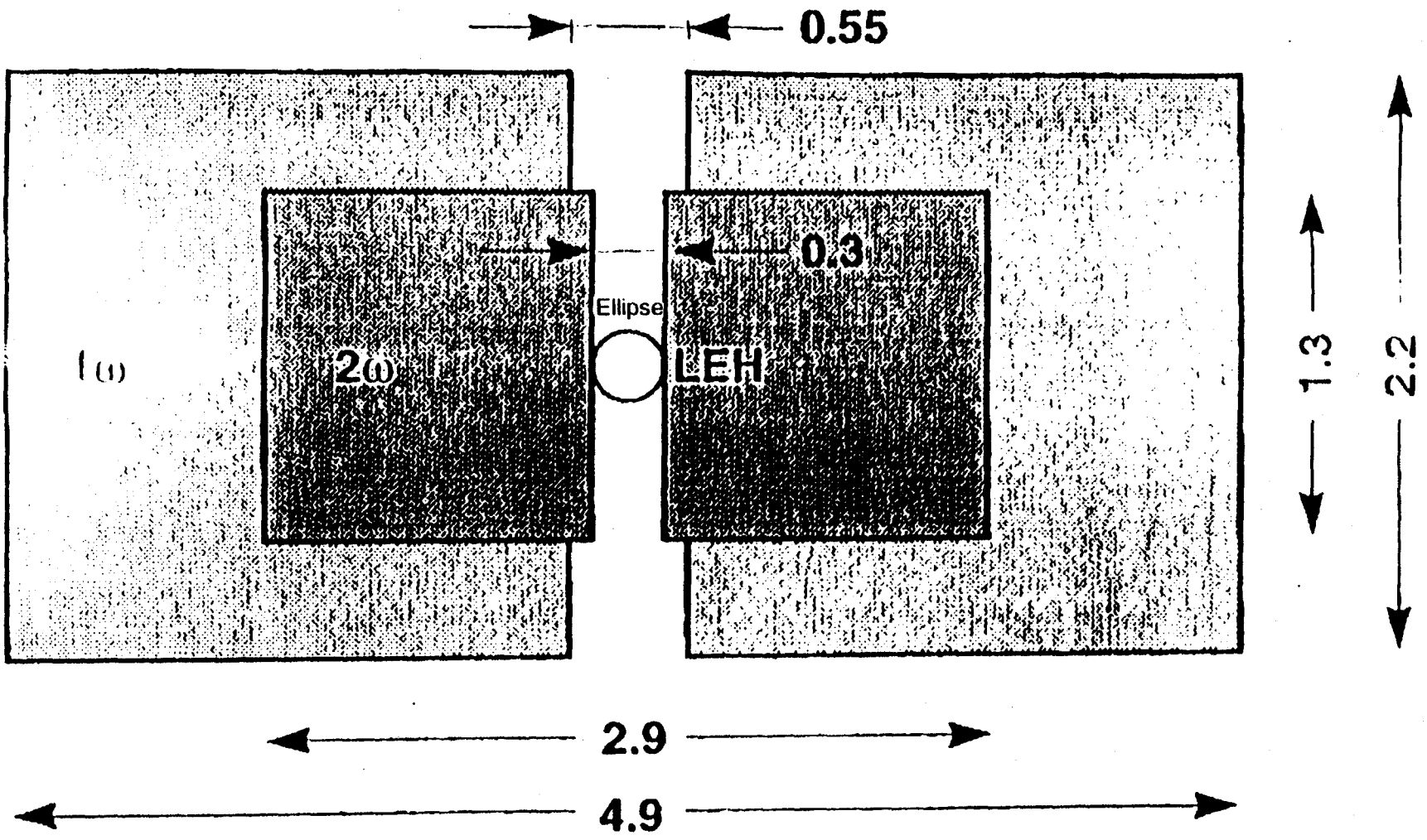

Figure 2: Representative pattern of 1ω and 2ω light for a single beam at chamber center (dimensions in cm)

50° Worst Case

RELATIVE INTENSITY ON A 26x26 mm QUADRANT OF 2w
BEAM PATTERN ON SHINE SHIELDS

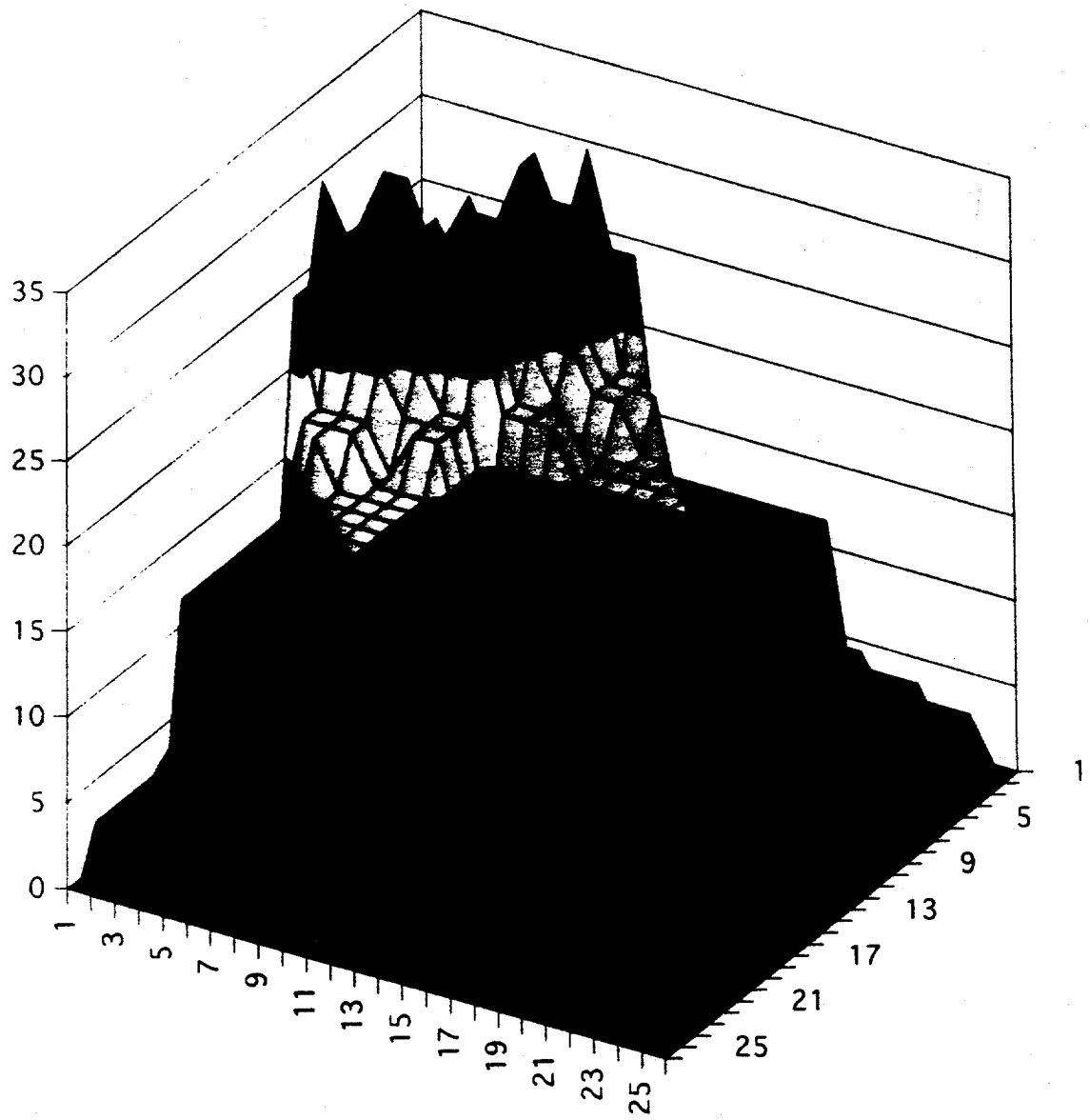

RELATIVE INTENSITY ON A 26x26 mm QUADRANT OF 2w
BEAM PATTERN ON SHINE SHIELDS

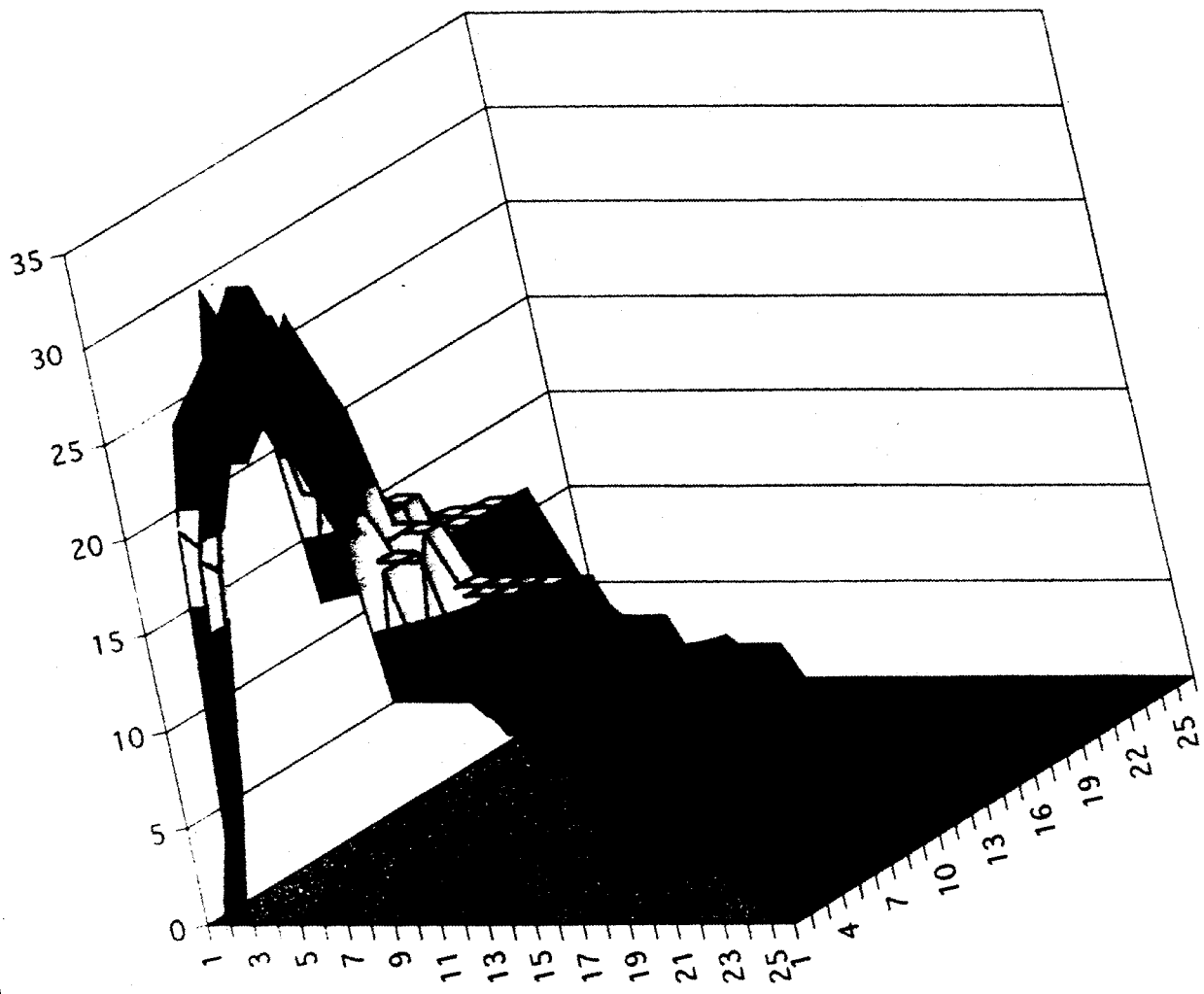

RELATIVE INTENSITY ON A 40x40 mm QUADRANT OF 1w
BEAM PATTERN ON SHINE SHIELDS

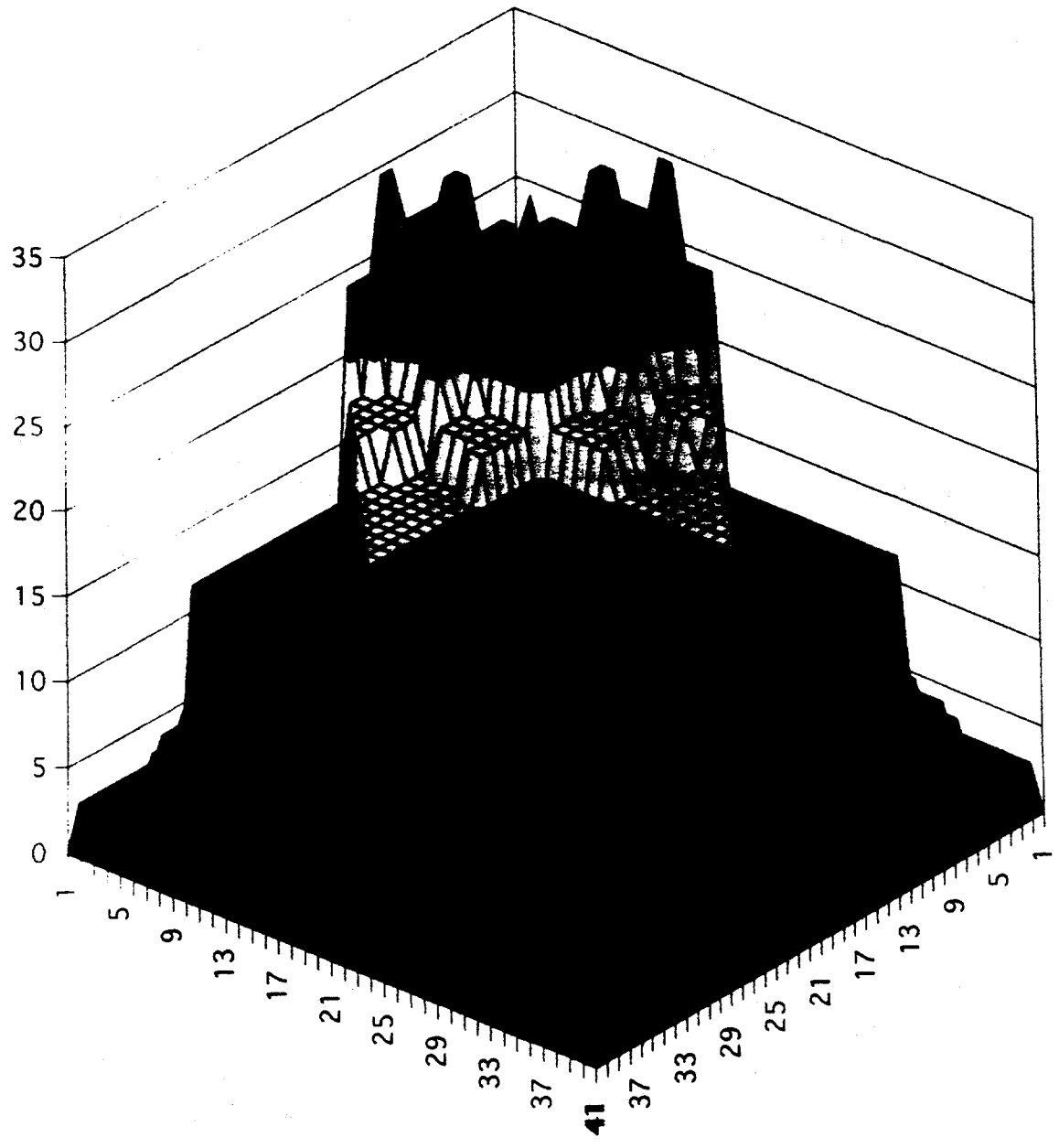

RELATIVE INTENSITY ON A 40x40 mm QUADRANT OF 1w
BEAM PATTERN ON SHINE SHIELDS

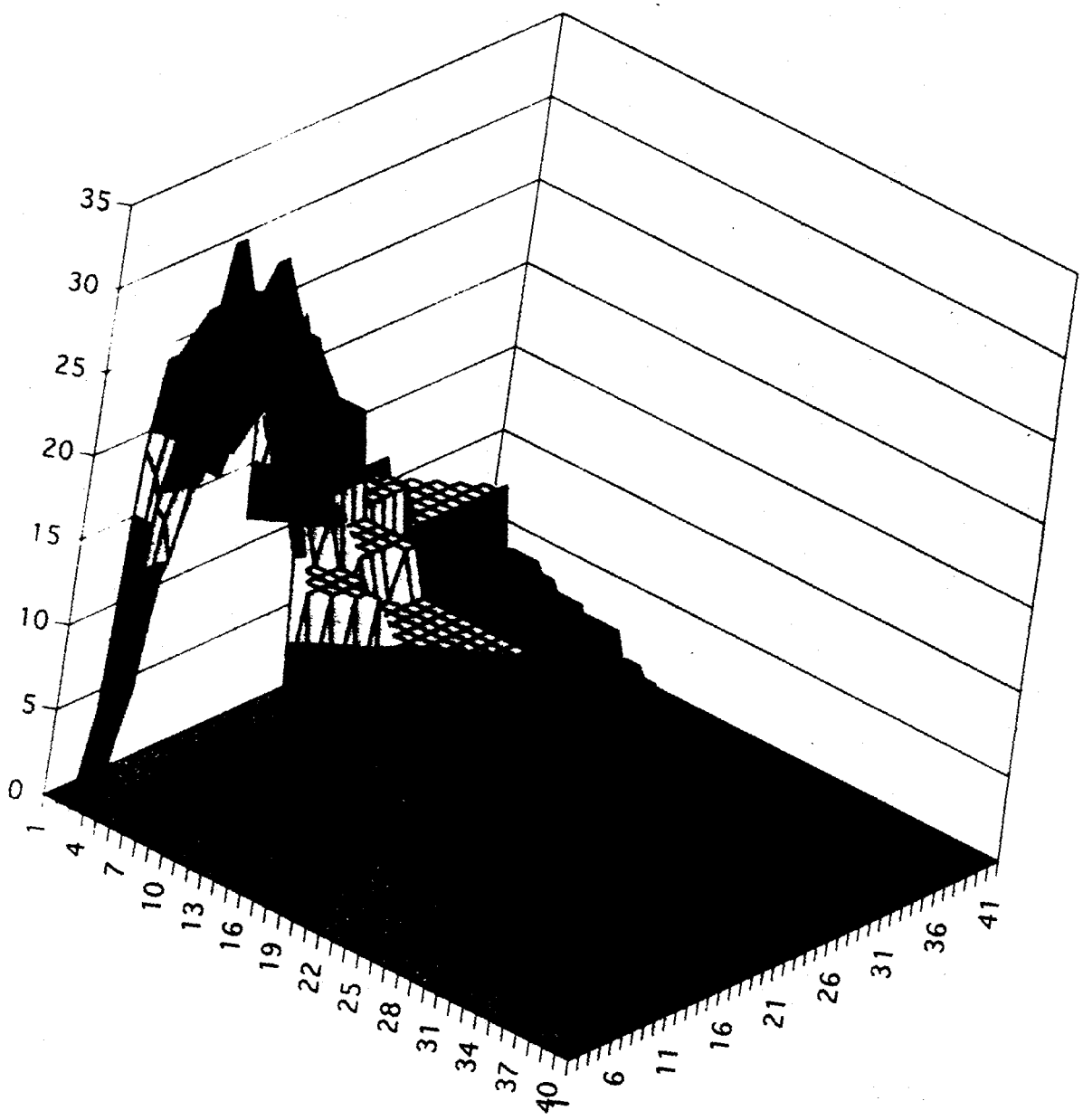

RELATIVE INTENSITY ON A 26x26 mm QUADRANT OF 2w
BEAM PATTERN ON SHINE SHIELDS

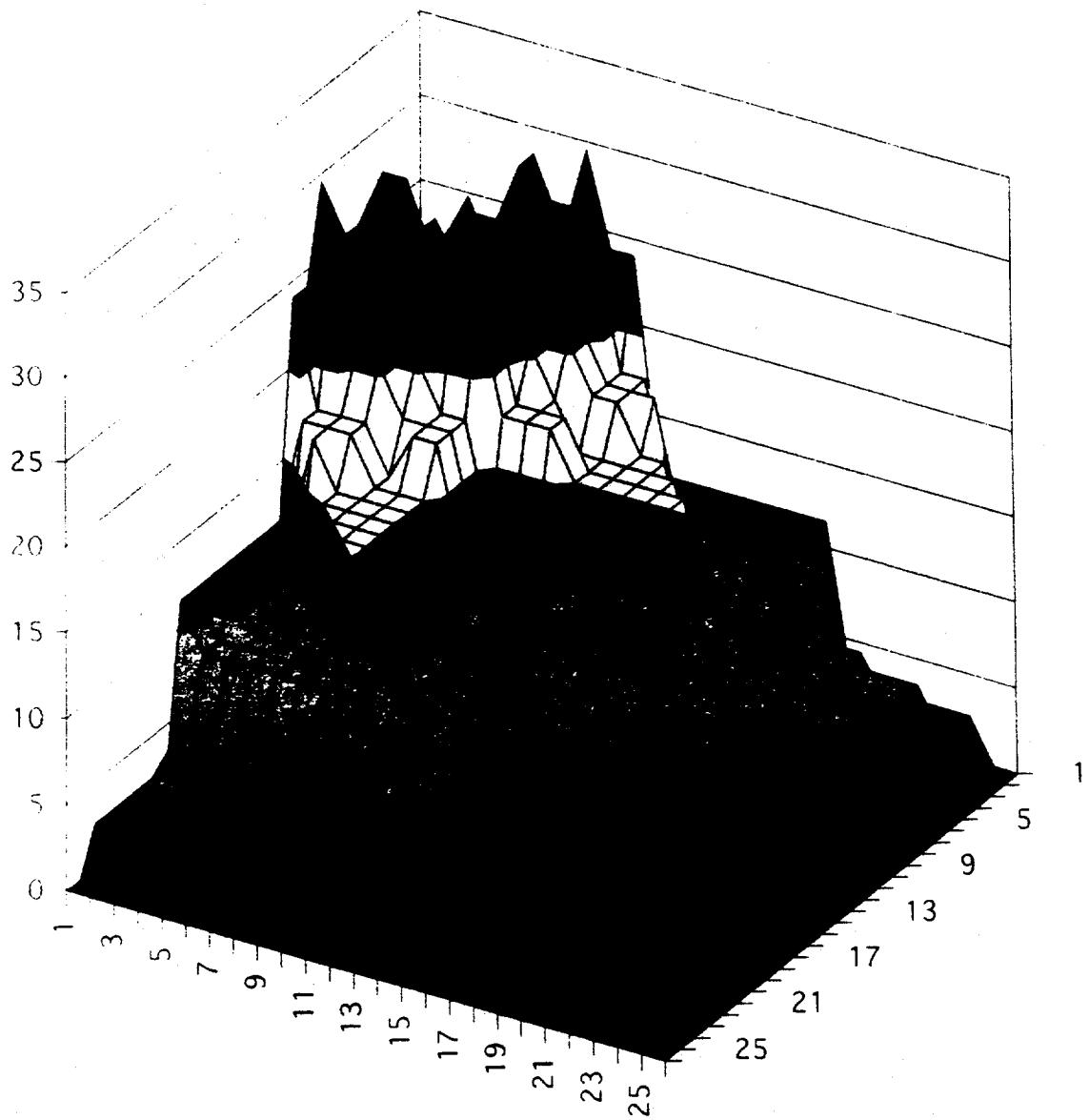

RELATIVE INTENSITY ON A 26x26 mm QUADRANT OF 2w
BEAM PATTERN ON SHINE SHIELDS

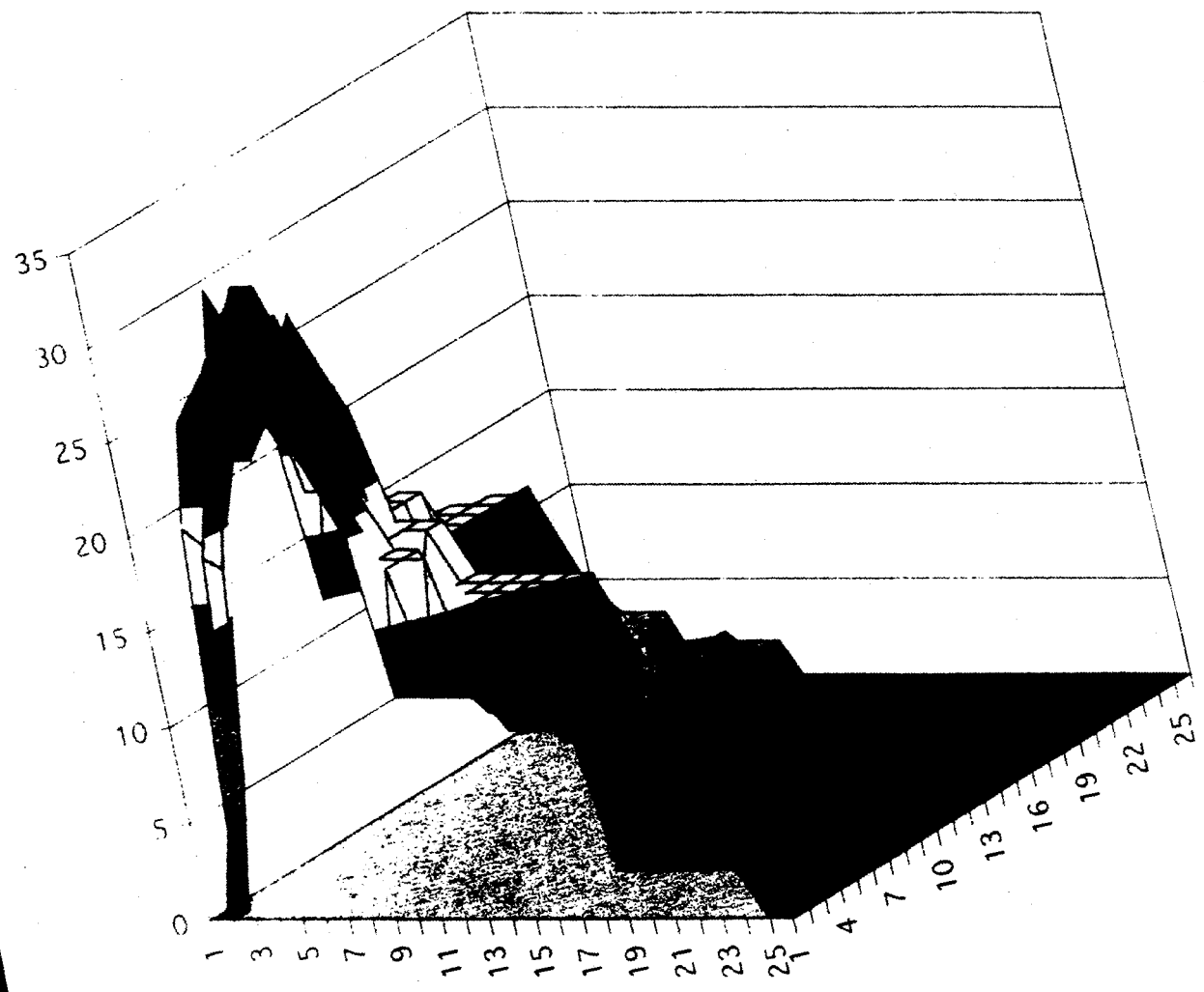

RELATIVE INTENSITY ON A 40x40 mm QUADRANT OF 1w
BEAM PATTERN ON SHINE SHIELDS

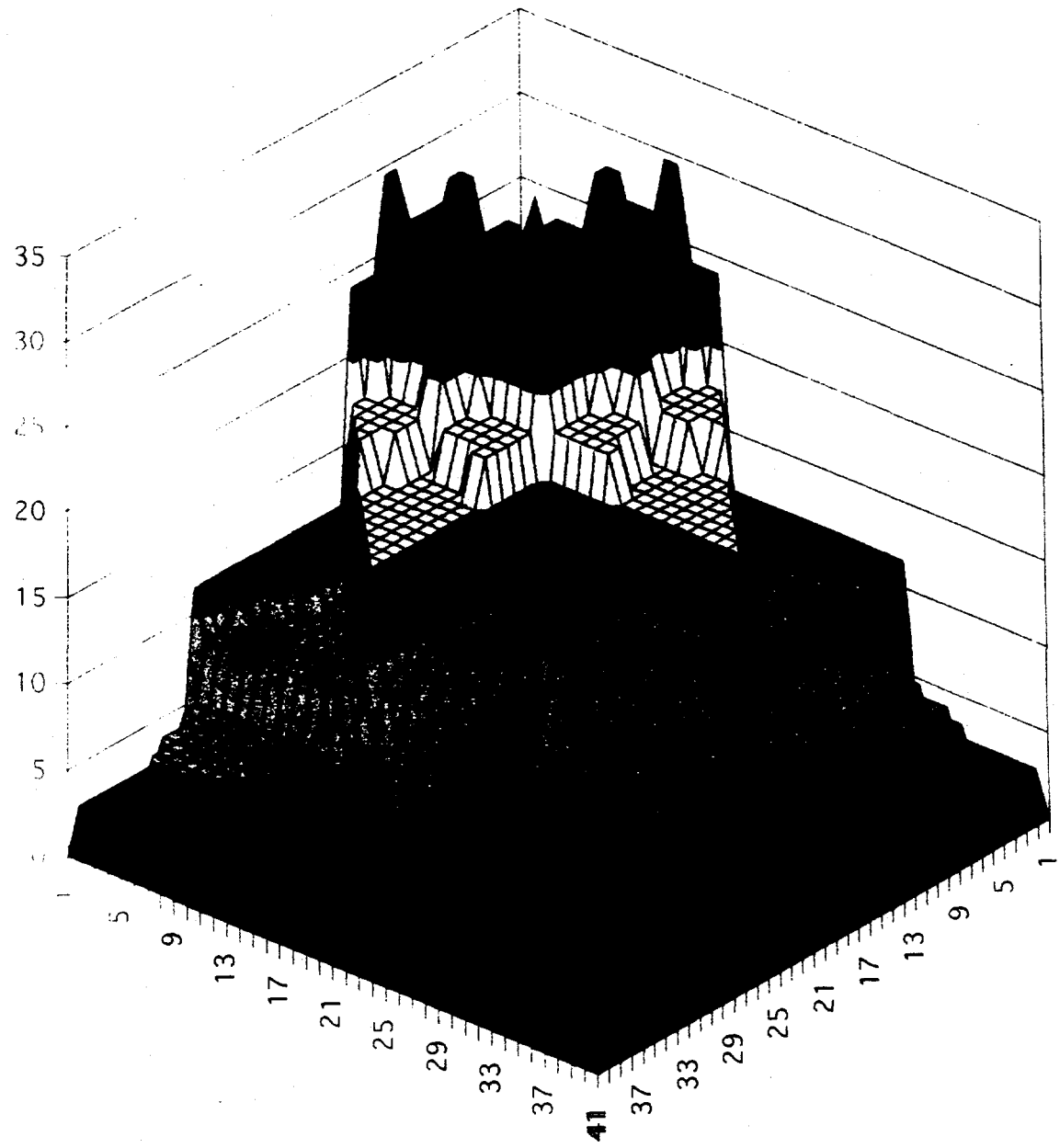

RELATIVE INTENSITY ON A 40x40 mm QUADRANT OF 1w
BEAM PATTERN ON SHINE SHIELDS

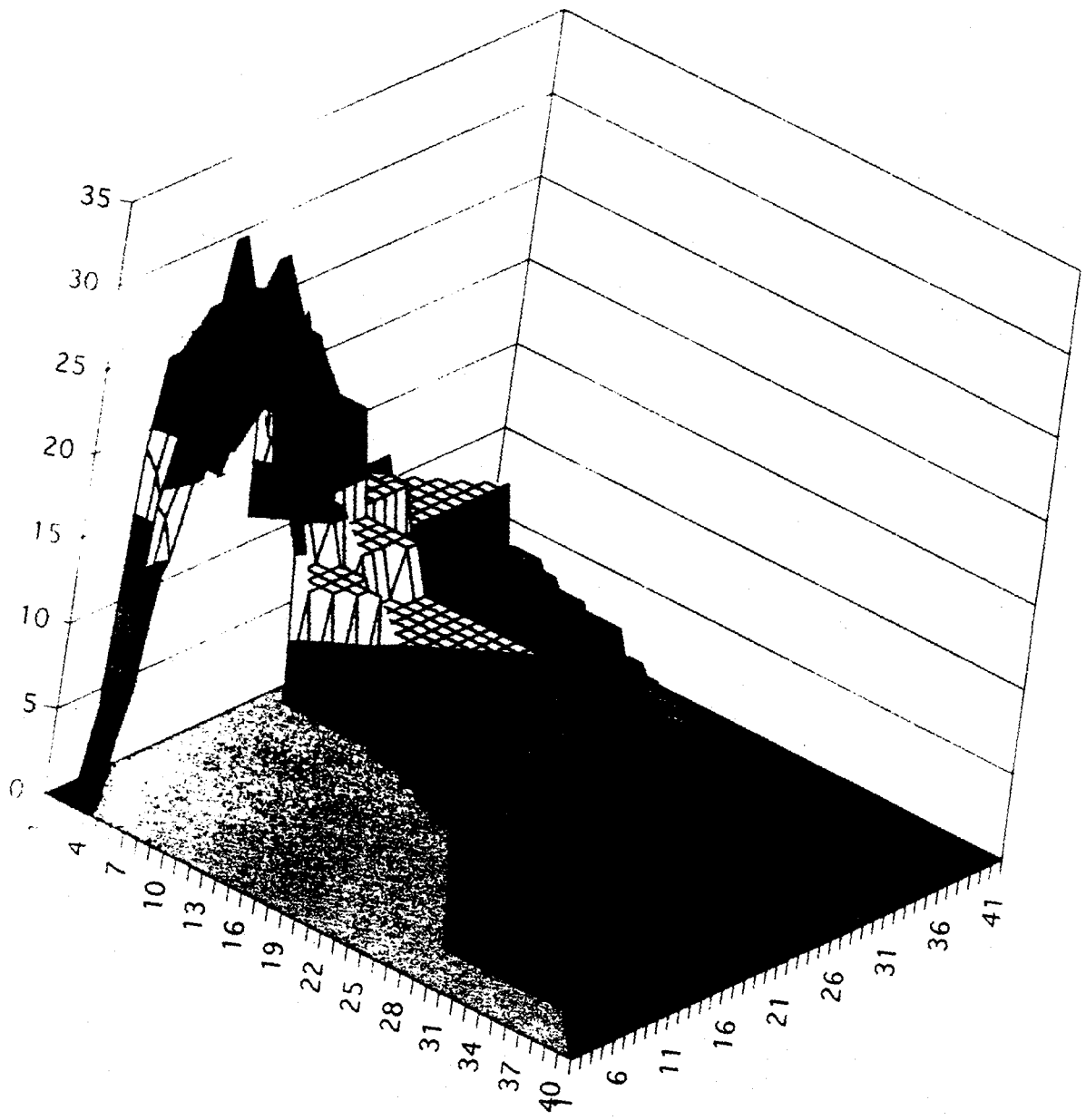

Case 1

1 ω Laser Light (1.06 μm)

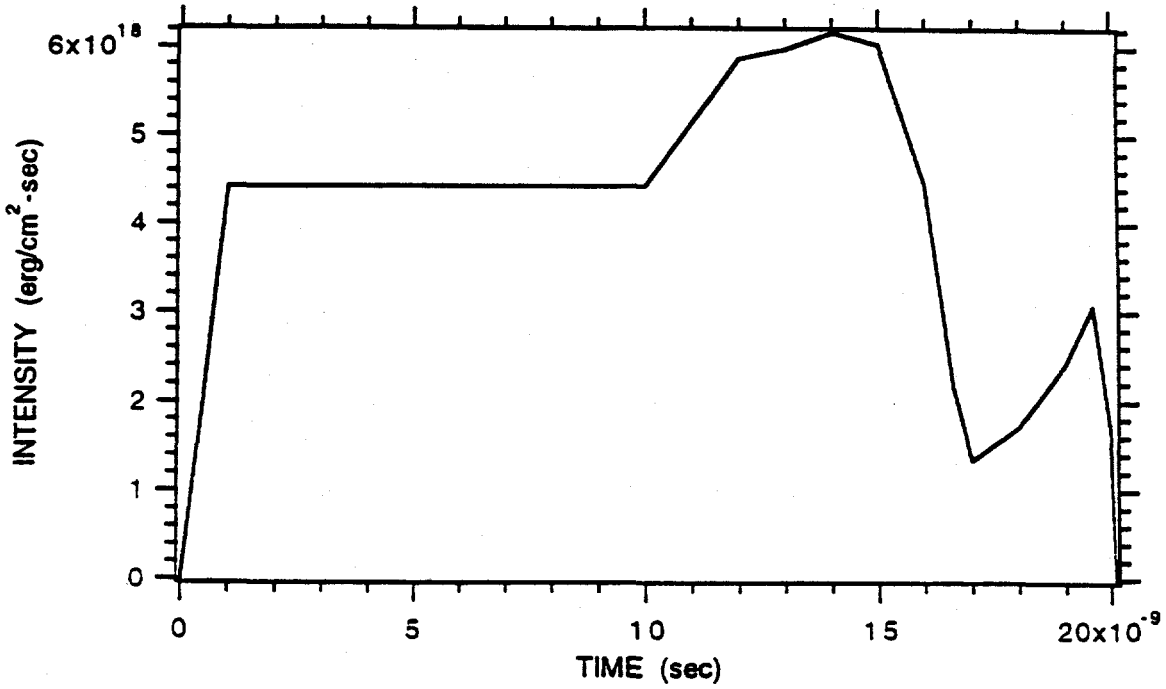

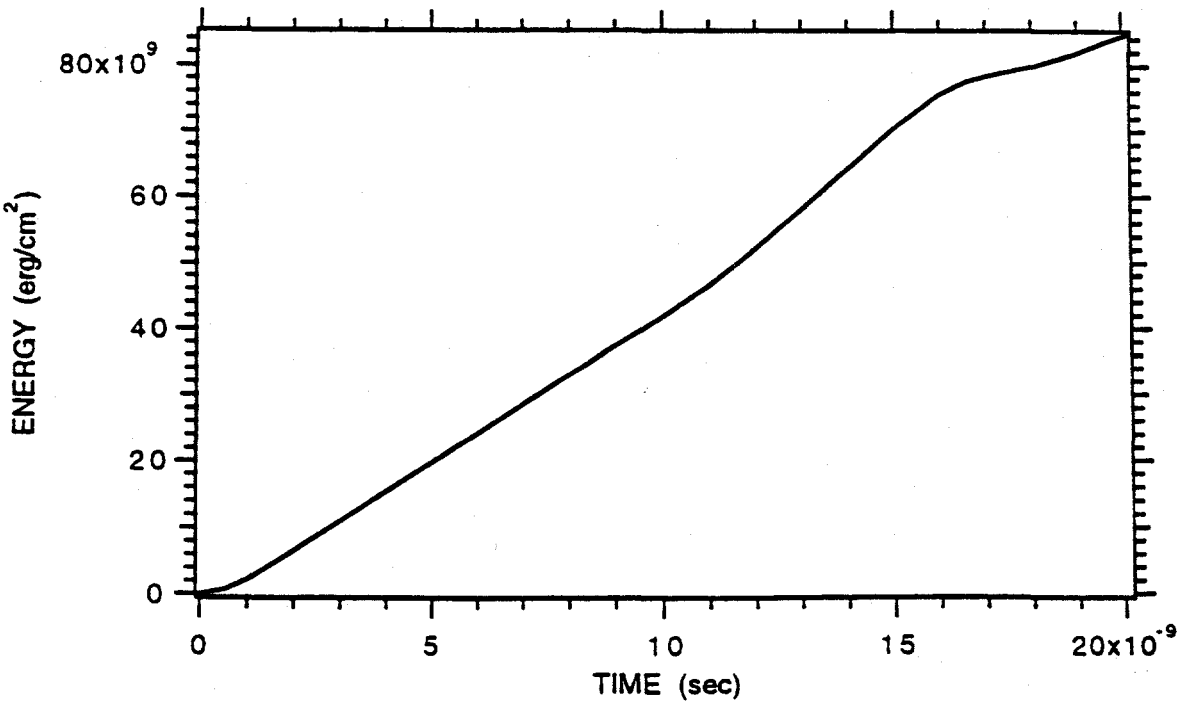

Case 1

2 ω Laser Light (0.53 μm)

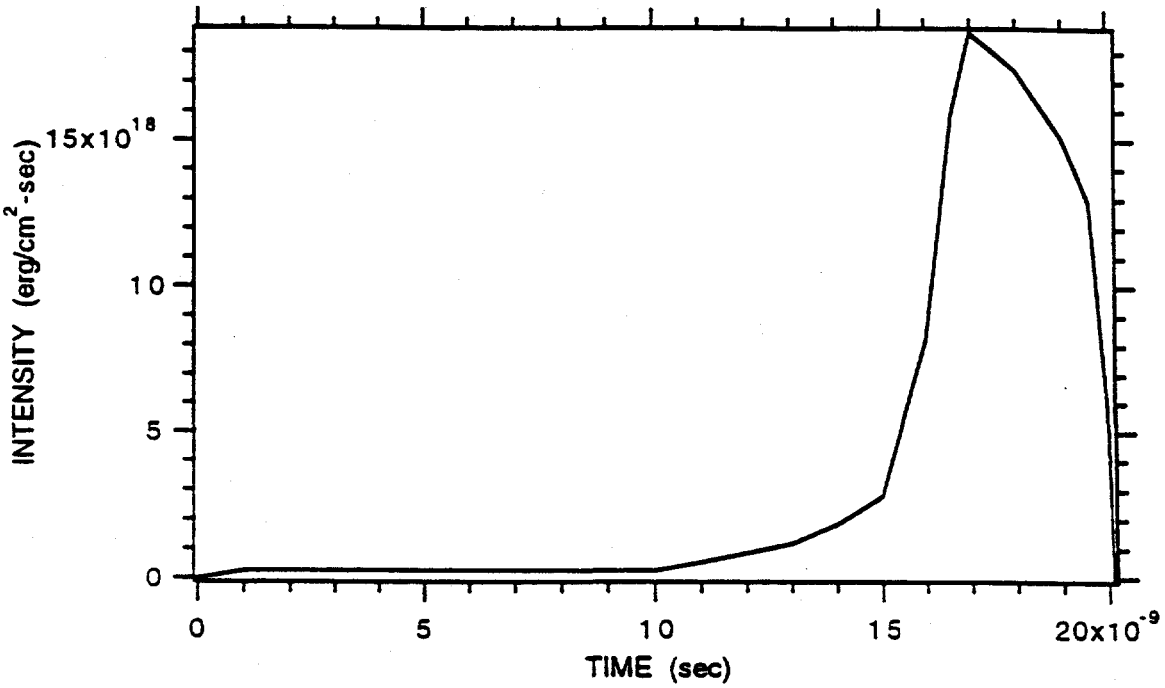

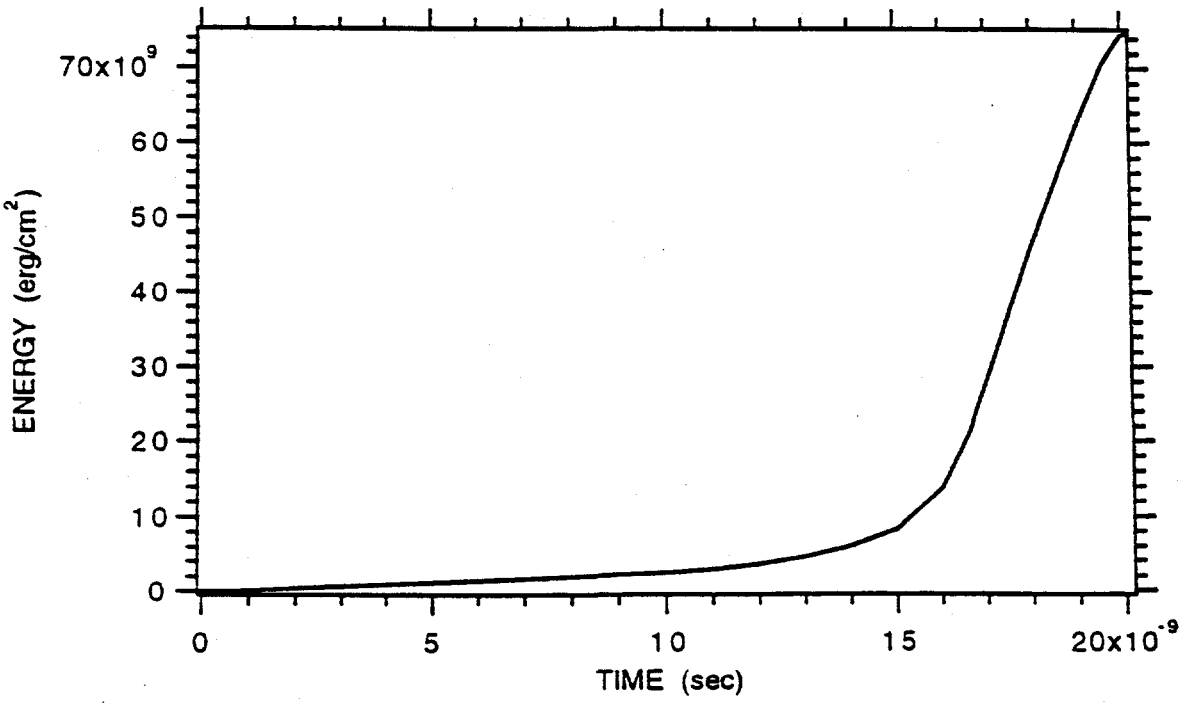

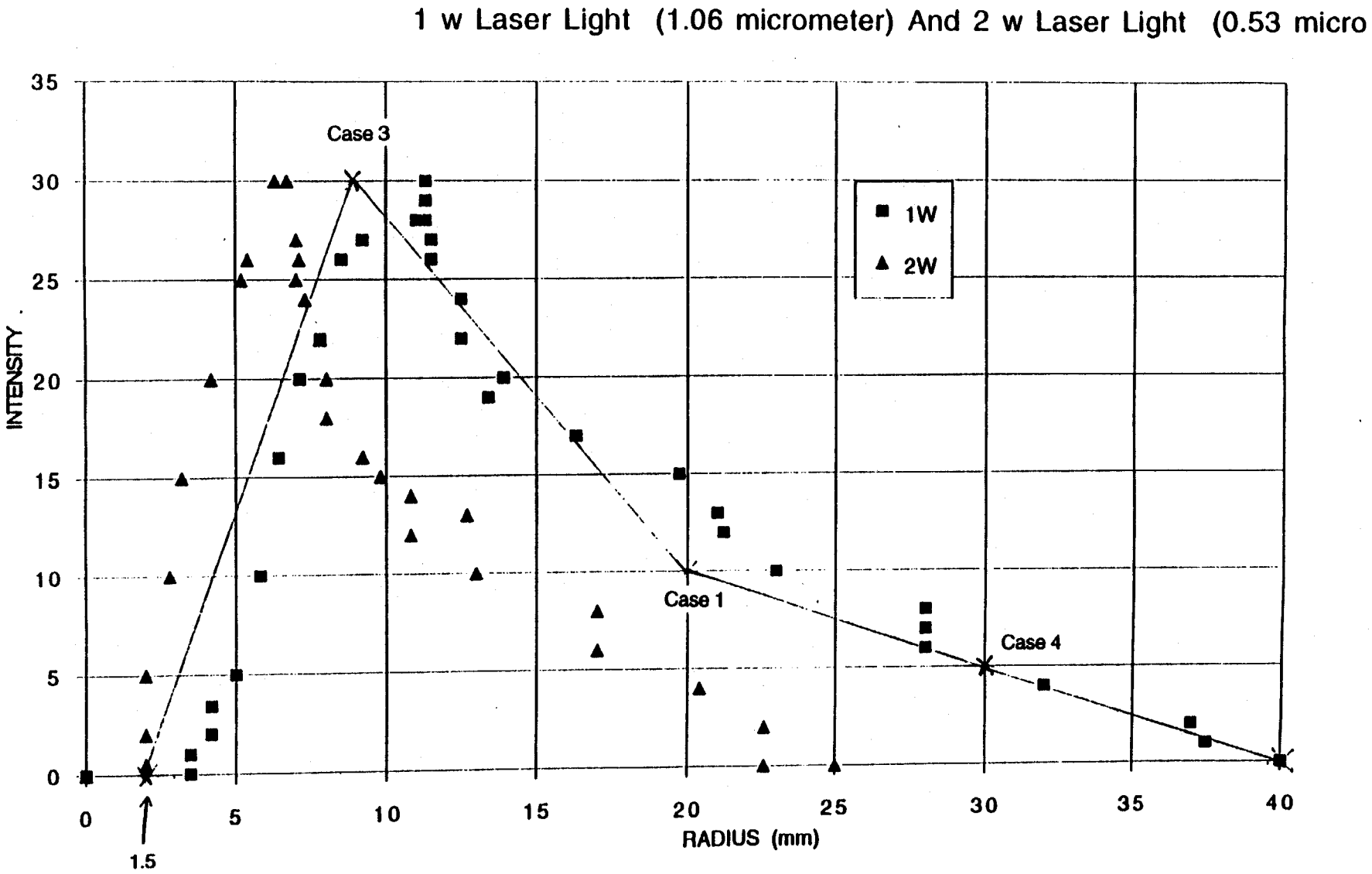
1 w Laser Light (1.06 micrometer) And 2 w Laser Light (0.53 micro
INTENSITY
RADIUS (mm)
Case 3
Case 1
Case 4
1W
2W
1.5
0
5
10
15
20
25
30
35
40

T =0.00 US
DT=.100 PS
CYCL= 0
DUMP= 1
Z IN CM
3
2.75
2.5
2.25
2
1.75
1.5
1.25
1
0.75
0.5
0.25
0
0.25
0.5
0.75
1.25
1.5
1.75
2
2.25
2.5
2.75
3
3.25
3.5
3.75
4
0.15
0.89
2.0
3.0
4.0
R, IN CM
002
I 2 D
10-Sep-95 18:00:56 CH2AU, mod 1/31/94 .ROUNDED CORNERS, NIF PROBLEM 1/1994

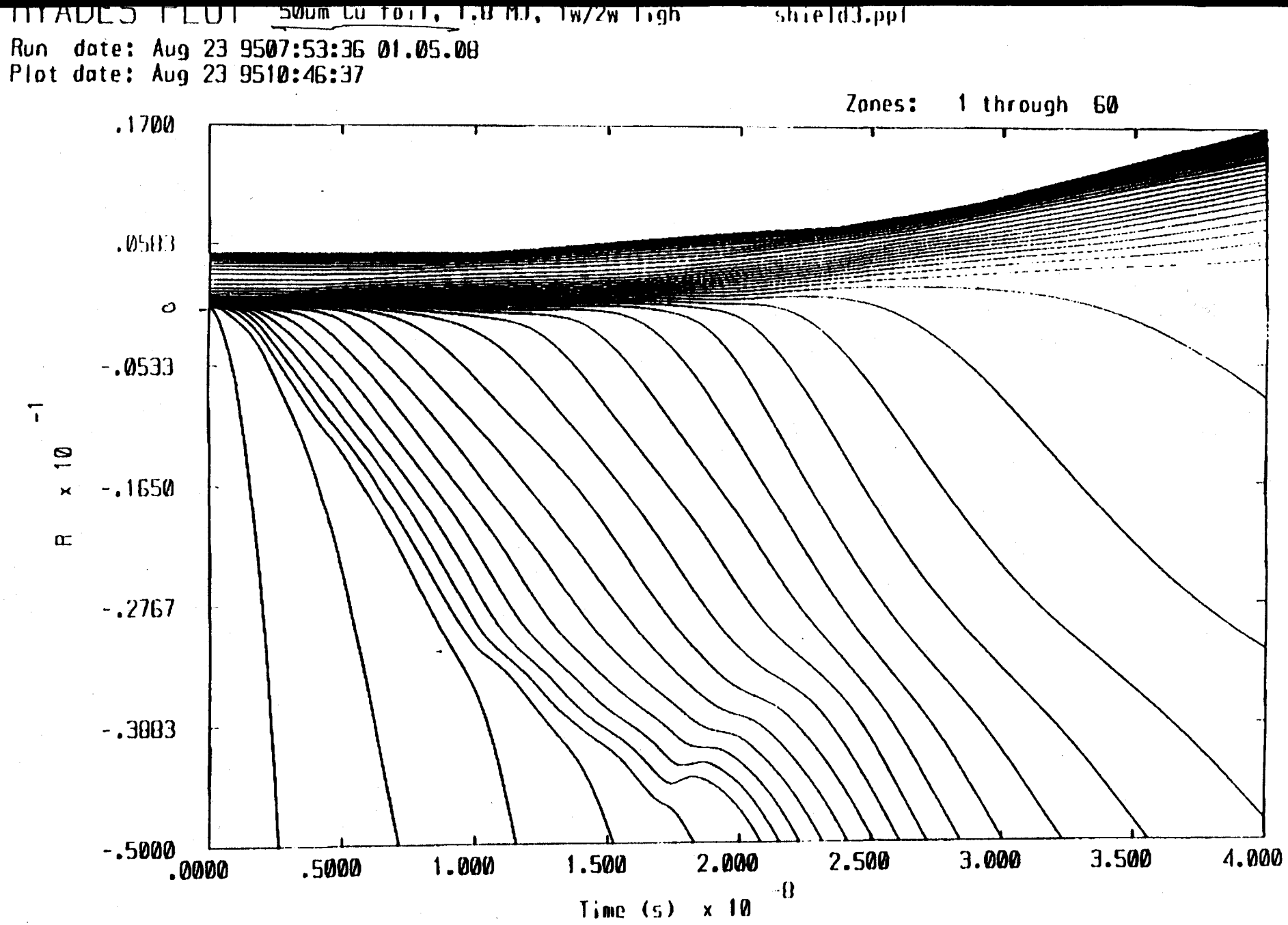

Figure 4: Plot of node location vs. time for Case 3. Laser is incident on the lower surface until t = 2E-08.

Results:

Fused-Silica Impact Data from NASA

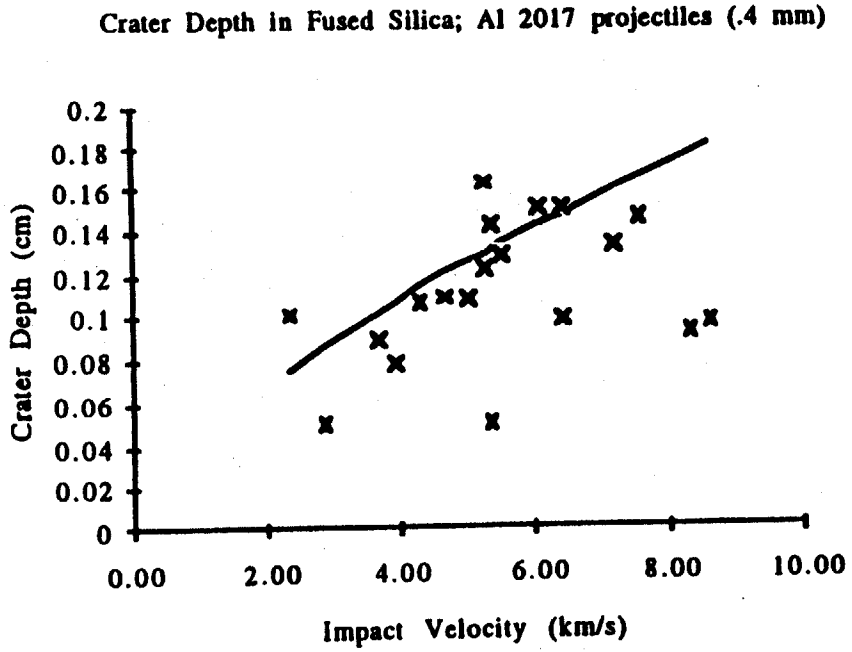

$$P_c = D_p V_p^{\frac{2}{3}} \left(\frac{\rho_t}{K_t}\right)^{\frac{1}{3}} \left(\frac{\rho_p}{\rho_t}\right)^{\frac{1}{2}} \left(\frac{C_{v_p}}{C_{v_t}}\right) \left(\frac{K_p}{K_t}\right)$$

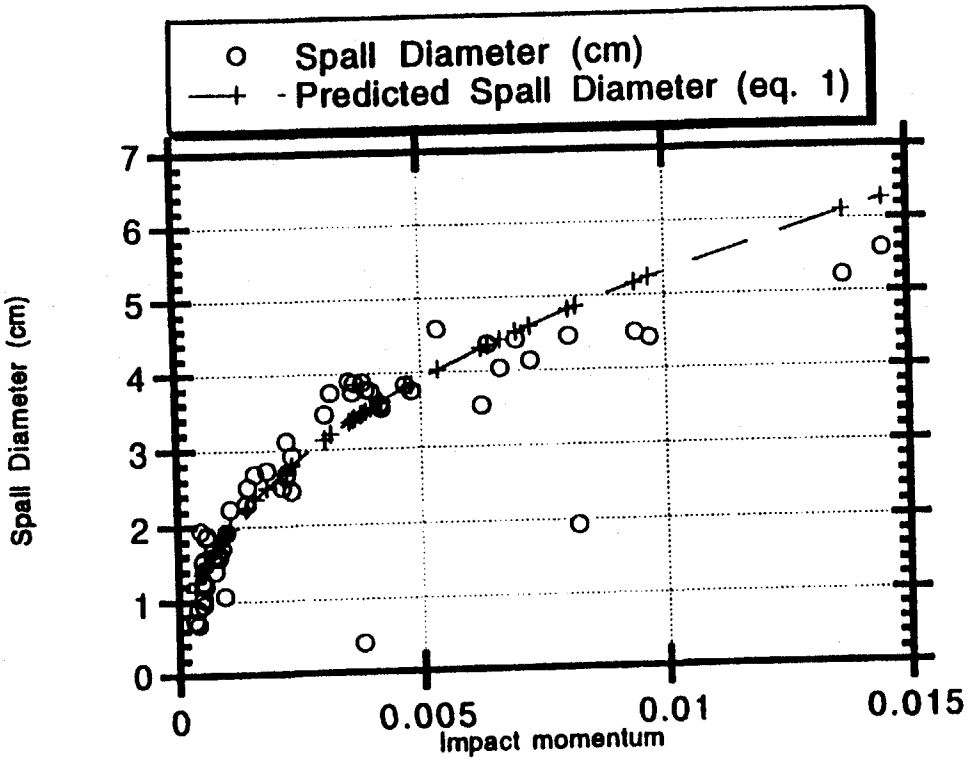

$$D_{spall} = kP^{0.4445}$$

File Edit

SAI's Accident Analysis Computer Algorithm (aka MacBomb™)

SRI International's

McNIF: ALGORITHM ANALYSIS CODE FOR NIF

DEMONSTRATION FOR

NATIONAL IGNITION FACILITY

File Edit Setup P/T Curves Damage Tools 3-D Views

SRI's Accident Analysis Computer Algorithm (aka MacBomb™)

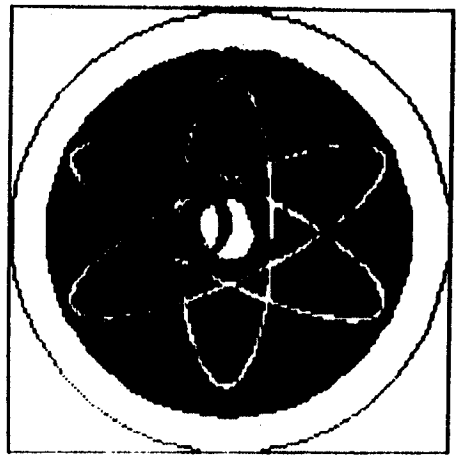

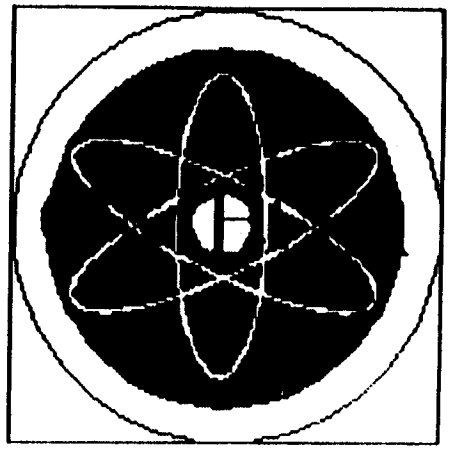

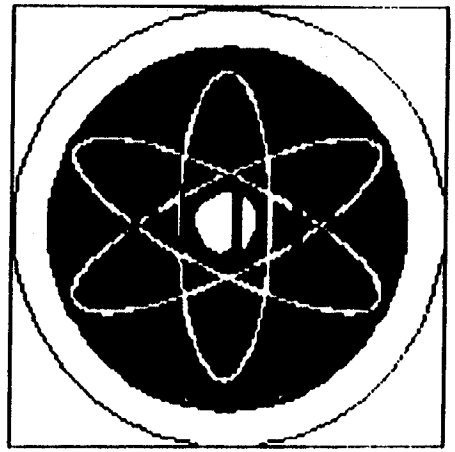

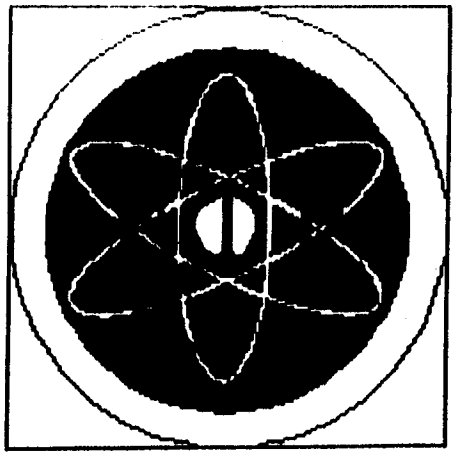

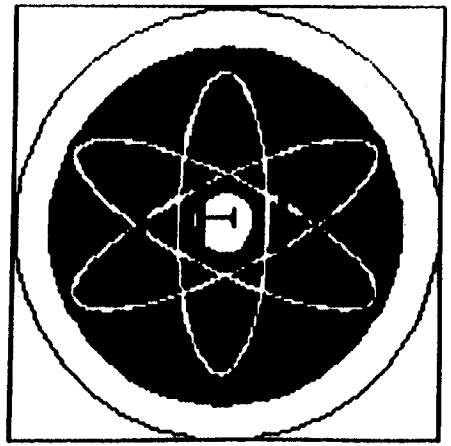

INITIAL SETUP FOR MCNIF: MENU CHOICES

- Nova, Omega Upgrade, NIF, ETF, IFE
- General Features
  - --Coordinate System and Layout
  - --3-D Display
  - --Timeline of Effects
  - --Damage memory of all nonvolatile components
  - --Sensitivity analysis and optimization
- NIF
  - --NIF Baseline Design
  - --Chamber Dynamics
  - --Optics Degradation from Neutrons and Gammas\
  - --Fast Ignitor
  - --EMI and Controls
  - --Weapons Effects
  - --Weapons Physics

- NIF Baseline Design

  Target Chamber Geometry
  - --Wall
  - --Laser ports
  - --Optics debris shields
  - --Shine shields
  - --Target support cone
  - --Target holder
  - --Diagnostics

  Source Specifications
  - --Driver mode (direct or indirect)
  - --Target source
    - Gas bag
    - Disk
    - Hohlraum
  - --Laser light energies
  - --Debris
  - --X rays
  - --Neutrons

  General Analysis
  - --Direct effects from target source debris, x rays, neutrons at
    - Wall
    - Optics debris shields (cratering)
    - Shine shields
    - Target support cone
    - Target holder
    - Diagnostics
  - --Critical irradiation analysis

- Chamber Dynamics
  - --Debris shield degradation
  - --Diagnostics' survivability
  - --Target technology
  - --Mechanical responses of chamber components
  - --Dose rates from target area
- Debris shield degradation
  - --Direct effects from hohlraum debris, x rays and neutrons
  - --Secondary effects of hohlraum debris, x rays and neutrons

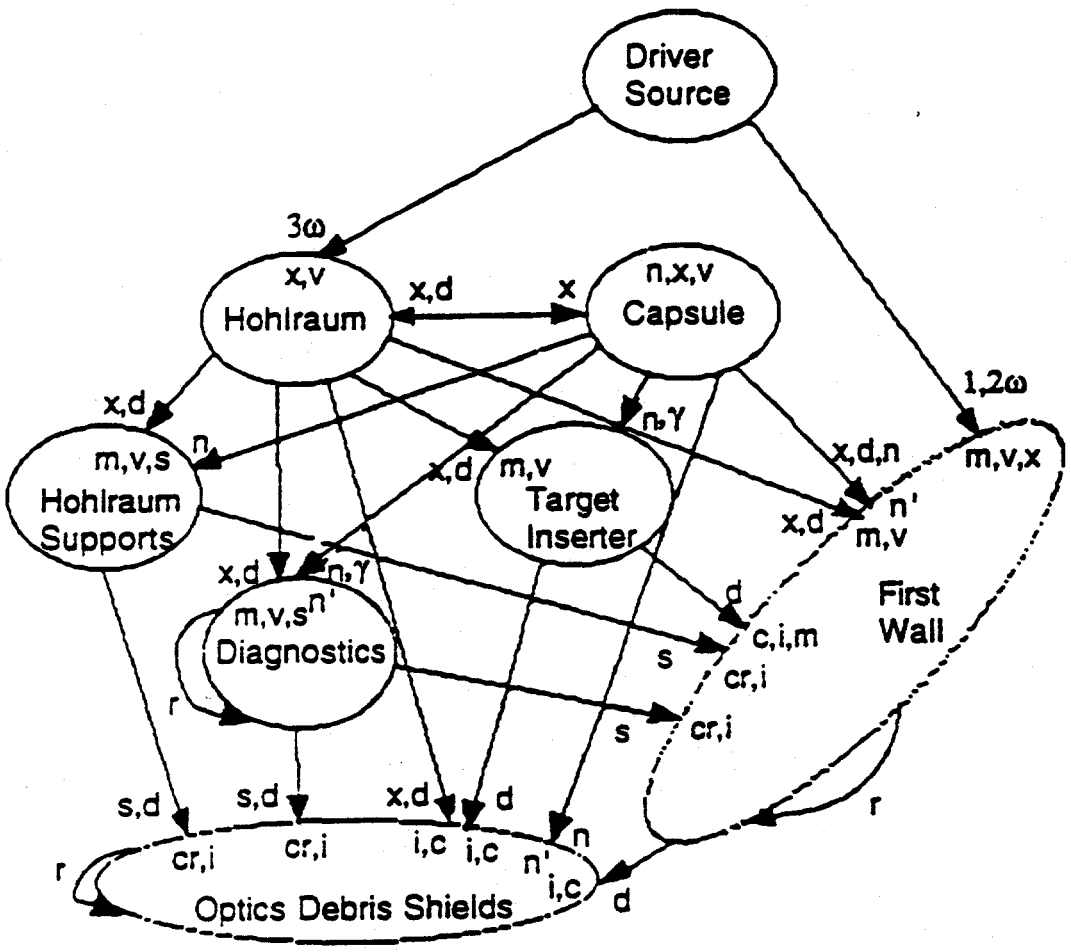

n = neutrons
x = X-rays
d = debris (usually hi vel m,v)
s = shrapnel
m = melt
v = vapor or gas
c = condensation
i = ion implantation
cr = cratering
n' = neutron particle damage
γ = gamma ray effects
r = recycled or cumulative effects

CAM-5543-11

Figure 2-7. NIF target chamber interactions for assessing NIF operations.

Summary/Conclusions:

- A code methodology has been developed for computing the combined effects of hohlraum and shine-shield debris.
- Extrapolations based on NASA data for fused silica should be useful for predicting optics debris-shield damage.
- McNIF appears to have the potential of being a useful high-level, organizational and analytical design tool containing relevant physics and supporting documentation.

POSSIBLE McNIF FROST ALGORITHMS

D. R. Curran & R. E. Tokheim

13 September 1995

Background:

- Detailed LLNL hydrocode calculations
- GAMBLE-II experiments

Candidate algorithms:

- Snowplow
- HPOL (Highly Porous Overlay Model)

Appendix II

POSSIBLE McNIF FROST ALGORITHMS

[FROST ALGORITHM]

SIMPLE DESIGN ALGORITHMS FOR ATTENUATION OF STRESS PULSES IN FROST LAYERS; APPLICATION TO NIF TARGET SUPPORT PROTECTION

D. R. Curran and R. E. Tokheim

24 July 1995

Introduction and summary

Preliminary National Ignition Facility (NIF) chamber designs utilize frost layers several mm thick to protect the target support cone and possibly other objects in the chamber from stress wave damage caused by absorbtion of cold x-rays emanating from the Hohlraum. Detailed hydrocode computations and ion beam experiments have been performed by LLNL personnel [1995] to study the feasibility of the concept, and the results were very encouraging. Ion beam fluences up to 400 J/cm^2 were tested, the deposition time was about 40 ns, and the deposition profile closely matched that expected from 1 Kev BBT x-rays of the same fluence. About 1 cm of frost was apparently sufficient to reduce initial front surface pressures to very low values (bars).

Detailed hydrocode calculations are time-consuming and expensive, therefore simple design algorithms would be extremely useful for use in a McNIF menu to evaluate and optimize this "frost shielding" concept. In the following paragraphs we explore the feasibility of such algorithms, compare them with LLNL calculations, and apply them to a "worst case, non-cryogenic" NOVA experiment: A 50ev BBT, 0.74 MJ point x-ray source that produces a fluence of 590 J/cm^2 at normal incidence at a 10 cm radius with a deposition time of 20 ns .

The results show that simplified algorithms appear practical, and that about a 1-cm layer of frost will be required to protect the target positioner cone in the worst case NOVA non-cryogenic environment.

More comparisons with detailed hydrocode calculations are needed to confirm the above conclusion.

Prior work

Although snow has long been known to be a good shock wave attenuator, little quantitative data are available. Gas gun data are reported in work by Brown et al [1988], and more recent work by Erlich and Curran [1994] reported measurement of attenuation of shock waves caused by explosively-launched flyer plates into snow samples roughly 60cm x 60 cm x 25cm in size. The large sample sizes were required to maintain uniaxial strain flow conditions for the duration of the in-material particle velocity measurements.

For peak pressures less than 100 MPa, the Erlich and Curran work showed that the "snowplow model" to be discussed next agrees with the experimental shock wave attenuation data to within the experimental scatter of about plus or minus 20%. However, the lowest snow density studied in the above-referenced work was about 0.3 g/cm^3, whereas the frost has a much lower density, about 0.1 g/cm^3. Furthermore, the peak pressures of interest in the NIF chamber are many orders of magnitude higher than 100 MPa.

As mentioned above, LLNL personnel [1995] performed ion beam experiments with the Gamble-II facility at the Naval Research Laboratory at fluences up to 400 J/cm^2. These

experiments no doubt produced the high pressures of interest, although successful pressure measurements were not attained. It was observed that about 1 cm of frost of density about 0.1 g/cc was sufficient to prevent damage in aluminum substrates. Furthermore, LLNL performed detailed hydrocode calculations for 1 kev BBT x-ray fluences of 100 J/cm^2.

Approach

We will describe two simple algorithms, a snowplow model algorithm for pressures below about 100 MPa, and a Highly Porous Overlay (HPOL) model algorithm for higher pressures. We will then compare predictions of the algorithms with LLNL hydrocode calculations. Finally, we will use the algorithms to estimate a "sure-safe" frost layer for the worst case non-cryogenic exposure of the target support cone.

Snowplow model algorithm

The snowplow model assumes that the porous material is compacted by a steady shock wave to a fully compacted, rigid solid whose equation of state is simply, $\rho = \rho_S$, where ρ_S is the density of the fully compacted state (for our frost case, we choose ρ_S = 1g/cc).

We define $\mu = 1-\rho_O/\rho_S$, where ρ_O is the initial density. Then the junp conditions become:

$$P = \rho_O u^2/\mu \qquad (1)$$
$$u = \mu U \qquad (2)$$
$$E = \mu P/2\rho_O \qquad (3)$$

where P is the compressive shock stress in the direction of wave propagation, u is the particle velocity behind the shock, U is the shock velocity, and E is the internal energy behind the shock. For frost with an initial density of 0.1 g/cc, μ = 0.9.

During x-ray deposition, the foot of the pulse will travel into the frost, shocking up as it goes. Simultaneously, unloading from the front surface will be occuring, so that at the end of the deposition a shock pulse will exist that has a duration roughly equal to the deposition time τ. To derive a simple algorithm for shock attenuation, we assume that this initial pulse can be approximated by a square pulse of instantaneous rise to a peak compressive stress, followed by a duration of time τ. During propagation of this pulse the shock front travels with a shock velocity U, and the unloading wave behind it overtakes it with velocity (in laboratory coordinates) u+c, where c is the sound speed in the fully dense water (≈ 1.5 km/s for pressures below about 100 MPa). Then the depth D at which the unloading wave overtakes the shock front is given by:

$$D = \frac{U(u+c)\tau}{u+c-U} \qquad (4)$$

where D is a conservative estimate of the depth of frost required to completely attenuate a shock with front surface compressive stress P and duration τ, and where u and U are obtained from Eqs (1) and (2). That is, $U = (P/\mu\rho_O)^{1/2}$, and:

$$D = \frac{(\mu U^2 + cU)\tau}{c-(1-\mu)U} \qquad (5)$$

The above estimate of D is conservative because the actual initial pulse is more triangular, and will attenuate faster, thereby resulting in a smaller value of D than that given by Eq (4) or (5).

Eq (5) is plotted below (for c = 1.5 km/s).

Figure1 Pressure vs shock penetration depth

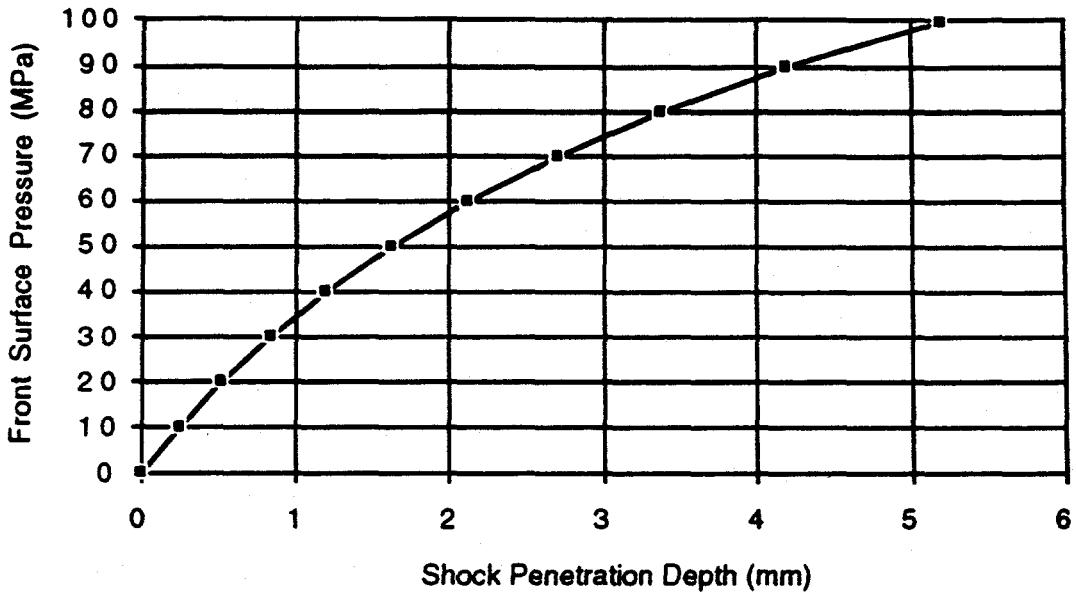

Thus, once the shock has decayed to below about 100 MPA, only a few mm of frost will be required to further attenuate it to zero.

However, this pressure region, where the strength of the frost plays a role, is only a small part of the problem. Of real interest is the high pressure region produced when the x-ray fluence is sufficient to produce a very high pressure vapor. For example, for the worst case, non-cryogenic case mentioned above, an FSCATT deposition calculation in water yields a front surface deposition of about 2×10^{14} erg/g, and the depth of vaporization in the frost is about 0.1 mm. With a Gruneisen ratio for water of about 0.3, and ignoring expansion during deposition, this would produce about 3000 GPa (30 Mbar) front surface pressure, a very large pressure indeed. Such conditions defy the above simple snowplow algorithm, and we must take a different approach, as discussed next.

Highly Porous Overlay (HPOL) Concept

The HPOL concept is illustrated in the sketch below. The frost is so porous that it is an open structure in which dendritic ice fibers form a low-density "brush" [LLNL, 1995], but the fiber density is nonetheless assumed high enough to prevent x-ray shine-through. Thus, all the x-ray photon deposition occurs in the fibers at some distance H from the target surface. We also assume that the fiber spacing is large enough that only insignificant stress waves can be transmitted through the fibers to the target. Therefore, the impulse is delivered only after the

blowoff gases expand to impact the target surface.

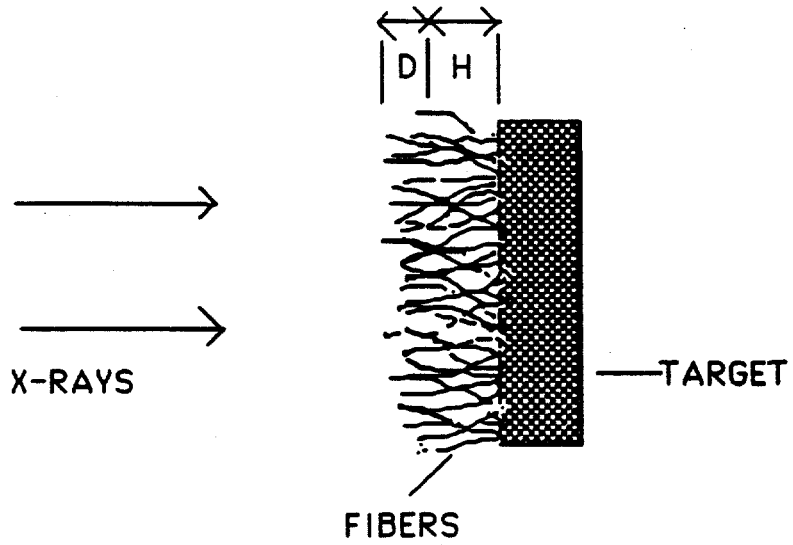

Figure 2 Fibrous Overlay Concept

The x-ray deposition is defined to occur to a depth D in the overlay. It is interesting to note that the mass and specific energy of the blowoff gases from a fiber are to a first approximation independent of the angle of the fiber to the incoming radiation. This fact is illustrated by the (2-dimensional) sketch below, in which the fiber is replaced by a plate.

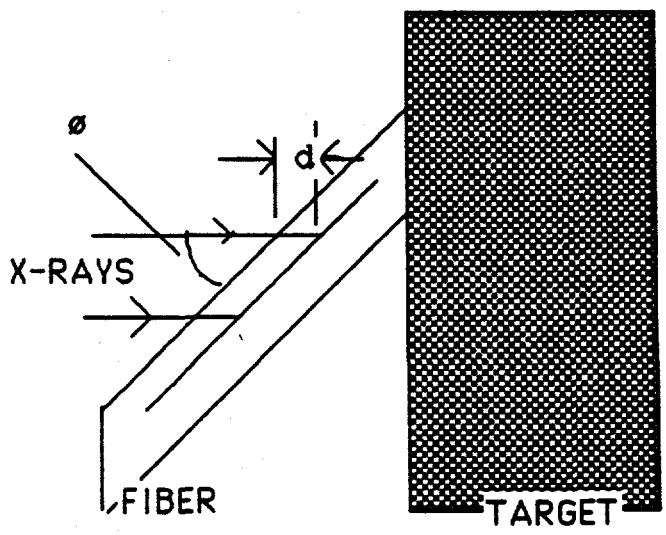

Figure 3 X-ray Deposition Geometry

If one neglects second order effects such as scattering, the deposition depth d is independent of the angle of incidence ø. If d is defined as the deposition depth corresponding to vaporization,

then the mass of the blowoff from the plate is the plate (fiber) density times the irradiated area times dsinø. But the irradiated area varies as 1/sinø. Thus, the blowoff mass is independent of the x-ray incidence angle. Furthermore, since the number of absorbed photons is the same in both cases, the deposited specific energy is also constant. This result will also hold for the 3-dimensional fiber case.

The design approach in general is thus to use low density fibers with high vaporization and melt energies to minimize blowoff mass, to maximize H/D within allowable weight penalties to reduce the gas pressure when the expanding gas impacts the target, and to delay the impulse delivery. We note that the total impulse reduction possible with the fibrous overlay concept is thus equal to that of a porous material. However, as discussed below, the impulse delivery is delayed by the time it takes the gas to expand to the target surface. Furthermore, the subsequent impulse delivery time is increased, and these effects can be used in some cases to good effect.

In our specific case, frost is chosen to minimize NIF chamber contamination, so we do not have the option of varying the fiber density or vaporization and melt energies.

It is easy to estimate an approximate impulse delivery time as a function of impulse and fiber geometry parameters. The fibers must be closely enough spaced compared to their lengths to prevent shine-through. Therefore, the blowoff gases will rapidly fill the space between the fibers before expanding toward the target, and to a first approximation this "channel fill up" time can be neglected. Thus, the initial conditions can be assumed to consist of gases filling the cavity between the fibers to the depth D shown in Figure 2 The gas front then expands toward (and away from) the target surface with velocity u. If we assume a linear velocity gradient from the gas front to the center of the cloud, the momentum toward the target is

$$I = (1/2)\, m\, u$$

where m is the areal mass of the blowoff gas. If the gas molecules have elastic collisions with the target surface, the momentum per unit area delivered to the target will be double that given above, i.e.

$$I = m\, u \qquad (6)$$

Thus, to a reasonable approximation, the total impulse delivered to the target will be the same as if the fiber material had been put on the target surface as a fully dense coating, but the peak pressure will be delayed and lower, and the load duration will be longer.

The impulse delivery will be delayed by the time it takes for the gas front to reach the target surface:

$$t_d = H/u = m\, H/I \qquad (7)$$

Since the areal mass m of the blowoff is independent of fiber orientation, it is the same as for normal incidence of radiation on a plate of the fiber material, i.e.

$$m = \rho d \qquad (8)$$

where ρ is the initial density of the fiber material, and d is the deposition depth corresponding to vaporization. Furthermore, to a good approximation, I in Eq.(6) can be obtained from a BBAY formula, e.g. the McCloskey-Thompson version:

$$I = 1.2\{2\int_{0}^{z(E_m)} z[E - E_m(1 + \ln(E/E_m))]dz\}^{1/2} \qquad (9)$$

where E_m is the melt (or more properly the vaporization) energy, z is the areal mass in g/cm^2 at a particular depth in the target, $z(E_m)$ (called m in Eq.(7) and (8)) corresponds to the depth where the deposited specific energy equals the vaporization energy , and I is the total impulse in taps ($dyne\text{-}sec/cm^2$).

Pressure reduction over that in the initial blowoff gas occurs as the gas expands to fill the cavities between the fibers and the volume between the deposition region and the target surface. The ratio of the initial gas volume to the volume when the gas front reaches the target is roughly $d/\mu(D + 2H)$, where μ as before is the volume porosity of the fibrous layer. Since the gas expansion is nearly free, the pressure reduction at the beginning of impulse delivery to the target, under the ideal gas approximation, is given by

$$P/P_0 = [d/\mu(D + 2H)]^{\gamma} \qquad (10)$$

where P_0 is the pressure in the unexpanded blowoff gas, and γ is the ratio of specific heats of the gas. Note that under the approximation of free expansion of a gas into a constant volume, the final state of the gas does not follow the PV^{γ} = constant law, which holds only for "quasistatic" processes [Zemansky, 1951]. We are therefore assuming that the expanding gas front is pushing a frost piston slowly enough that wave reverberations in the gas keep the gas at a uniform pressure. This assumption is dubious because the estimated sound speed in the gas is on the order of the estimated piston speed. Nonetheless, we will proceed with it.

The total impulse delivery time t_D is the sum of the impulse delay time from Eq.(7) and the delivery time t_L after the gas has contacted the target. For a given total impulse, t_L will be roughly inversely proportional to P. Thus,

$$t_D = mH/I + t_{()}\, P_{()}/P \qquad (11)$$

where t_0 is the delivery time for the prompt impulse when the deposition is in a plate of fully dense fiber material, and is approximately equal to the deposition time t.

The performance bounds of this concept can be inferred from a few numerical examples from Eq(10). The examples are listed in the following table.

Table 1 Predictions of HPOL algorithm

Case	BBT	fluence	d	D	μ	P_0	comments
LLNL hydo. calc.	1 kev	100 J/cm^2	0.0003 cm	0.003 cm	0.9	≈12 GPa at 0.003 cm depth	Decays to 1 MPa at 0.6 cm depth
HPOL algorithm calc.	1 kev	100 J/cm^2	0.0003 cm	0.003 cm	0.9	$\rho\Gamma E \approx 6$ GPa at 0.003 cm depth, ρ=1 (Assumes Γ=1.3, uses LLNL deposition profile)	Decays to 1 MPa at 1.0 cm depth
Worst case non-cryo	50 ev	590 J/cm^2	0.0001 cm	0.001 cm	0.9	$\rho_0\Gamma E \approx$ 3000 GPa at 0.001 cm depth	

In the HPOL model, we assume a frost fiber density of 1 g/cc, a porosity μ of 0.9, and a vapor γ of 1.3. Figure 4 shows a plot of P as a function of overlay depth from the HPOL algorithm for the above 100 J/cm^2 case, and compares it to the LLNL calculation for the same conditions. The simple algorithm agrees with the more rigorous LLNL calculation to within less than a factor of 10 over the range of interest. Moreover, below 100 MPa (1 kbar), the snowplow algorithm could be invoked to predict that an additional 0.5 cm of frost would completely attenuate the pulse, in rough agreement with the LLNL calculations.

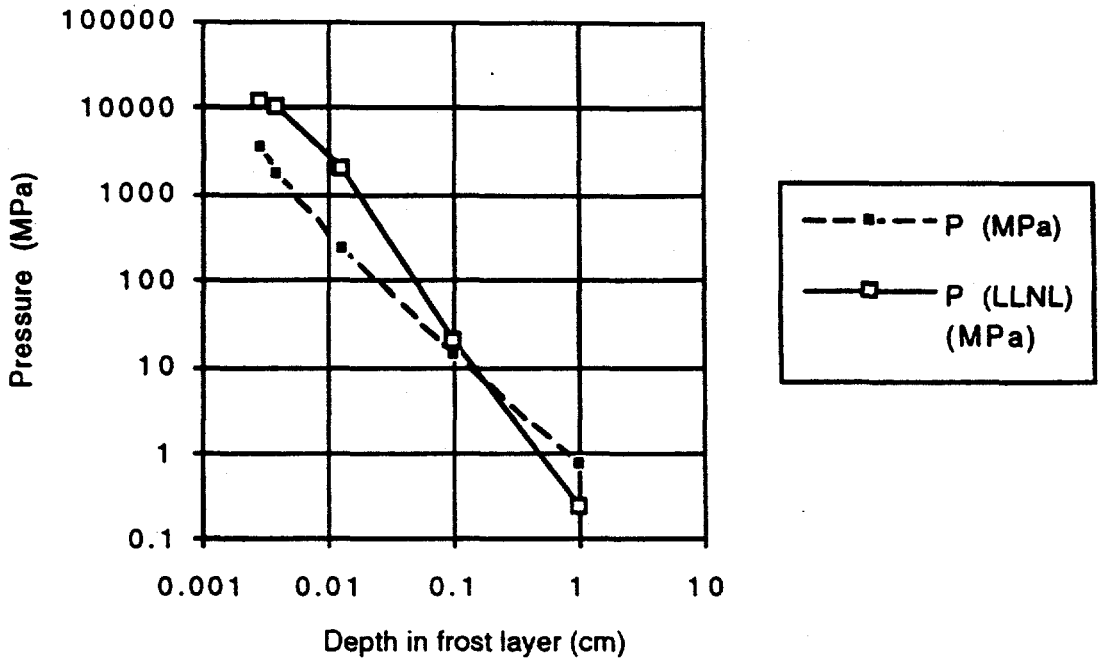

Figure 4 Attenuation of pressure in frost layer

We next use the HPOL and snowplow algorithms to evaluate the NOVA "worst case" for the target positioner: 590 J/cm^2 , 50 ev BBT. The prediction of the HPOL model is shown in Figure 5 below.

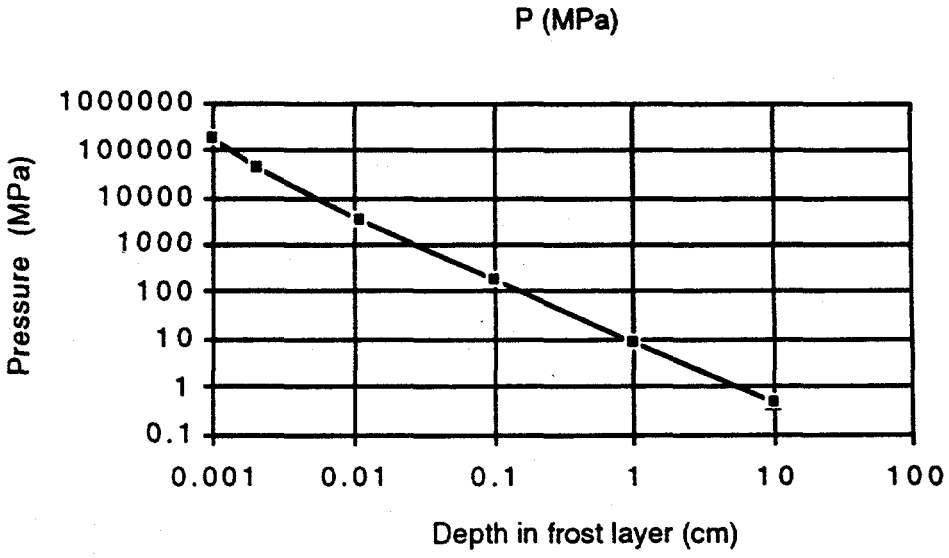

Figure 5 HPOL model estimate of attenuation in frost layer for worst case non-cryogenic case

In this case, we see that the HPOL model predicts that the pressure will be reduced to 100 MPa (1 kbar) at a depth of 1mm. Then the snow plow model predicts that 5 additional mm would

reduce the presure to negligible amounts. Thus, 10 mm of frost would appear to be suficient protection for the target positioner cone for the worst case non-cryogenic environment, even at normal incidence. However, a detailed hydrocode calculation with relevant physics is needed both to confirm this conclusion, and to validate the simple algorithms.

However, the target holder would appear to be vulnerable to higher fluences, since more than 1 cm of frost may be impractical. Thus, for cases involving nuclear burn, it may be impossible to prevent the target holder from forming shrapnel.

Summary

The simple HPOL algorithm at high pressures combined with the snowplow model below 100 MPa appears to give a reasonable estimate of the frost layer thickness required to reduce the incident pressure to safe levels.

More comparisons of these algorithms with detailed hydrocode calculations containing the relevant physics are needed to validate these potential McNIF algorithms.

Then the McNIF algorithm should be used early in the program to define the bounds of where frost protection is viable.

References

J. A. Brown, E. S. Gaffney, G. L. Blaisdell, and J. B. Johnson. "Techniques for Gas Gun Studies of Shock Wave Attenuation in Snow", in *Shock Waves in Condensed Matter 1987*, S. C. Schmidt and N. C. Holmes, editors, Elsevier Science Publishers, Amsterdam (1988).

D. C. Erlich and D. R. Curran, "An Experimental Study of Shock Wave Transmission through Snow, a Snow Simulant, and Freon Gas", Defense Nuclear Agency Report No. DNA-TR-93-95 (Feb. 1994).

Lawrence Livermore Laboratory unpublished document, provided by Per Peterson [1995].

M. W. Zermansky, Heat and Thermodynamics, McGraw-Hill, (1951), p125.

SUMMARY

- Postulated simple McNIF algorithms look promising

- But need validation with further hydrocode calculations and experiments

Appendix III

POSSIBLE PHOEBUS OR NOVA EXPERIMENTS

POSSIBLE PHOEBUS or NOVA EXPERIMENTS
Bob Tokheim and Don Curran
10/19/95

1. All-purpose experimental fixture: A possible all purpose experimental fixture might look something like the sketch shown below.

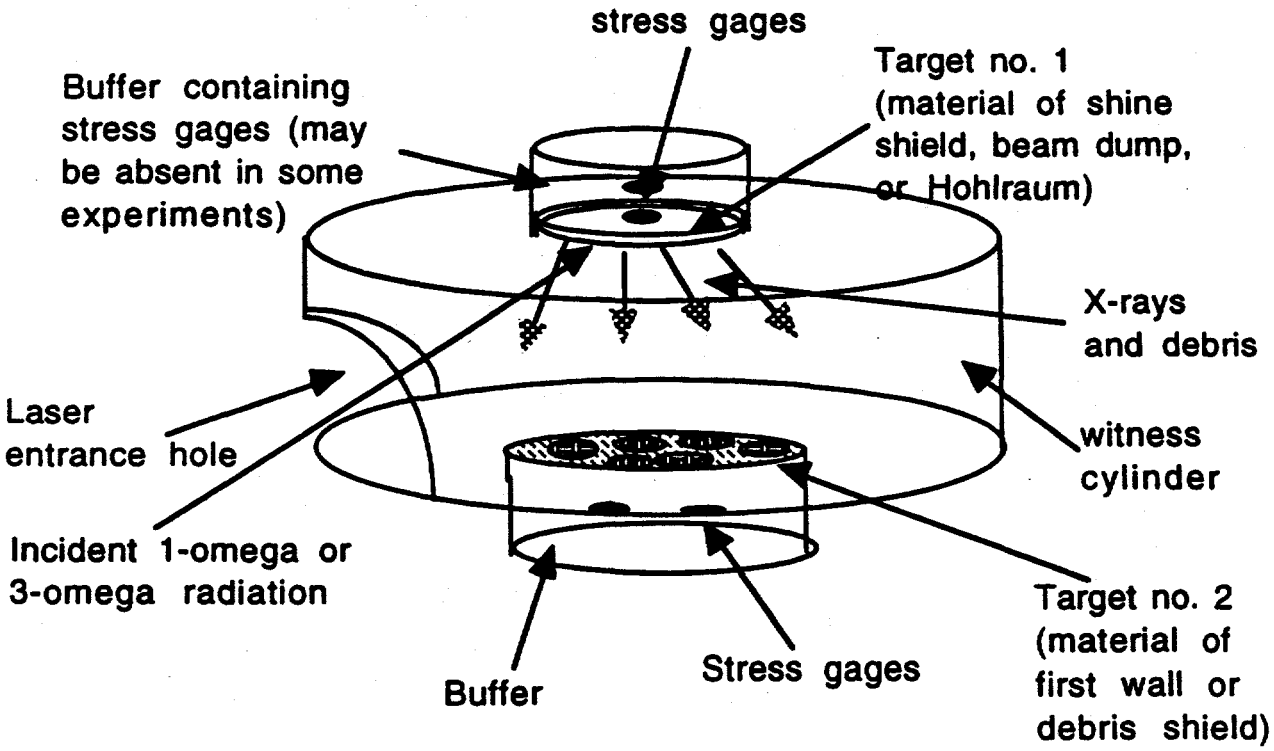

The idea is to have a standard fixture that could be used in either Phoebus or Nova experiments, thereby standardizing as much as possible the experimental procedures.

This is just a first cut; many improvements can no doubt be made, e.g. the witness cylinder could be a hemisphere.

Some possible experiments with this fixture are listed next.

2. Experiments: A few proposed experiments with the above fixture are listed in the following table.

Purpose of experiment	Incident radiation on Target no. 1	Target no. 1	Target no. 2	Comments
Measure the effects of x-rays and debris from shine shields on 1st wall and debris shield materials	1-ω	Copper disk (with and without rear surface buffer & gages)	Side-by-side: • B4C & B • Fused silica & fused silica over methyl-cellolose	Vary spot size on target no. 1 to vary fluence. Rear surface gages only used for large spot sizes
Measure the effects of 1-ω on beam dumps, capture beam dump ablated material	1-ω	Beam dump layers with rear surface buffer & gages	Witness material selected to best capture beam dump ablated material	
Measure the combined effects of Hohlraum x-rays and debris on 1st wall and debris shield materials	3-ω	Gold disk (with and without rear surface buffer & gages)	Side-by-side: • B4C & B • Fused silica & fused silica over methyl-cellolose	• Vary spot size on target no. 1 to vary fluence. Rear surface gages only used for large spot sizes • Gages behind target no. 2 allow measurement of debris arrival time, and possibly validate code calculations of debris impulse

3. Multiexposure effects: The above experiments can be performed several times with the same samples and/or witness plates to explore cumulative effects.

4. Debris measurement diagnostics:

Figure 1 shows how a target (debris source [Target no. 1] or debris sink [Target no. 2]) might be instrumented to measure debris characteristics. Additionally a time resolved history of the debris can be obtained by employing a rotating drum technique developed for radiation simulators (both as a diagnostic and as a component of a debris shield), see **figure 2. Table 1**

details the attributes and liabilities of various diagnostic measurements that can be made of debris generation and deposition on the NIF.

Figure 1. Possible sensors installed into a debris diagnostic target.

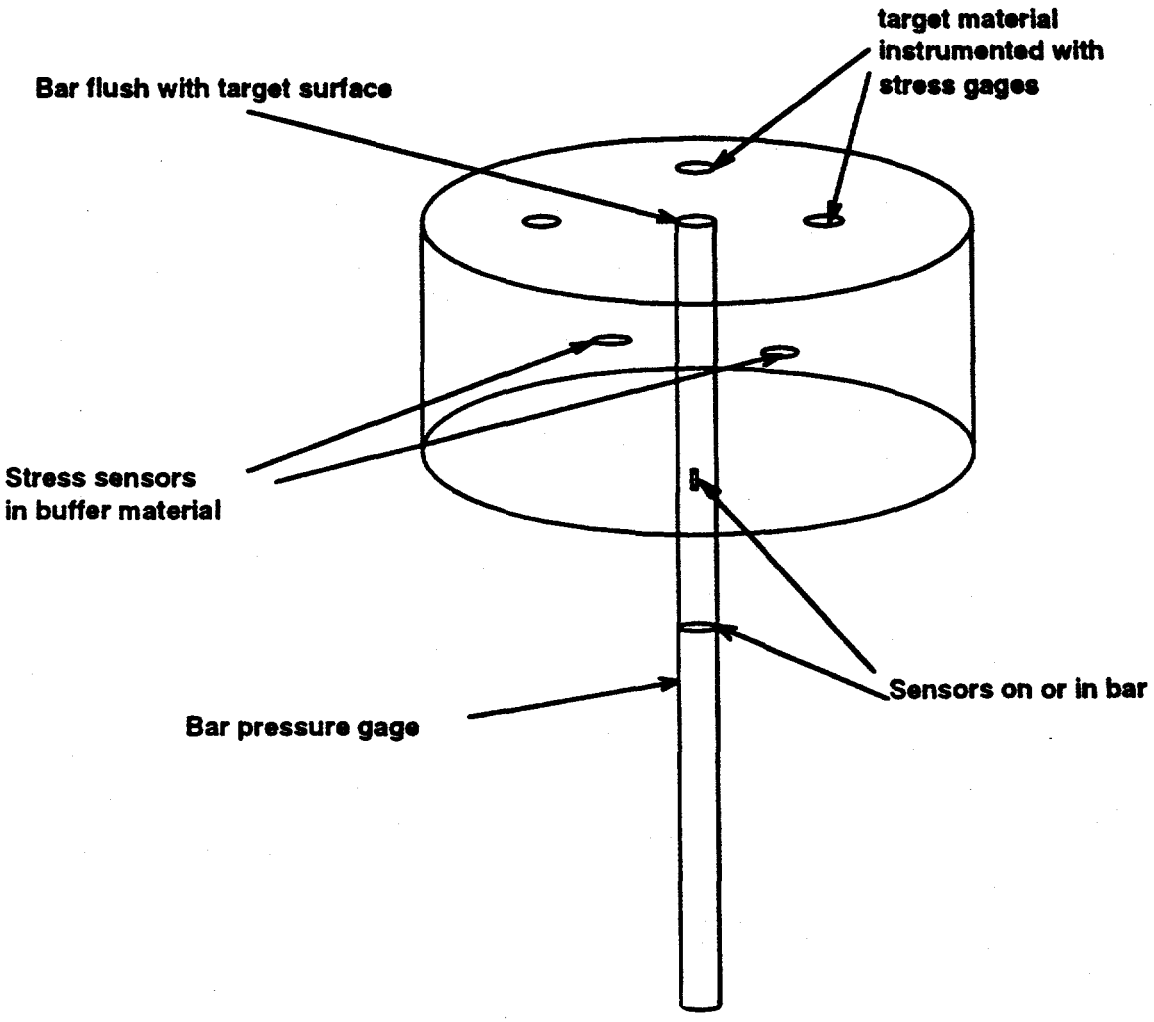

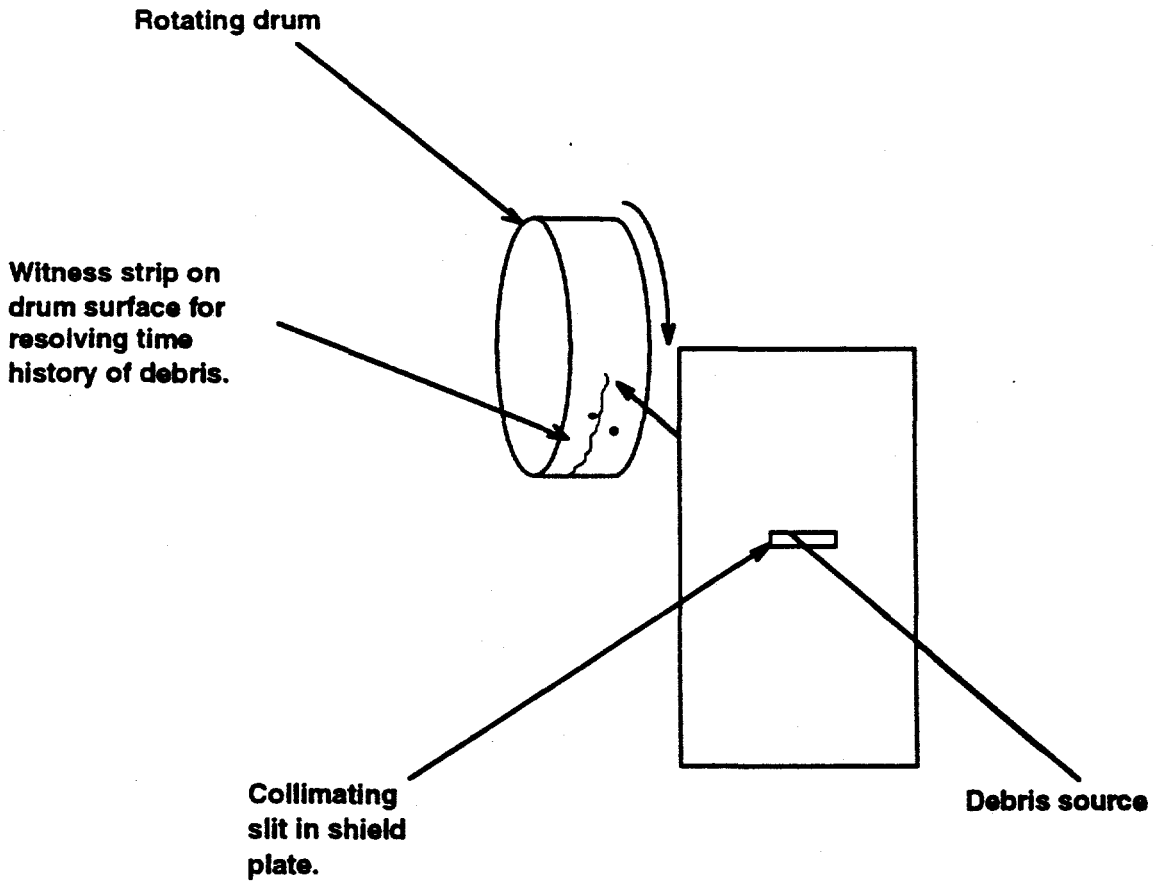

Figure 2. Test configuration for making time-dependent debris measurements.

TIME RESOLVED MEASUREMENT OF DEBRIS

A possible technique for capturing a time resolved history of NIF debris would be to use a fast rotating drum covered with a collecting strip see **figure 2**. This concept has been previously developed and some preliminary testing was done to collect debris generated on an x-ray simulators.

The concept consists of a hollow aluminum drum rotating with a maximum surface velocity of 200 m/s to 300 m/s, limited by the material properties (this corresponds to 20,000 rpm to 30,000 rpm for a 100 mm radius drum). The surface of the drum can be covered with a flexible strip such as Mylar or Kapton which can capture a time history of the debris through condensation or impact of liquid or solid particles. This strip can be removed and inspected using a scanning electron microscope where debris content can be ascertained through elemental analysis, craters can be measured and counted and the speed of each debris component determined. Alternatively the drum can be slotted to capture and time resolve a specific

component of the debris stream. As the drum rotates the slot will pass through the debris line-of-site and some of the material will pass through to the interior of the drum. In this case the collector strip is placed on the inner surface of the hollow drum.

The drum is housed in a cassette where the front face can be slotted to collimate the debris beam improving the time resolution of the technique, a 0.3 mm slit width corresponds to a nominal 1 μsec resolution on the collector strip. Additionally the cassette serves to contain material in the event of a catastrophic failure. A secondary shutter can be used to block the collimating slot preventing any "re-write" on the collector strip.

The drum runs on high speed vacuum rated bearings driven by a vacuum rated high speed motor (approximately 1 hp for a 100 mm radius by 130 mm long hollow aluminum drum), both of these require active cooling in a vacuum environment. The drum speed and orientation are computer controlled to interface with NIF timing. Once the desired rotational rate is achieved a timing pulse is issued when the drum is in a specific rotational orientation. This pulse can be used to either trigger the source or be recorded and thus establish an absolute time reference for the debris collecting strip.

Table 1. Potential sensors and diagnostics for debris characterization.

GAGE TYPE	MEASUREMENT	ATTRIBUTES	LIMITATIONS
Rotating drum	Collect samples of debris material.	Time history of debris field (What arrives when, what state it is in and how much). • Debris velocity. • Debris phase state (i.e. vapor, liquid, solid). • Elemental analysis.	Rotational rate limited by material properties of drum. (Surface velocity limited ≤ about 300 m/s).
Quartz Stress short-circuit or current mode	Stress induced in material by "blow-off" of surface.	Minimum rise-time. Noise immunity (low impedance in short - circuit mode) History of successful use on radiation simulators.	Very short recording time (~1 μsec). Diameter ≥ ~3 times the thickness. Stress ≤ ~1000 MPa.
Quartz Stress differential voltage mode	Stress induced in material by "blow-off" of surface.	Long duration recording time. Diameter can cover large range, ~ 6 mm to ~ 13 mm. Noise immunity for differential design . History of successful use on radiation simulators.	Rise-time is dependent on overall sensor thickness, ≥ ~ 40 nsec. Stress ≤ ~1000 MPa. Difficult to make (differential design).
Ytterbium Stress	Stress induced in target by debris impact. Stress induced in material by "blow-off" of surface.	Noise immune design evolved from UGT testing. Can sense over large areas.	Low stress sensitivity limits measurement to between about 10 MPa and 2000 MPa. Sensitive to strain.

Table 1. Potential sensors and diagnostics for debris characterization (continued).

GAGE TYPE	MEASUREMENT	ATTRIBUTES	LIMITATIONS
Manganin Stress	Stress induced in material by "blow-off" of surface.	Linear response. Low temperature coefficient. Noise immune design evolved from UGT testing. Can sense over large areas.	Very low sensitivity to stress, measurement of stress above about 500 MPa.
Carbon Stress	Stress induced in target by debris impact. Stress induced in material by "blow-off" of surface.	Robust . Can sense over large areas.	Low stress sensitivity.
PVDF Stress	Stress induced in target by debris impact. Stress induced in material by "blow-off" of surface.	Generally the same as quartz in either current mode or voltage mode. Sensor can be made very thin, ~ 10 μm to 50 μm. Low-Z material.	Generally the same as quartz either current mode or voltage mode. Perhaps not as well understood as quartz. Small area only, 1 mm to 25 mm^2. Sensitive to strain.

Instrumented pressure bar	Pressure-time history of debris deposition on target. Pressure of "blow-off" layer.	Removes sensor(s) to a less severe environment. Noise immune design evolved from UGT testing. Bar can be instrumented with multiple sensors to enhance confidence in measurement. Diameter can cover large range, ~ 3 mm to ~ 13 mm. Can measure pressures as low as about .01 MPa.	Dispersion in bar material complicates measured signal (rise-time typically ≥1 μsec). Upper stress limit determined by yield point of bar material. Recording duration generally* limited by acoustic length of bar, a few hundred μsec. * Techniques to extend measurement time have been developed.

Appendix IV

MINIMUM REQUIRED THICKNESS FOR NIF CHAMBER FIRST WALL AND DEBRIS SHIELD COATING

Table 1. Potential sensors and diagnostics for debris characterization (continued).

GAGE TYPE	MEASUREMENT	ATTRIBUTES	LIMITATIONS
Ruby stress gage	Stress induced in material by "blow-off" of surface.	High frequency response. Diameter can cover large range, ≤ ~ 1 mm to ~ 20 mm. Upper stress range ≥ 30 GPa. Stress sensitivity is well characterized.	Development stage Signal conditioning cost* Lower limit of resolution about 200 MPa to 300 MPa. * DNA currently funding effort.

Minimum Required Thicknesses for NIF Chamber First Wall and Debris Shield Coating Materials to Counter the Expected Shrapnel Threat

D. R. Curran and R. E. Tokheim

7 November 1995

Abstract

We have combined available data and simple theory to estimate the minimum required thicknesses of ceramic first wall materials and plastic debris shield coating materials to afford reliable protection against debris and shrapnel in 20 Mj yield shots. The results are summarized in the following table.

Table 1. Minimum thicknesses for debris and shrapnel protection

Material	Minimum thickness (mm)	Comments
Fully dense B4C, B, or SiC for first wall protection	5	Criterion is that the layer thickness be five times the damage radius. The craters are shallow, but a large sub-crater fractured zone is probable. A thinner layer may be possible if the fractured material remains bonded to the substrate.
85% dense B4C, B, or SiC for first wall protection	4 - 6	"
Debris shield coating plastic	3.5	Criterion is that the layer thickness be five times the damage radius. Lack of large sub-crater fracture zone allows thinner layer than for the first wall ceramics.

The relatively thick layer requirements for the first wall material comes from the extensive fracturing that may occur in these brittle materials, but does not occur in soft materials like plastic or aluminum. However, the soft materials make deeper craters. Thus, the extent of damage is comparable for the soft and hard materials.

The most dangerous fragments appear to be the 150 μm steel shrapnel particles impacting at about 400 m/s. Therefore, initial "certification testing" should focus on producing these conditions.

The effect of 15% porosity in the first wall material appears to be mixed, with the porous material exhibiting more damage at lower impact velocities corresponding to the "worst case" shrapnel, and less damage at the high velocities corresponding to the small debris particles.

Shrapnel and debris threat

The threat considered here consists of gold Hohlraum and copper shine shield debris as well as steel shrapnel originating from the cryogenic tubes. The shrapnel is created as the tubes expand due to neutron heating, and the shrapnel is then accelerated further by absorption of Hohlraum x-rays and by the gold debris "wind" from the Hohlraum.

Preliminary estimates for a 20 MJ shot give shrapnel particles in the size range of 1-150 μm-diameter, with the smaller particles impacting the first wall or debris shields at about 10 km/s, and the larger particles impacting at about 400 m/s. Only a few hundred of the larger shrapnel particles will be produced, but 10^7 - 10^8 of the smaller particles will be produced. The current chamber design geometry will tend to concentrate the larger particles on the beltline away from the debris shields, and to concentrate the smaller particles on the debris shields. However, some particles of all sizes will impact at every location.

Hardening materials

First wall material candidates are ceramics, either plasma-sprayed to about 85% of full density, or sintered and/or pressed to nearly full density. The debris shield material is fused silica, but a candidate design has a methyl-cellulose plastic coating to mitigate shrapnel and debris damage.

Problem: Determine the minimum ceramic and plastic thicknesses required to survive a large number of yield shots before needing to be replaced.

Approach

Our initial approach is empirical. We have surveyed damage observations from tests over the particle size and velocity ranges of interest for ceramics and plastics, and have scaled the results to particle size. We checked these conclusions for plausibility by applying simple penetration models.

Data for plastics

NASA data exist for teflon targets impacted by 3.2 mm glass spheres at velocities from 1 to 7 km/s [1]. The results were similar to those obtained later for 1100 aluminum targets over the same impact velocity range, although the teflon craters showed short cracks radiating from the crater whereas the aluminum showed classic plastic craters. In both materials the craters were roughly hemispherical in shape. The similarity of results is not surprising because at these high impact velocities the forces exerted on the target are well above the yield strengths of the flowing penetrator and target materials, and a simple law in which the crater depth is equal to the interface velocity times the "impactor erosion time" may be reasonable.

That is, assume that the impactor is a rod of length L. The rear of the rod moves towards the target at the impact velocity v, while the eroding nose moves into the target at the slower interface velocity av. The depth of penetration corresponding to complete erosion of the penetrator is

$$P = aL/(1-a)$$

If the crater is hemispherical, the ratio of the diameter D of the crater to the characteristic impactor size L is

$$D/L = 2P/L = 2a/(1-a) \qquad (1)$$

An estimate for a can be obtained from impedance matching of impactor/target materials. Such estimates are given in the table below.

Table 2. Impedance matching estimates for a, and the associated values of D/L, for several materials. Comparison with experimental data.

Impactor material/target material	a	D/L	Observed D/L for impact velocities between 1 and 7 km/s	Comments
Glass/teflon	≈ 0.6	≈ 1.8	0.8 - 3.5	Ref. 1
Steel/teflon	≈ 0.75	≈ 4.5		
Gold/teflon	≈ 0.8	≈ 6.4		
Copper/teflon	≈ 0.75	≈ 4.5		
Glass/aluminum	≈ 0.5	≈ 2	1.5 - 4.0	Ref. 2
Gold/dense armor ceramic (e.g. B4c or SiC)	≈ 0.7	≈ 3.3		Craters expected only for impact velocities > ≈ 2 km/s
Steel/dense armor ceramic (e.g. B4c or SiC)	≈ 0.65	≈ 2.4	≈ 2 for the crater, but ≈ 7 for fractured zone in novaculite at 500 m/s	"
Copper/dense armor ceramic (e.g. B4c or SiC)	≈ 0.65	≈ 2.4		"
Aluminum/fused silica	≈ 0.5	≈ 2	2 - 8	Ref. 3. Sub-crater damage not recorded
WC/Si3N4	≈ 0.5	≈ 2	No crater, but crack lengths with D/L ≈ 2 at 170 m/s	Ref. 4.

Increasing values of D/L are expected for the higher impact velocities because the crater cavity continues to grow after the impactor is consumed. The growth stops after the kinetic energy in the target after the impactor is consumed is dissipated by work against the target yield strength. If the kinetic energy in the target after the impactor is consumed is proportional to the initial kinetic energy in the impactor, then the post-consumption cavity growth would be proportional to $v^{2/3}$, where v is the impact velocity. A dimensional analysis with this velocity dependence was derived more rigorously, and applied to the aluminum/fused silica data, in Ref. 3.

The teflon and aluminum target data also show this type of weak increase with impact velocity, as reported in References 1 and 2.

The above data for teflon suggest that a conservative teflon thickness T/L would be about 5 times the calculated D/L in the above table. Since the largest shrapnel fragment is expected to have a size of 150 μm (0.15 mm), this criterion would yield a minimum teflon thickness of 3.4 mm. This thickness could also be expected to survive many shots because most of the fragments are

expected to be much smaller than 150 μm, and the probability of the larger shrapnel particles impacting in an earlier large crater should be small.

Since the mechanical properties of most plastics under hypervelocity impact conditions are similar, the above results for teflon are probably reasonable for other plastics such as methyl-cellulose. Of course, we need to confirm this conclusion with impact experiments on the plastics of interest.

Ceramic first wall materials

Impact damage from metallic impactors against brittle target materials with high compressive yield strengths is fundamentally different than damage in soft target materials at impact velocities below about 2 km/s, because the high strength target causes the impactor material to flow, and the impactor is "consumed" without penetrating the target. However, tensile stresses are produced in the targets, resulting in "Herzian cone cracks" and "lateral cracks" that can excavate surface material and produce shallow craters. The extent of the fractured zone beneath the impactor can be quite large, even though the craters are shallow, as noted in Table 2 for novalulite targets.

At impact velocities greater than about 2 km/s, metallic impactors will produce "stagnation pressures" ($= \rho v^2/2$) that exceed 10 GPa, which is roughly the compressive yield strength of a good ceramic, and "plastic" penetration can occur. Thus, for impact velocities above 2 km/s, we can use the rough formula of Table 2. Again, however, we expect the fractured zone to be more extensive than the plastic crater.

Some of these data appear in Reference 4 and 5.

Hypervelocity impacts at of "chunky" fragments at velocities well in excess of 2 km/s will produce localized surface loads with energy densities well in excess of those in chemical high explosives. For example, a steel fragment impacting at 10 km/s has a kinetic energy density of about 10,000 cal/g, or ten times that of a typical chemical high explosive. For such cases, meteor impact, chemical explosive, and nuclear crater data are relevant. For such cases in "hard rock", shallow craters are formed with a D/L = 2 (where L is the dimension of the charge, i.e. the size of the intensely loaded surface area), and with a heavily fractured sub-crater zone with a D/L of 7 -10. Hydrocode cratering calculations are in fair agreement with these results [5,6].

The observations in Reference 4 suggest that the 85% dense material produced a damage radius about 30% larger for a given impact velocity than the fully dense material. However, this does not agree with observations in Reference 6 for explosive charges in contact with 85% porous calcite grout, which appeared to show less damage than the fully dense case. This is possibly explained by the higher importance of the stress attenuation properties of the porous material at hypervelocities.

Our tentative conclusion is that the performance of the 85% dense and the fully dense material is comparable, but with the porous material perhaps showing better performance at hypervelocities. On the other hand, the greatest threat appears to be the 150 μm steel shrapnel fragments impacting at 400 m/s. In that case, the fully dense material may be superiior.

The above results are summarized in Table 1 above.

Impact testing should obviously be performed on these candidate matrerials as soon as possible.

Appendix V

SHRAPNEL AND DEBRIS GENERATION IN NIF CHAMBER FROM CRYO TUBES AND HOHLRAUM

Summary and conclusions

The results of our preliminary analysis are given in Table 1 above. The minimum first wall thicknesses are larger than desired (≈ 5 mm instead of ≈ 1 mm), primarily because of the possibility of extensive sub-crater fracturing. A 2 mm thickness might work because of the low probability of a second impact at the same location.

The worst case impact appears to be 150 μm steel shrapnel particles impacting at about 400 m/s. Therefore, initial "certification testing" should focus on producing these conditions.

Since these estimated first wall thicknesses are on the borderline of being practical, impact testing should be done soon to resolve the issue.

References

1. F. Hoerz, M. Cintala, R. P. Bernhard, F. Cardenas, W. Davidson, G. Haynes, T. H. See, and J. Winkler, "Cratering and Penetration Experiments in Teflon Targets at Velocities from 1 to 7 km/s", NASA Technical Memorandom 104797 (July 1994).

2. F. Hoerz, M. Cintala, R. P. Bernhard, F. Cardenas, W. Davidson, G. Haynes, T. H. See, and J. Winkler, "Penetration Experiments in Aluminum 1100 Targets Using Soda-Lime Glass Projectiles", NASA Technical Memorandom 104813 (July 1995).

3. K. S. Edelstein and M. L. Fudge, "Penetration and Surface Spalling due to Hypervelocity Impact into Fused Silica", personal communication (1995).

4. K. C. Dao, D. A. Shockey, L. Seaman, D. R. Curran, and D. J. Rowcliffe, "Particle Impact Damage in Silicon Nitride", SRI International Annual Report to the Office of Naval Research, Contract No. N000114-76-0657 (May 1979).

5. D. R. Curran,, D. A. Shockey, L. Seaman, and M. Austin, "Mechanisms and Models of Cratering in Earth Media, in Proc. of Symp. on Planetary Cratering Mechanics - Impact and Explosion Cratering, eds. D. J. Roddy, R. O. Pepin, R. B. Merrill (Pergamon Press, 1977).

6. D. R. Curran, J. B. Antoun, and T. Cooper, "Cratering in Porous Carbonate Rock", unpublished.

SHRAPNEL AND DEBRIS GENERATION IN NIF CHAMBER FROM CRYO TUBES AND HOHLRAUM

R. E. Tokheim and D. R. Curran
SRI INTERNATIONAL

Presented at Oak Ridge, 5-6 December 1995

OUTLINE

- NO-YIELD HOHLRAUM DEBRIS COMPUTATIONS
- COMPUTATIONS OF SHRAPNEL/DEBRIS FROM NEUTRON DEPOSITION IN CRYO TUBES
- PROJECTION OF SHRAPNEL/DEBRIS TO FIRST WALL
- CONCLUSIONS

NO-YIELD HOHLRAUM DEBRIS COMPUTATIONS

- 1.8 MJ with shine shields
- 1.0 MJ with shine shields

Configuration for Hohlraum with Shine Shields:

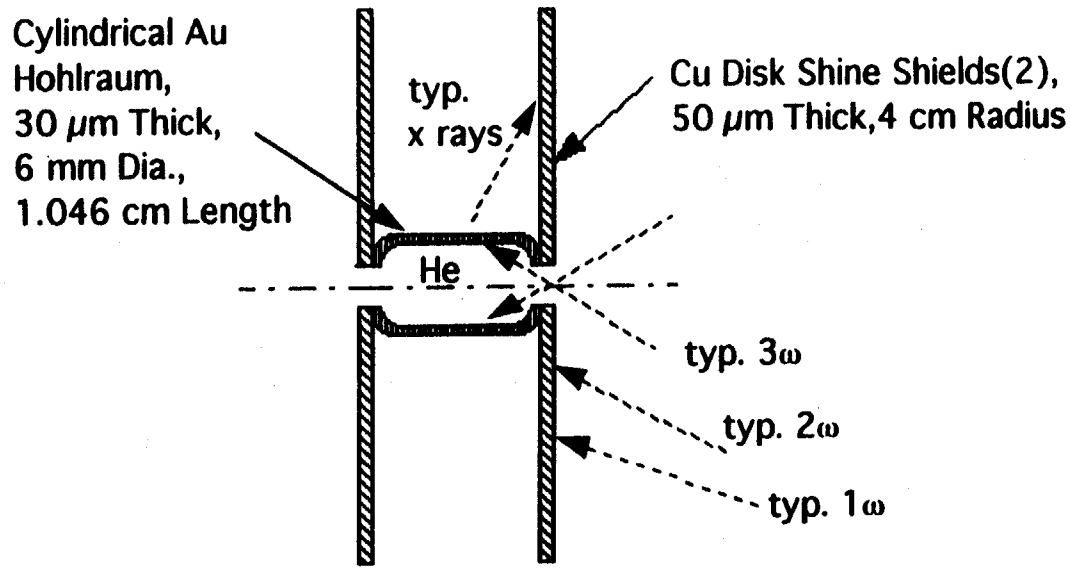

Approach:

- LLNL computations of $1\omega/2\omega$ intensity onto Cu shine shields
- Plot of typical intensity variation on shine shields
- Use of HYADES runs at certain locations for initialization of shine-shield L2D computations
- Modified use of previous L2D Au hohlraum computations
- Energy deposition of mixed-blackbody x rays through hohlraum to inside of shine shields during L2D run

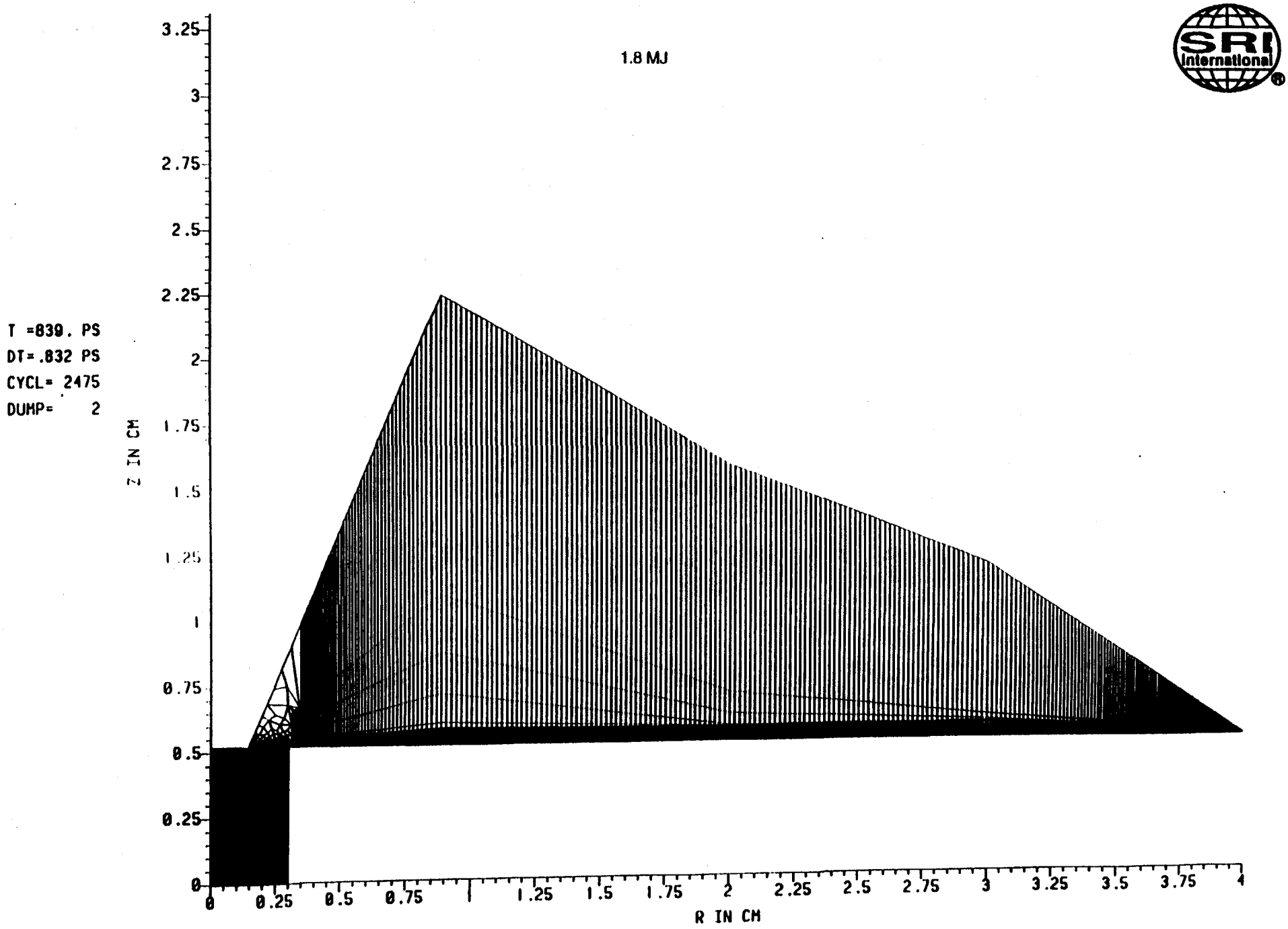

002

I 2 D

15-Sep-95 20:50:50 mod 9/8/95.ROUNDED CORNERS.NIF WITH SHIELD

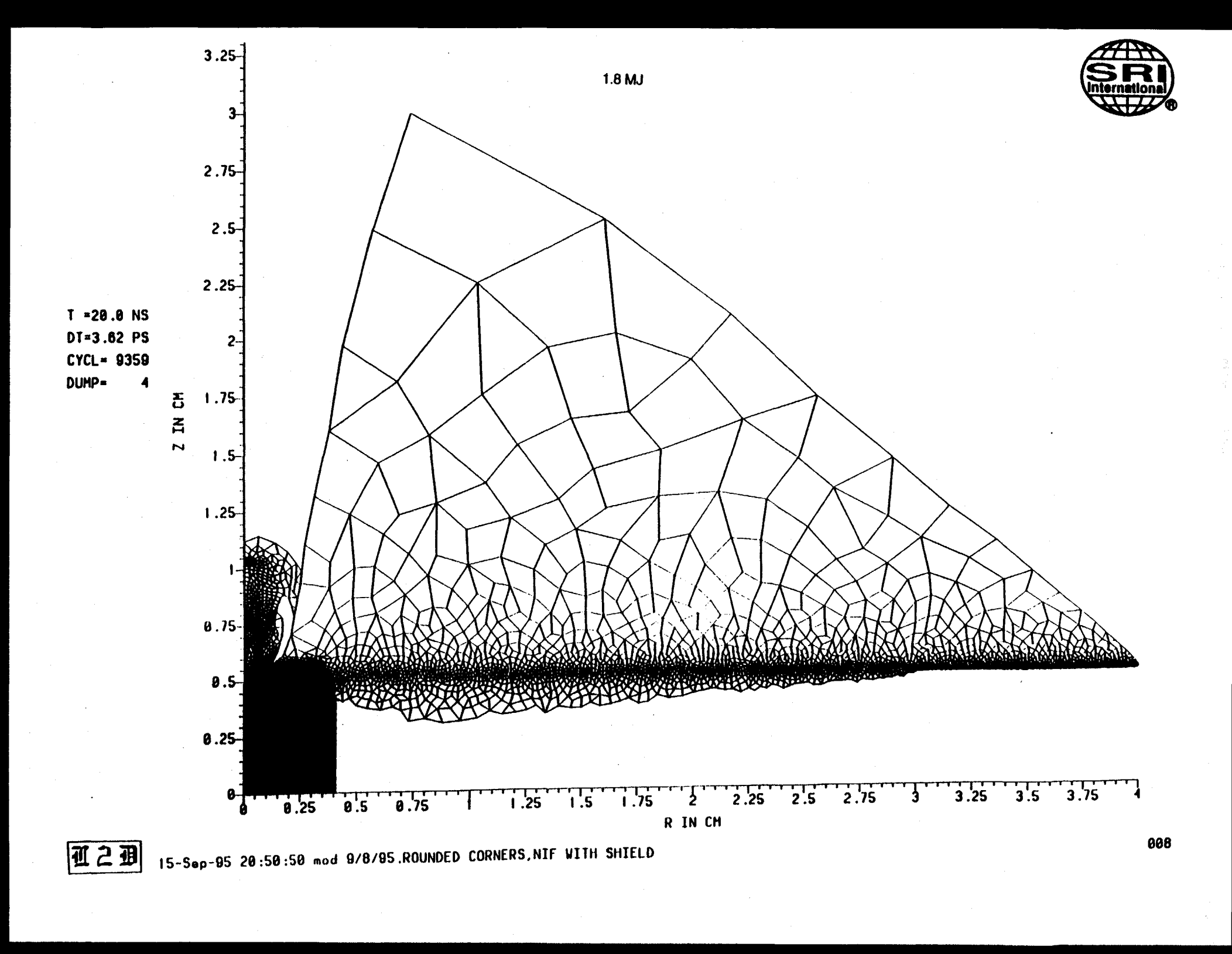
1.8 MJ
T =20.0 NS
DT=3.62 PS
CYCL= 9359
DUMP= 4
Z IN CM
R IN CM
3.25
3
2.75
2.5
2.25
2
1.75
1.5
1.25
1
0.75
0.5
0.25
0
0.25
0.5
0.75
1.25
1.5
1.75
2
2.25
2.5
2.75
3
3.25
3.5
3.75
4
SRI International
I 2 D
15-Sep-95 20:50:50 mod 9/8/95.ROUNDED CORNERS,NIF WITH SHIELD
008

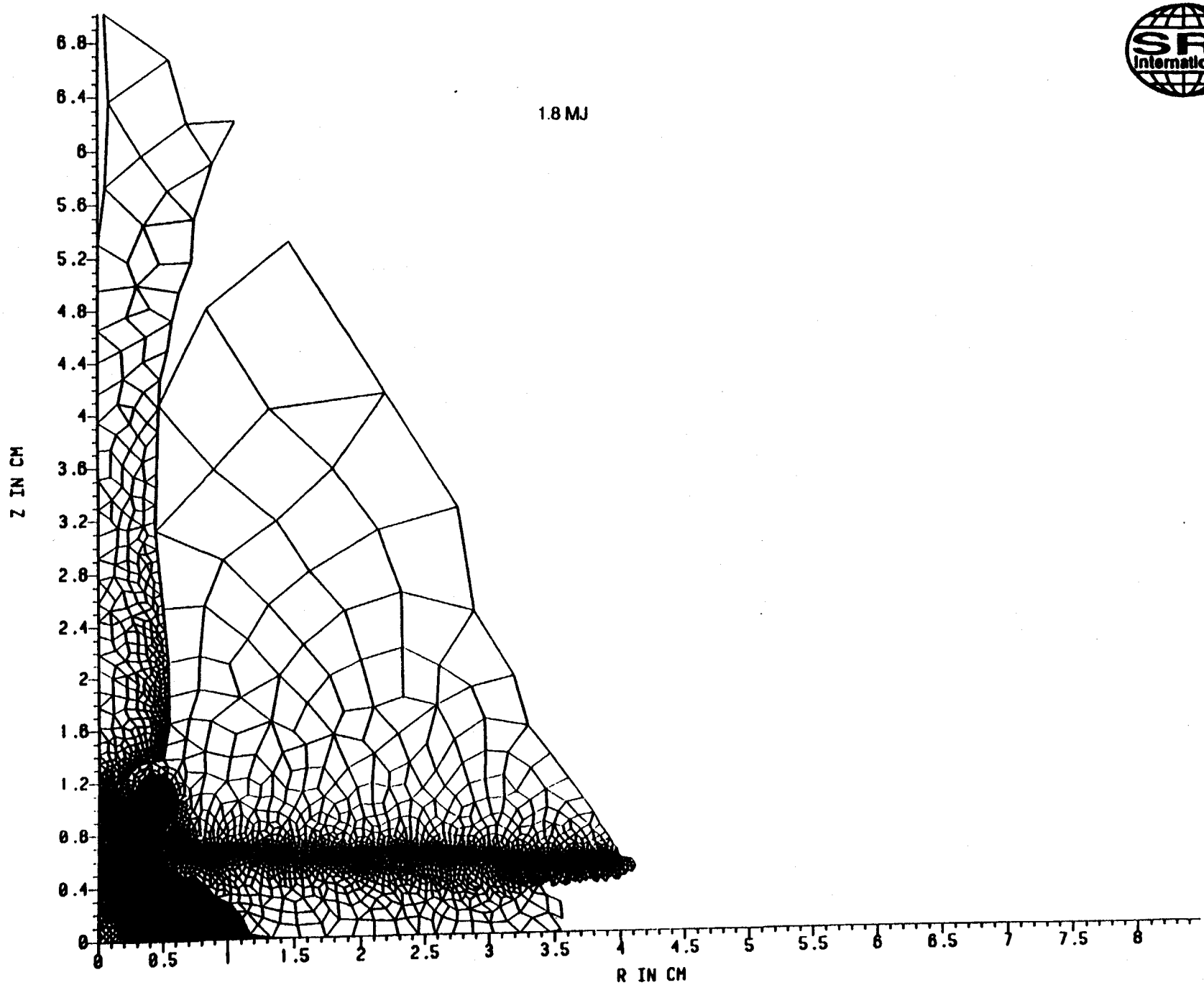

I 2 D 15-Sep-95 20:50:50 mod 9/8/95.ROUNDED CORNERS,NIF WITH SHIELD

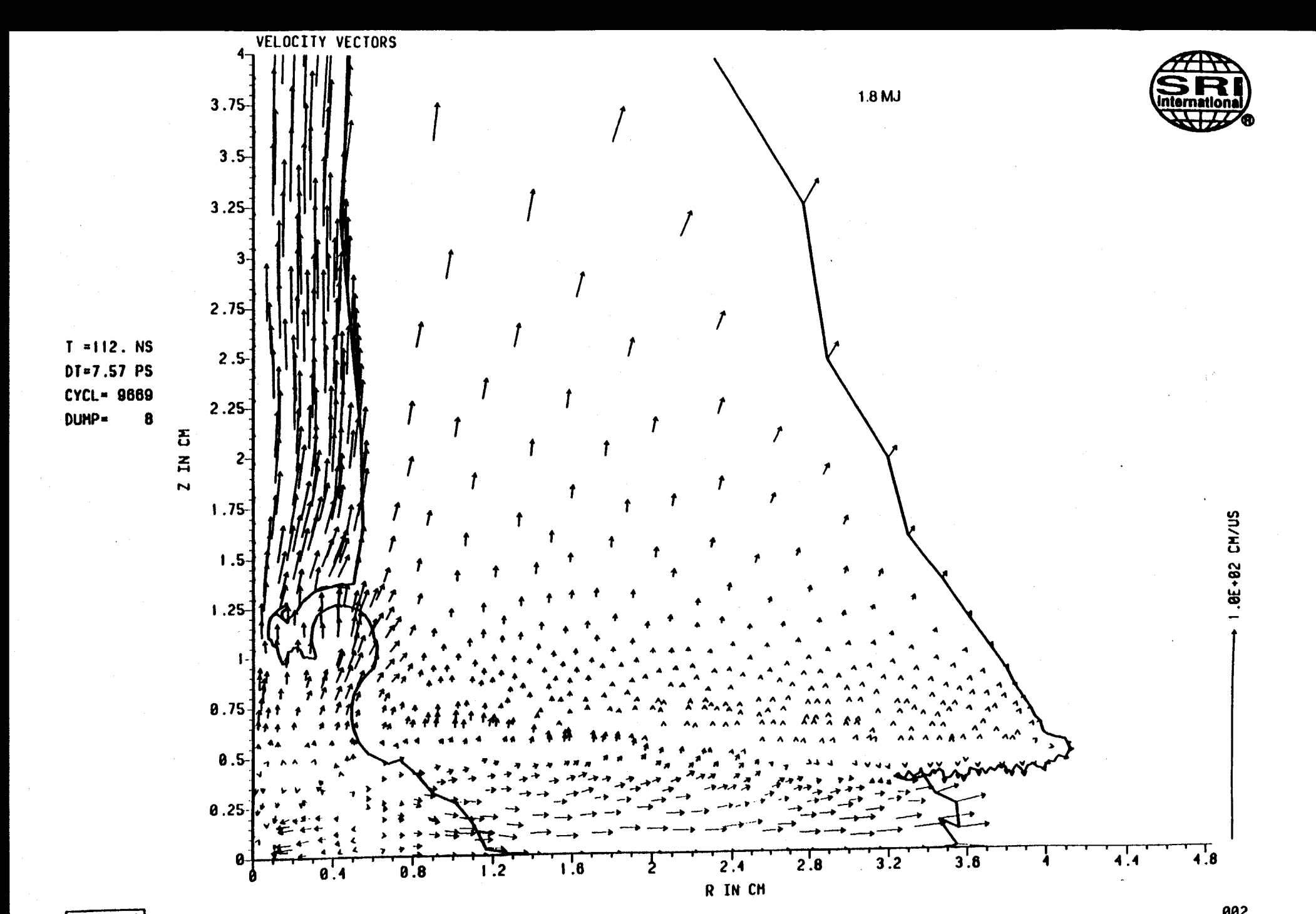

SRI International

M 2 B

15-Sep-95 20:50:50 mod 9/8/95.ROUNDED CORNERS,NIF WITH SHIELD

002

1.8 MJ

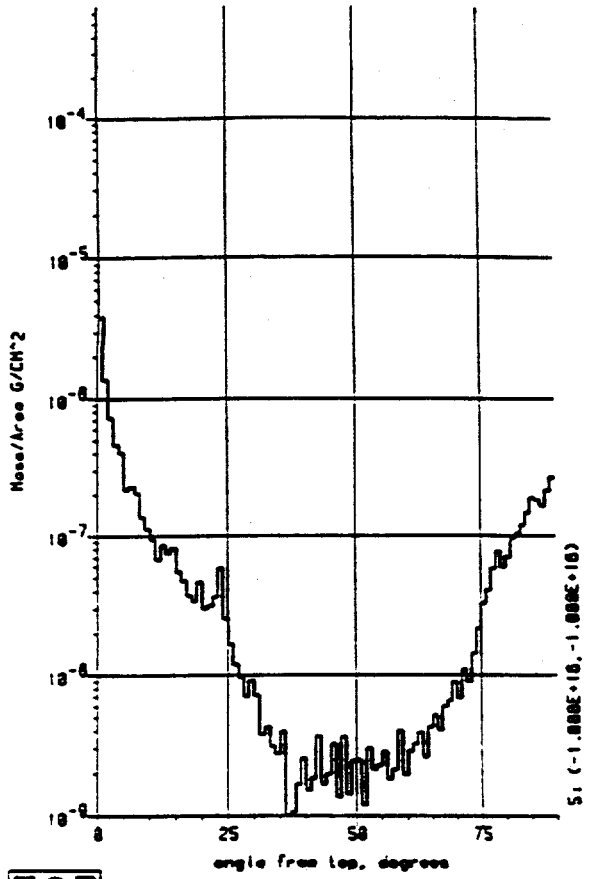

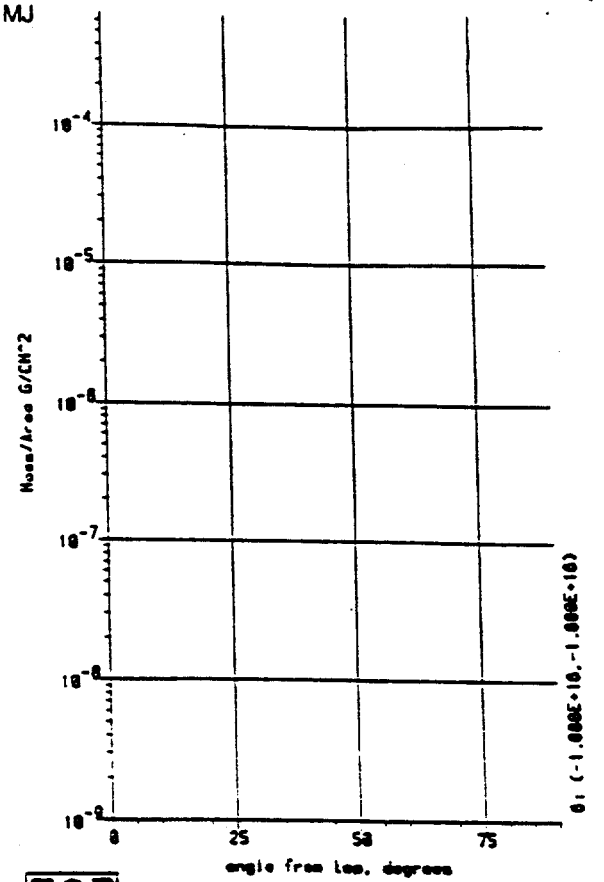

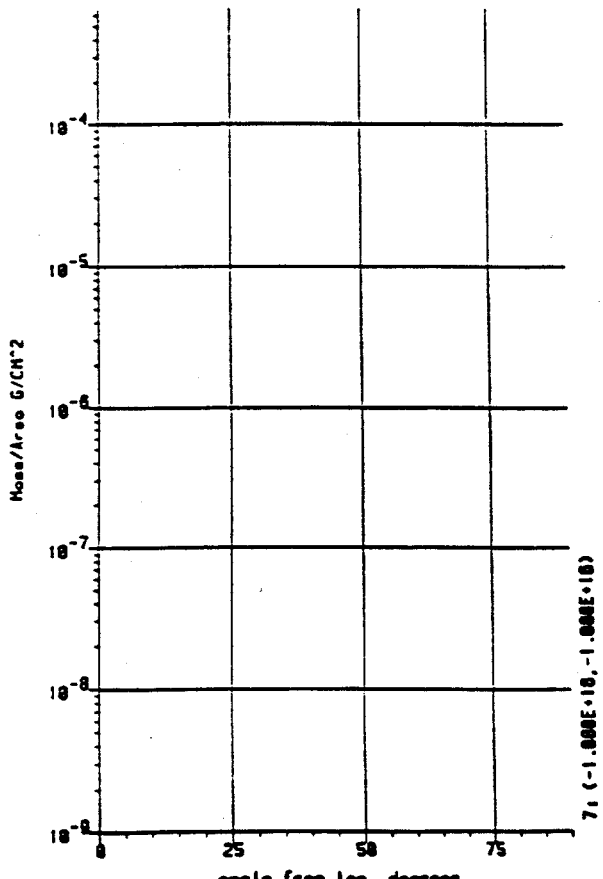

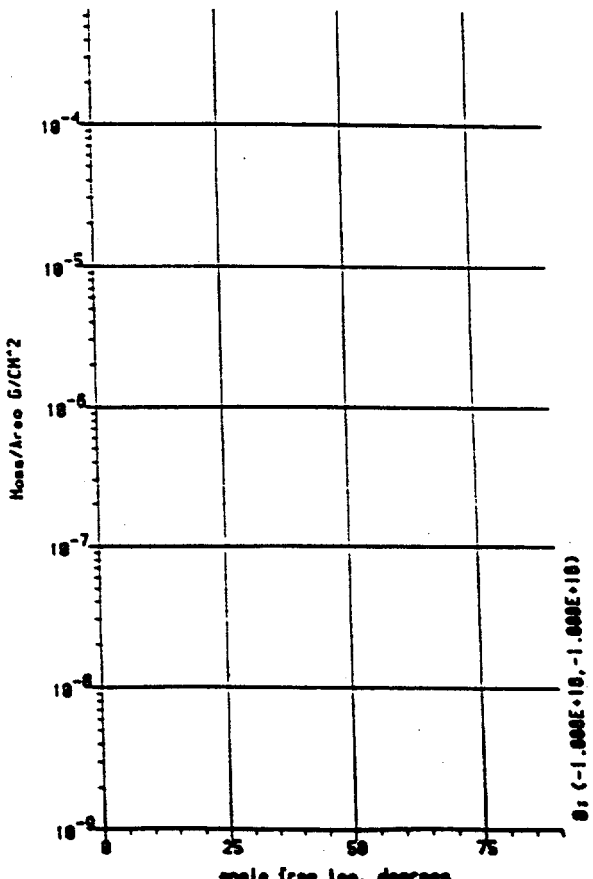

885 ..... at 112 ns on 500 cm, ionized GOLD

886 ..... at 112 ns on 500 cm, solid CU

887 ..... at 112 ns on 500 cm, melted CU

888 ..... at 112 ns on 500 cm, vaporized CU

1.8 MJ

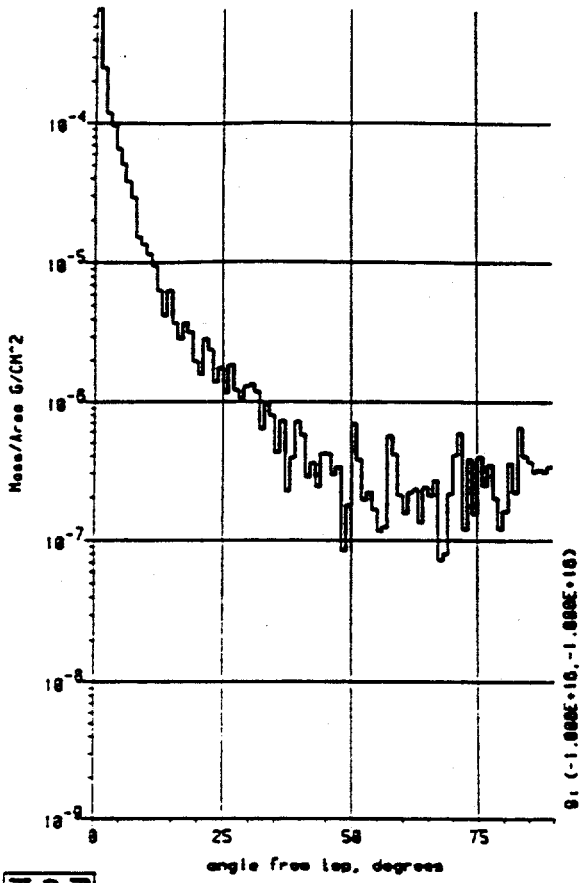

道 之 道 ..... at 112 ns on 500 cm. ionized CU 888

1 MJ

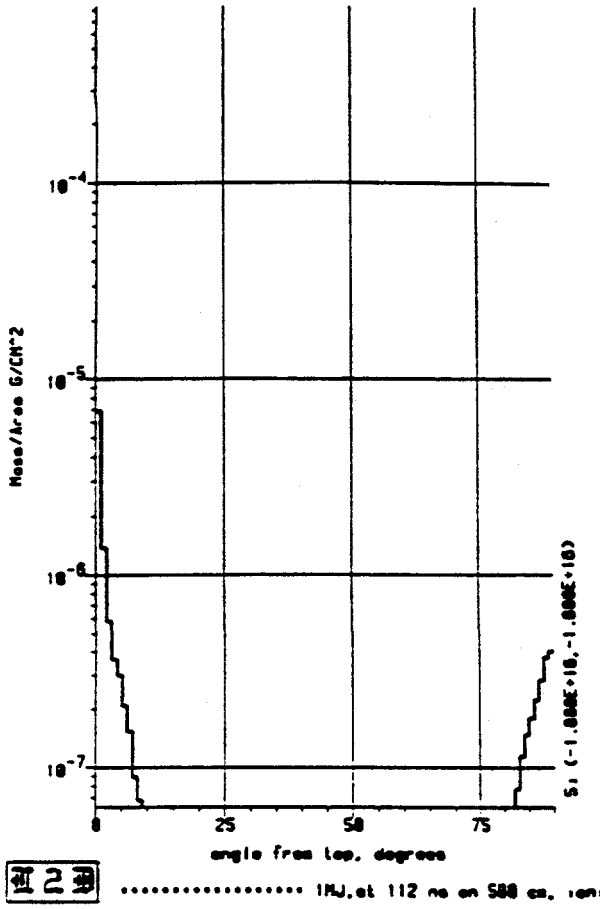

図2(a) ..... 1MJ,at 112 ns on 500 cm, ionized CO 005

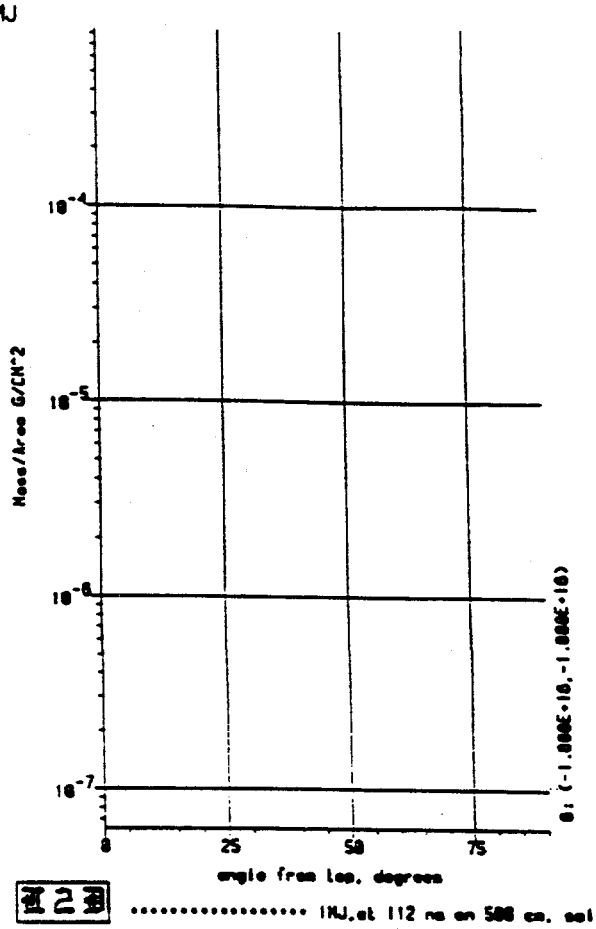

図2(a) ..... 1MJ,at 112 ns on 500 cm, solid CU

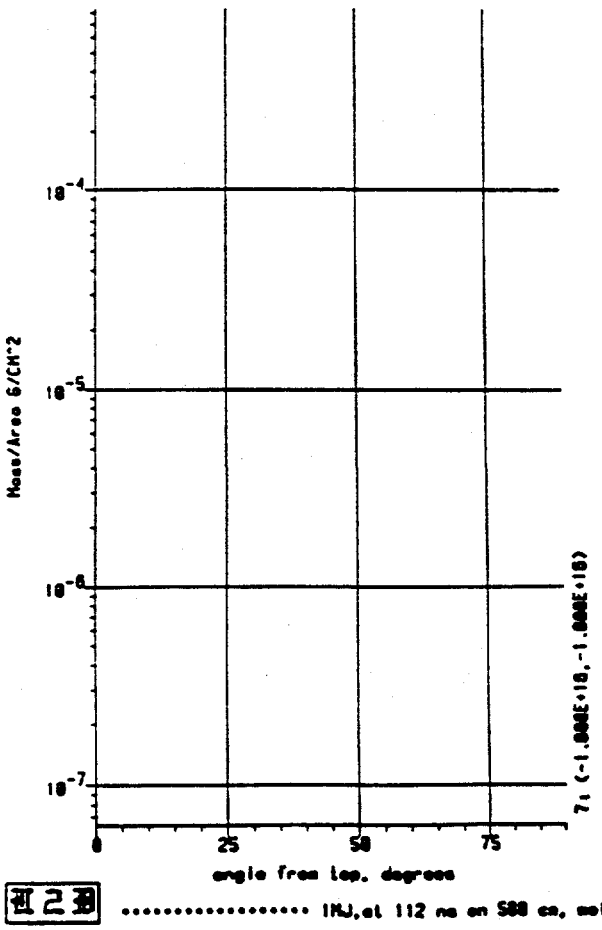

図2(a) ..... 1MJ,at 112 ns on 500 cm, melted CU 007

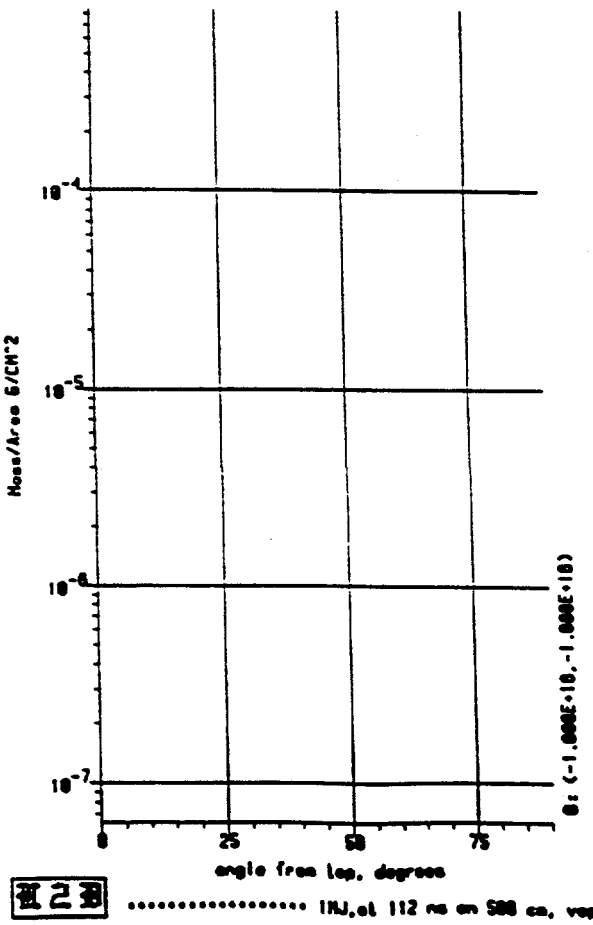

図2(a) ..... 1MJ,at 112 ns on 500 cm, vaporized

1 MJ

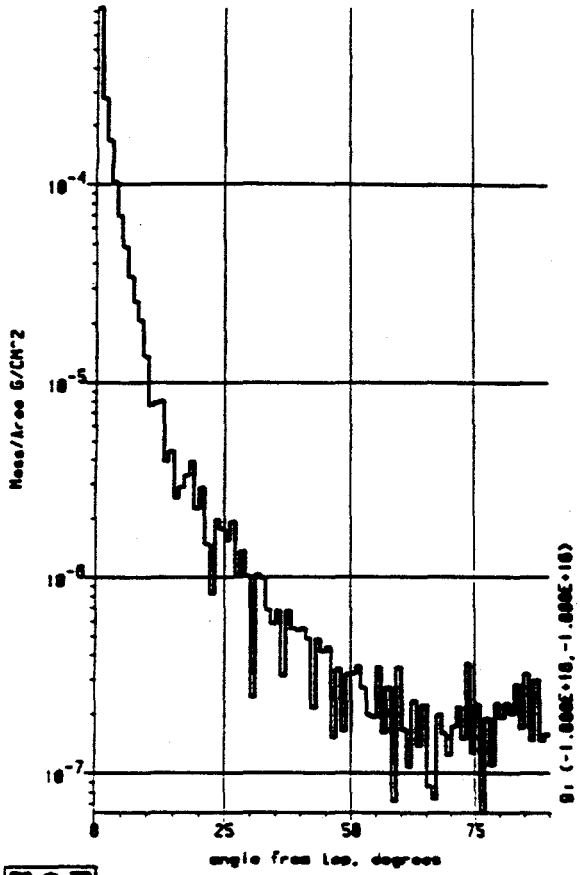

図2(3)

..... 1MJ,at 112 ns on 500 cm, ionized CU 000

COMPUTATIONS OF SHRAPNEL/DEBRIS FROM NEUTRON DEPOSITION IN CRYO TUBES

- Focus on 20 MJ yield case (16 MJ neutrons)

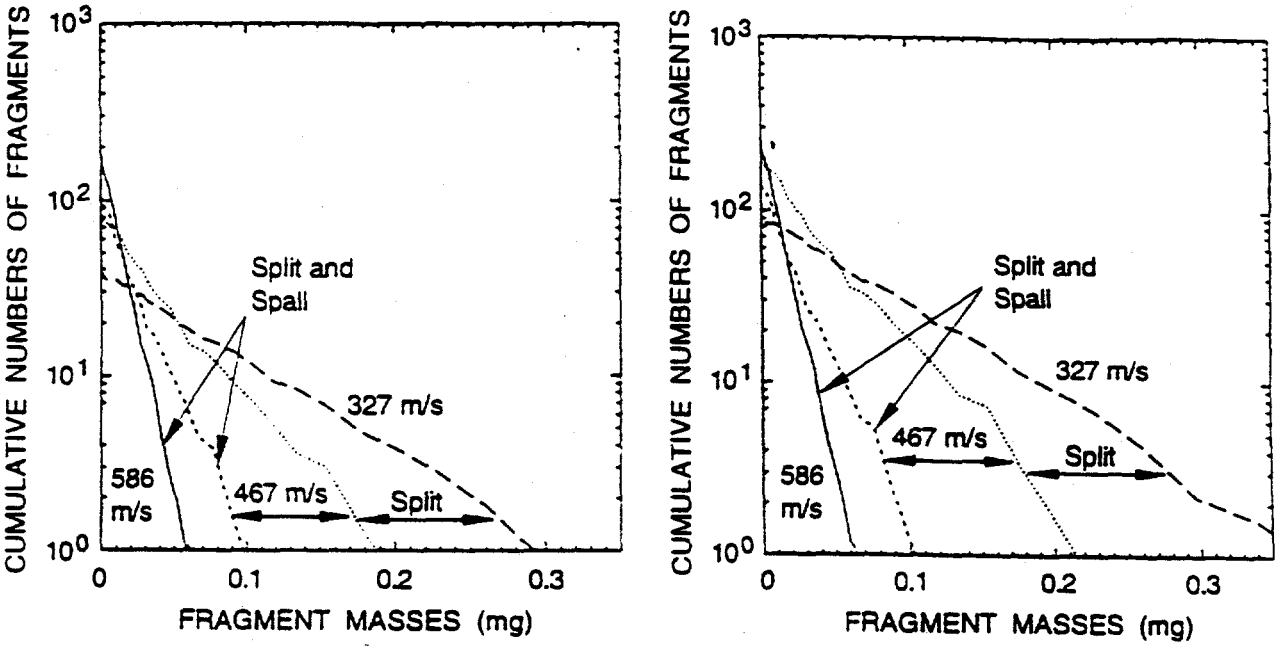

(a) 4 MJ of neutron energy

(b) 16 MJ of neutron energy

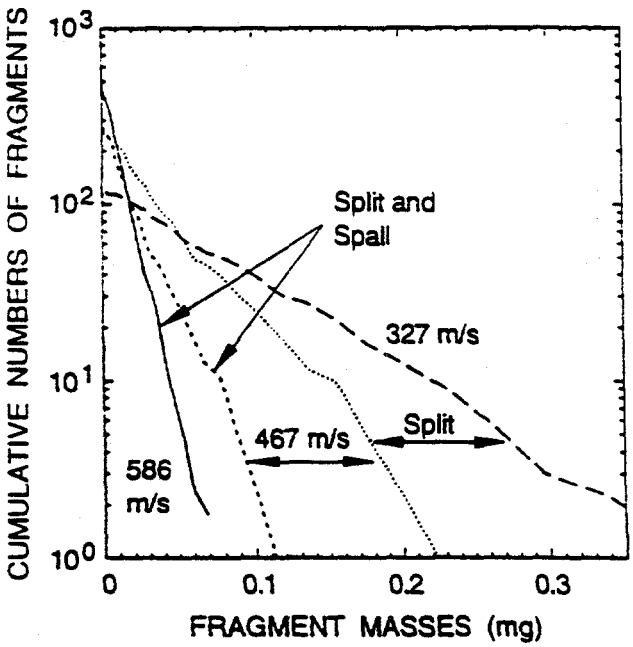

(c) 36 MJ of neutron energy

CAM-2802-44

Figure 4-2. Fragment sizes of stainless steel tubes.
(Fragment velocities of 327, 467, and 586 m/s.)

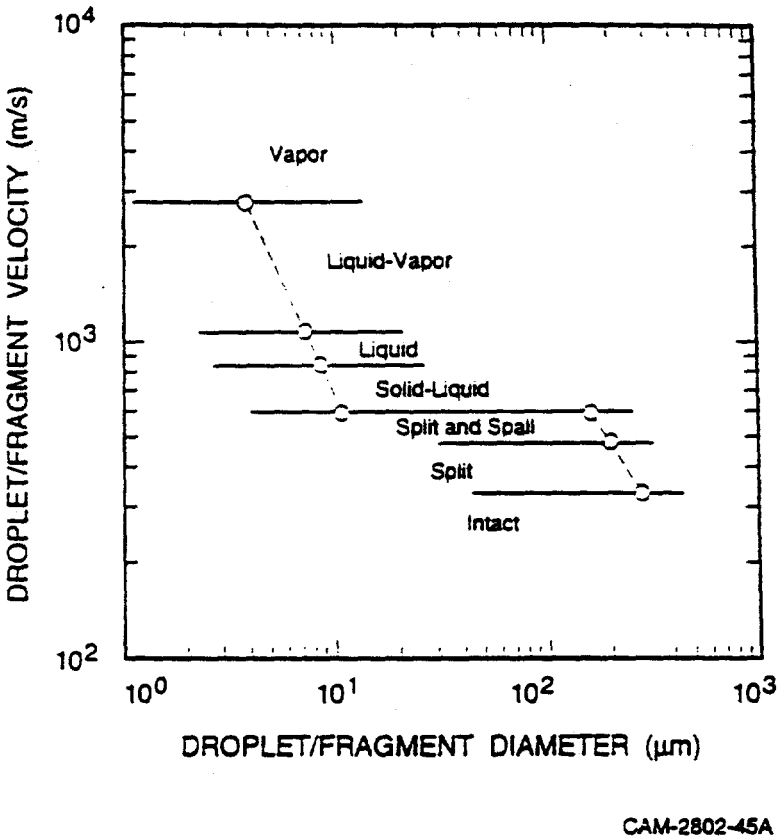

Figure 4-3. Velocity of droplets from stainless steel tubes.

11/21/95							
Shrapnel per stainless steel tube for 16 MJ neutron energy deposition							
Energy	Frac.Condit.	Dist.(cm)	Vel	M1	R1	Vol/tube	No/tube
(cal/g)	Abv Energy		(m/s)	(mg)	(cm)	(cm3)	
400	Intact	3.2	327				
	Split	2.6	397	8.337E-02	1.355E-02	1.149E-04	1.102E+01
700	Split	2	467	4.424E-02	1.097E-02	1.149E-04	2.077E+01
	Split/Spall	1.8	526.5	2.170E-02	8.652E-03	3.829E-05	1.411E+01
1040	Split/Spall	1.6	586	1.110E-02	6.919E-03	3.829E-05	2.760E+01
	Melt	1.375	717.5	5.575E-06	5.500E-04	4.307E-05	6.181E+04
1650	Melt	1.15	849	2.884E-06	4.415E-04	4.307E-05	1.195E+05
	Liquid	1	953.5	2.145E-06	4.000E-04	2.872E-05	1.071E+05
2305	Liquid	0.85	1058	1.796E-06	3.770E-04	2.872E-05	1.279E+05
	Liq/Vapor	0.425	1679	9.048E-07	3.000E-04	8.136E-05	7.194E+05
7000	Liq/Vapor	0	2300	3.802E-07	2.247E-04	8.136E-05	1.712E+06

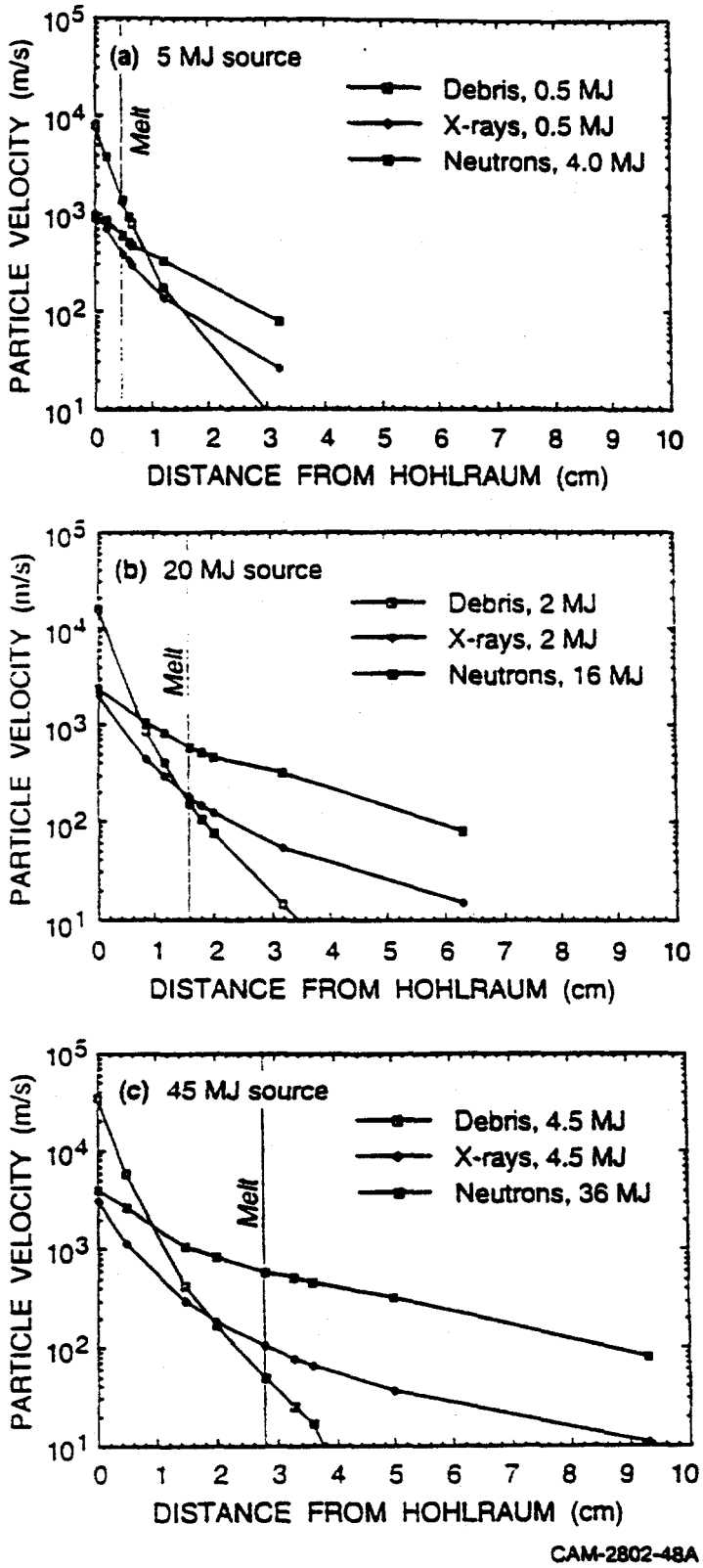

Figure 4-13. Particle velocities in stainless steel tubes.

PROJECTION OF SHRAPNEL/DEBRIS TO FIRST WALL

- Focus on 20 MJ yield case (16 MJ neutrons)

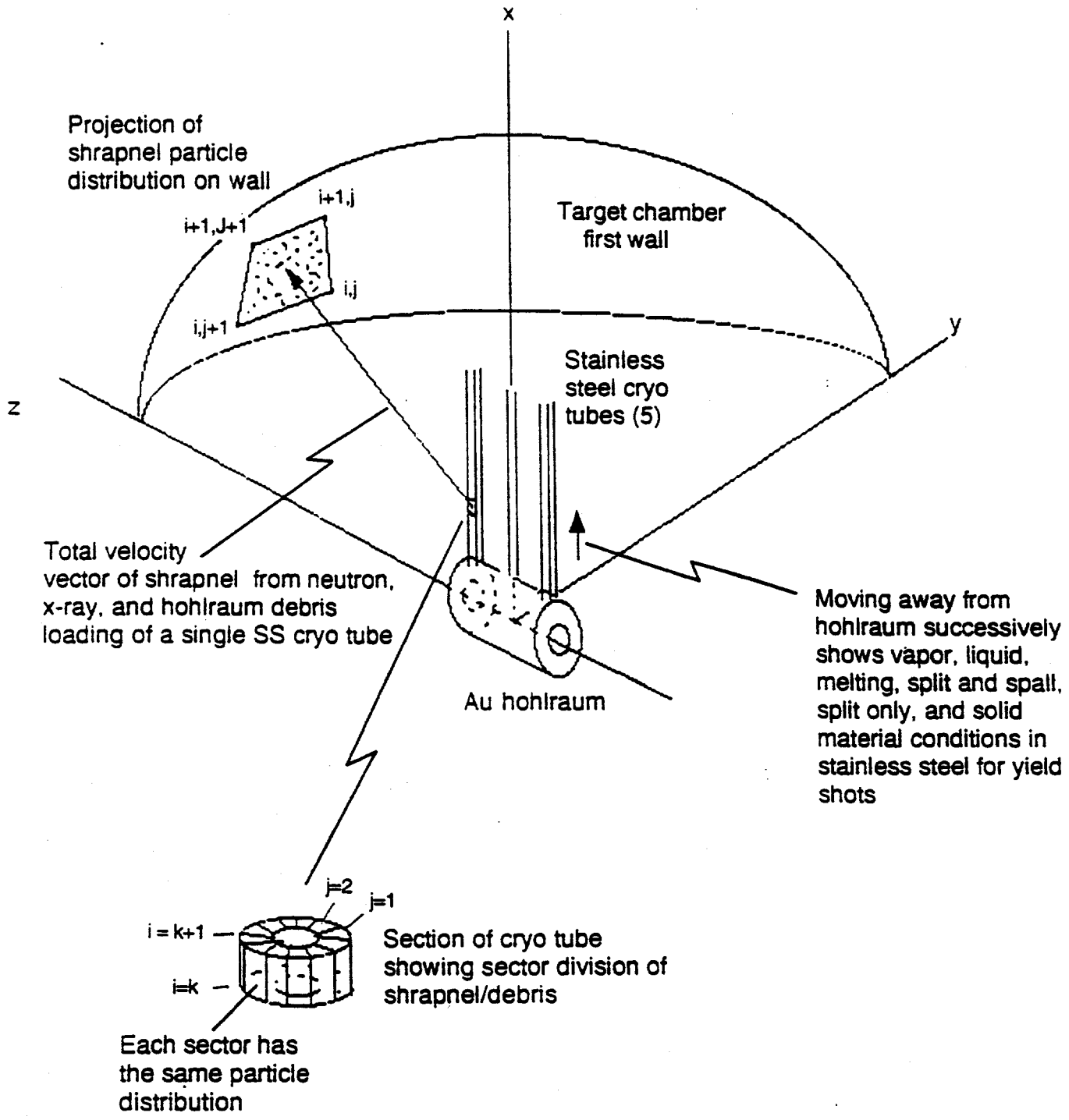

Figure1. Configuration for NIF yield shot showing treatment of cryogenic tube break-up and shrapnel/debris projection onto target chamber first wall

For 10 Sectors

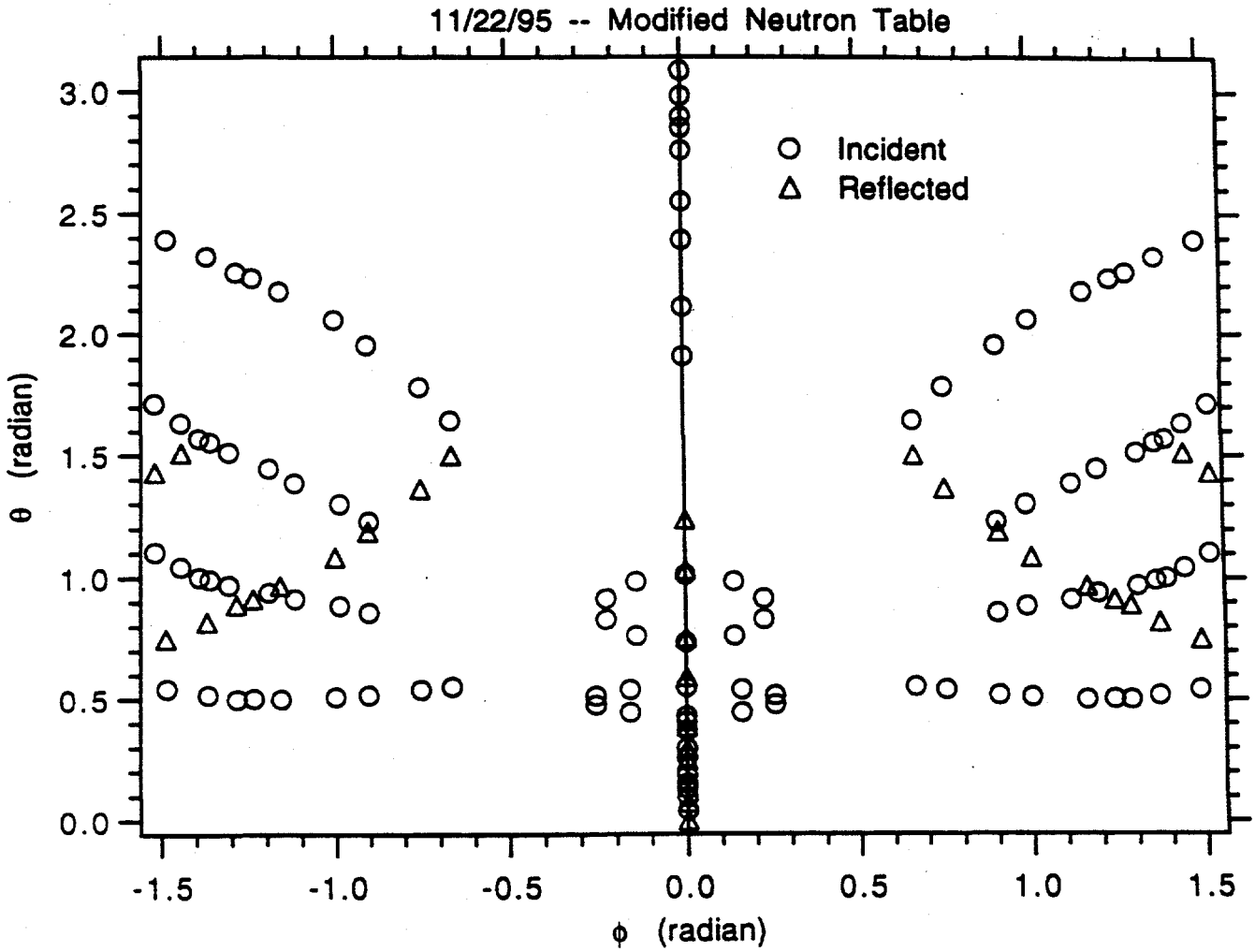

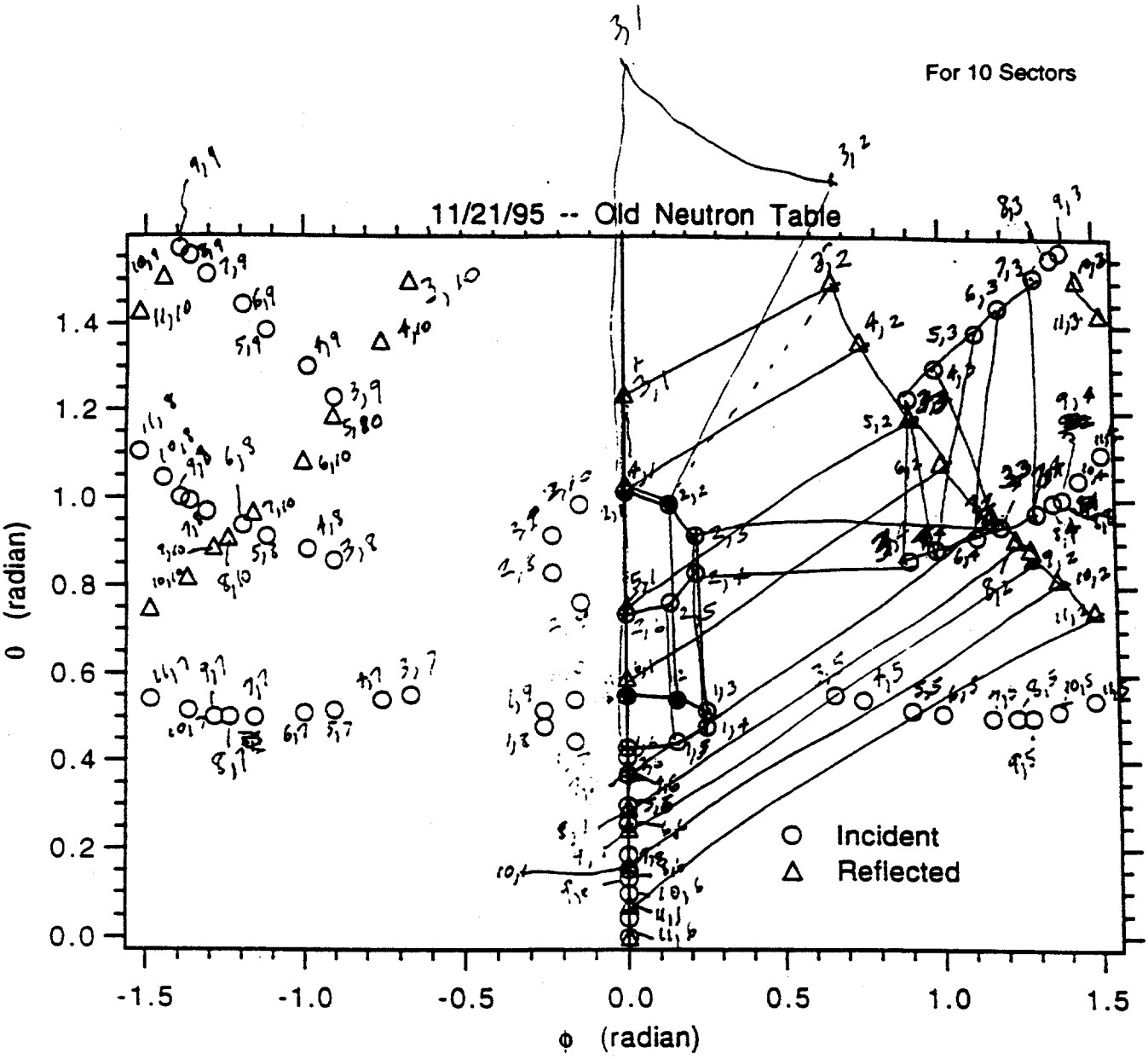
For 10 Sectors
11/21/95 -- Old Neutron Table
θ (radian)
φ (radian)
1.4
1.2
1.0
0.8
0.6
0.4
0.2
0.0
-1.5
-1.0
-0.5
0.0
0.5
1.0
1.5
Incident
Reflected

test

i	j	phi	theta	massdens1	nopart1	mompart1	area
1	1	0.000E+00	5.490E-01	0.000E+00	0.000E+00	0.000E+00	1.124E+04
1	2	1.596E-01	5.407E-01	0.000E+00	0.000E+00	0.000E+00	6.026E+03
1	3	2.548E-01	5.154E-01	0.000E+00	0.000E+00	0.000E+00	1.228E+03
1	4	2.548E-01	4.783E-01	0.000E+00	0.000E+00	0.000E+00	4.500E+03
1	5	1.596E-01	4.438E-01	0.000E+00	0.000E+00	0.000E+00	6.342E+03
1	6	9.831E-10	4.296E-01	0.000E+00	0.000E+00	0.000E+00	6.341E+03
1	7	-1.596E-01	4.438E-01	0.000E+00	0.000E+00	0.000E+00	4.473E+03
1	8	-2.548E-01	4.783E-01	0.000E+00	0.000E+00	0.000E+00	9.504E+02
1	9	-2.548E-01	5.154E-01	0.000E+00	0.000E+00	0.000E+00	5.987E+03
1	10	-1.596E-01	5.407E-01	0.000E+00	0.000E+00	0.000E+00	1.124E+04
2	1	0.000E+00	1.012E+00	0.000E+00	0.000E+00	0.000E+00	7.868E+04
2	2	1.402E-01	9.845E-01	0.000E+00	0.000E+00	0.000E+00	4.842E+04
2	3	2.245E-01	9.140E-01	0.000E+00	0.000E+00	0.000E+00	2.908E+04
2	4	2.244E-01	8.294E-01	0.000E+00	0.000E+00	0.000E+00	2.064E+04
2	5	1.401E-01	7.616E-01	0.000E+00	0.000E+00	0.000E+00	1.746E+04
2	6	8.615E-10	7.356E-01	0.000E+00	0.000E+00	0.000E+00	1.746E+04
2	7	-1.401E-01	7.616E-01	0.000E+00	0.000E+00	0.000E+00	2.061E+04
2	8	-2.244E-01	8.294E-01	0.000E+00	0.000E+00	0.000E+00	2.906E+04
2	9	-2.245E-01	9.140E-01	0.000E+00	0.000E+00	0.000E+00	4.842E+04
2	10	-1.402E-01	9.845E-01	0.000E+00	0.000E+00	0.000E+00	7.868E+04
3	1	0.000E+00	1.906E+00	1.424E-09	2.558E+04	1.517E-04	3.227E+04
3	2	6.646E-01	1.644E+00	2.961E-09	2.558E+04	1.944E-04	1.552E+04
3	3	9.024E-01	1.229E+00	0.000E+00	0.000E+00	0.000E+00	7.247E+03
3	4	9.019E-01	8.576E-01	0.000E+00	0.000E+00	0.000E+00	4.395E+03
3	5	6.633E-01	5.523E-01	0.000E+00	0.000E+00	0.000E+00	3.440E+03
3	6	4.771E-09	4.081E-01	0.000E+00	0.000E+00	0.000E+00	3.440E+03
3	7	-6.633E-01	5.523E-01	0.000E+00	0.000E+00	0.000E+00	4.377E+03
3	8	-9.019E-01	8.576E-01	0.000E+00	0.000E+00	0.000E+00	7.222E+03
3	9	-9.024E-01	1.229E+00	0.000E+00	0.000E+00	0.000E+00	1.549E+04
3	10	-6.646E-01	1.644E+00	1.424E-09	2.558E+04	1.517E-04	3.227E+04
4	1	0.000E+00	2.111E+00	9.455E-10	2.142E+04	1.494E-04	4.860E+04
4	2	7.537E-01	1.782E+00	1.844E-09	2.142E+04	1.907E-04	2.492E+04
4	3	9.879E-01	1.300E+00	0.000E+00	0.000E+00	0.000E+00	1.271E+04
4	4	9.873E-01	8.838E-01	0.000E+00	0.000E+00	0.000E+00	8.308E+03
4	5	7.520E-01	5.401E-01	0.000E+00	0.000E+00	0.000E+00	6.816E+03
4	6	5.411E-09	3.688E-01	0.000E+00	0.000E+00	0.000E+00	6.815E+03
4	7	-7.520E-01	5.401E-01	0.000E+00	0.000E+00	0.000E+00	8.298E+03
4	8	-9.873E-01	8.838E-01	0.000E+00	0.000E+00	0.000E+00	1.258E+04
4	9	-9.879E-01	1.300E+00	0.000E+00	0.000E+00	0.000E+00	1.498E+04
4	10	-7.537E-01	1.782E+00	9.455E-10	2.142E+04	1.494E-04	4.859E+04
5	1	0.000E+00	2.390E+00	2.282E-09	1.390E+04	1.661E-04	3.021E+04
5	2	9.356E-01	1.954E+00	4.216E-09	1.390E+04	1.891E-04	1.597E+04
5	3	1.119E+00	1.385E+00	0.000E+00	0.000E+00	0.000E+00	9.134E+03
5	4	1.119E+00	9.130E-01	0.000E+00	0.000E+00	0.000E+00	5.285E+03
5	5	9.334E-01	5.166E-01	0.000E+00	0.000E+00	0.000E+00	4.294E+03
5	6	7.748E-09	2.980E-01	0.000E+00	0.000E+00	0.000E+00	4.294E+03
5	7	-9.334E-01	5.166E-01	0.000E+00	0.000E+00	0.000E+00	5.279E+03
5	8	-1.119E+00	9.130E-01	0.000E+00	0.000E+00	0.000E+00	9.156E+03
5	9	-1.119E+00	1.385E+00	0.000E+00	0.000E+00	0.000E+00	1.592E+04
5	10	-9.356E-01	1.954E+00	2.282E-09	1.390E+04	1.661E-04	3.020E+04
6	1	0.000E+00	2.551E+00	1.716E-09	1.236E+04	2.655E-04	4.317E+04
6	2	1.302E+00	2.058E+00	2.901E-09	1.236E+04	3.259E-04	2.276E+04
6	3	1.194E+00	1.443E+00	0.000E+00	0.000E+00	0.000E+00	1.357E+04
6	4	1.193E+00	9.388E-01	0.000E+00	0.000E+00	0.000E+00	9.392E+03
6	5	9.991E-01	5.100E-01	0.000E+00	0.000E+00	0.000E+00	7.899E+03
6	6	9.487E-09	2.569E-01	0.000E+00	0.000E+00	0.000E+00	7.899E+03
6	7	-9.991E-01	5.100E-01	0.000E+00	0.000E+00	0.000E+00	9.384E+03
6	8	-1.193E+00	9.388E-01	0.000E+00	0.000E+00	0.000E+00	1.353E+04
6	9	-1.194E+00	1.443E+00	0.000E+00	0.000E+00	0.000E+00	2.370E+04
6	10	-1.302E+00	2.058E+00	1.716E-09	1.236E+04	2.655E-04	4.316E+04
7	1	0.000E+00	2.760E+00	3.409E-09	5.520E+00	4.552E-01	1.797E+04
7	2	1.162E+00	2.175E+00	5.409E-09	5.520E+00	5.437E-01	1.133E+04
7	3	1.308E+00	1.512E+00	0.000E+00	0.000E+00	0.000E+00	6.687E+03
7	4	1.308E+00	9.690E-01	0.000E+00	0.000E+00	0.000E+00	4.634E+03
7	5	1.159E+00	4.991E-01	0.000E+00	0.000E+00	0.000E+00	3.877E+03
7	6	1.397E-08	1.858E-01	0.000E+00	0.000E+00	0.000E+00	3.977E+03
7	7	-1.159E+00	4.991E-01	0.000E+00	0.000E+00	0.000E+00	4.628E+03
7	8	-1.308E+00	9.690E-01	0.000E+00	0.000E+00	0.000E+00	6.663E+03
7	9	-1.308E+00	1.512E+00	0.000E+00	0.000E+00	0.000E+00	1.129E+04
7	10	-1.162E+00	2.175E+00	3.410E-09	5.520E+00	4.552E-01	1.797E+04
8	1	0.000E+00	2.852E+00	6.686E-09	2.822E+00	8.059E-01	9.159E+03
8	2	1.240E+00	2.232E+00	9.981E-09	2.822E+00	9.470E-01	6.198E+03
8	3	1.361E+00	1.554E+00	0.000E+00	0.000E+00	0.000E+00	3.965E+03
8	4	1.360E+00	9.925E-01	0.000E+00	0.000E+00	0.000E+00	2.909E+03
8	5	1.237E+00	5.014E-01	0.000E+00	0.000E+00	0.000E+00	2.505E+03
8	6	1.760E-08	1.527E-01	0.000E+00	0.000E+00	0.000E+00	2.505E+03
8	7	-1.237E+00	5.014E-01	0.000E+00	0.000E+00	0.000E+00	2.909E+03
8	8	-1.360E+00	9.925E-01	0.000E+00	0.000E+00	0.000E+00	3.963E+03
8	9	-1.361E+00	1.554E+00	0.000E+00	0.000E+00	0.000E+00	6.194E+03
8	10	-1.240E+00	2.232E+00	6.686E-09	2.822E+00	8.059E-01	9.159E+03
9	1	0.000E+00	2.899E+00	1.112E-08	4.154E+00	1.470E+00	1.652E+04
9	2	1.287E+00	2.255E+00	1.575E-08	4.154E+00	1.689E+00	1.167E+04
9	3	1.392E+00	1.569E+00	0.000E+00	0.000E+00	0.000E+00	7.389E+03
9	4	1.391E+00	1.001E+00	0.000E+00	0.000E+00	0.000E+00	5.139E+03
9	5	1.284E+00	5.008E-01	0.000E+00	0.000E+00	0.000E+00	4.242E+03
9	6	2.066E-08	1.318E-01	0.000E+00	0.000E+00	0.000E+00	4.241E+03
9	7	-1.284E+00	5.008E-01	0.000E+00	0.000E+00	0.000E+00	5.107E+03
9	8	-1.391E+00	1.001E+00	0.000E+00	0.000E+00	0.000E+00	7.269E+03
9	9	-1.392E+00	1.569E+00	0.000E+00	0.000E+00	0.000E+00	1.150E+04
9	10	-1.287E+00	2.255E+00	1.114E-08	4.154E+00	1.470E+00	1.650E+04
10	1	0.000E+00	2.984E+00	1.906E-08	2.204E+00	2.468E+00	1.927E+04
10	2	1.370E+00	2.323E+00	1.249E-08	2.204E+00	2.722E+00	1.472E+04
10	3	1.445E+00	1.635E+00	1.704E-08	2.204E+00	3.093E+00	1.078E+04
10	4	1.444E+00	1.045E+00	0.000E+00	0.000E+00	0.000E+00	8.253E+03
10	5	1.366E+00	5.166E-01	0.000E+00	0.000E+00	0.000E+00	7.135E+03
10	6	2.934E-08	9.776E-02	0.000E+00	0.000E+00	0.000E+00	7.133E+03
10	7	-1.366E+00	5.166E-01	0.000E+00	0.000E+00	0.000E+00	8.201E+03
10	8	-1.444E+00	1.045E+00	0.000E+00	0.000E+00	0.000E+00	1.060E+04

10	9	-1.443E+00	1.635E+00	1.266E-08	2.204E+00	2.722E+00	1.451E+04
10	10	-1.370E+00	2.323E+00	1.007E-08	2.204E+00	2.468E+00	1.925E+04
11	1	0.000E+00	3.083E+00	0.000E+00	0.000E+00	0.000E+00	0.000E+00
11	2	1.488E+00	2.394E+00	0.000E+00	0.000E+00	0.000E+00	0.000E+00
11	3	1.519E+00	1.713E+00	0.000E+00	0.000E+00	0.000E+00	0.000E+00
11	4	1.519E+00	1.103E+00	0.000E+00	0.000E+00	0.000E+00	0.000E+00
11	5	1.484E+00	5.412E-01	0.000E+00	0.000E+00	0.000E+00	0.000E+00
11	6	7.030E-08	4.352E-02	0.000E+00	0.000E+00	0.000E+00	0.000E+00
11	7	-1.484E+00	5.412E-01	0.000E+00	0.000E+00	0.000E+00	0.000E+00
11	8	-1.518E+00	1.103E+00	0.000E+00	0.000E+00	0.000E+00	0.000E+00
11	9	-1.519E+00	1.713E+00	0.000E+00	0.000E+00	0.000E+00	0.000E+00
11	10	-1.488E+00	2.394E+00	0.000E+00	0.000E+00	0.000E+00	0.000E+00
i	j	phiref1	thetaref1	massdens2	nopart2	mcmpart2	area
1	1	0.000E+00	0.000E+00	1.158E-08	3.424E+05	4.683E-04	1.124E+04
1	2	0.000E+00	0.000E+00	2.160E-08	3.424E+05	4.904E-04	6.026E+03
1	3	0.000E+00	0.000E+00	1.061E-07	3.424E+05	5.244E-04	1.228E+03
1	4	0.000E+00	0.000E+00	2.893E-08	3.424E+05	5.565E-04	4.500E+03
1	5	0.000E+00	0.000E+00	2.053E-08	3.424E+05	5.756E-04	6.342E+03
1	6	0.000E+00	0.000E+00	2.053E-08	3.424E+05	5.756E-04	6.341E+03
1	7	0.000E+00	0.000E+00	2.910E-08	3.424E+05	5.565E-04	4.473E+03
1	8	0.000E+00	0.000E+00	1.370E-07	3.424E+05	5.244E-04	9.554E+02
1	9	0.000E+00	0.000E+00	2.174E-08	3.424E+05	4.904E-04	5.987E+03
1	10	0.000E+00	0.000E+00	1.158E-08	3.424E+05	4.683E-04	1.124E+04
2	1	0.000E+00	0.000E+00	1.655E-09	1.439E+05	4.194E-04	7.868E+04
2	2	0.000E+00	0.000E+00	2.689E-09	1.439E+05	4.495E-04	4.842E+04
2	3	0.000E+00	0.000E+00	4.476E-09	1.439E+05	4.932E-04	2.908E+04
2	4	0.000E+00	0.000E+00	6.309E-09	1.439E+05	5.326E-04	2.064E+04
2	5	0.000E+00	0.000E+00	7.415E-09	1.439E+05	5.554E-04	1.746E+04
2	6	0.000E+00	0.000E+00	7.456E-09	1.439E+05	5.554E-04	1.746E+04
2	7	0.000E+00	0.000E+00	6.319E-09	1.439E+05	5.326E-04	2.061E+04
2	8	0.000E+00	0.000E+00	4.480E-09	1.439E+05	4.932E-04	2.906E+04
2	9	0.000E+00	0.000E+00	2.689E-09	1.439E+05	4.495E-04	4.842E+04
2	10	0.000E+00	0.000E+00	1.655E-09	1.439E+05	4.194E-04	7.868E+04
3	1	0.000E+00	1.237E+00	0.000E+00	0.000E+00	0.000E+00	3.227E+04
3	2	6.646E-01	1.499E+00	0.000E+00	0.000E+00	0.000E+00	1.552E+04
3	3	0.000E+00	0.000E+00	6.239E-09	2.558E+04	2.505E-04	7.247E+03
3	4	0.000E+00	0.000E+00	1.048E-08	2.558E+04	2.968E-04	4.385E+03
3	5	0.000E+00	0.000E+00	1.336E-08	2.558E+04	3.222E-04	3.440E+03
3	6	0.000E+00	0.000E+00	1.336E-08	2.558E+04	3.222E-04	3.440E+03
3	7	0.000E+00	0.000E+00	1.050E-08	2.558E+04	2.968E-04	4.377E+03
3	8	0.000E+00	0.000E+00	6.261E-09	2.558E+04	2.505E-04	7.212E+03
3	9	0.000E+00	0.000E+00	2.966E-09	2.558E+04	1.944E-04	1.549E-04
3	10	-6.646E-01	1.499E+00	0.000E+00	0.000E+00	0.000E+00	1.227E+04
4	1	0.000E+00	1.032E+00	0.000E+00	0.000E+00	0.000E+00	4.960E+04
4	2	7.537E-01	1.361E+00	0.000E+00	0.000E+00	0.000E+00	2.492E+04
4	3	0.000E+00	0.000E+00	6.514E-09	2.142E+04	2.453E-04	1.171E-04
4	4	0.000E+00	0.000E+00	1.031E-08	2.142E+04	2.902E-04	8.358E+03
4	5	0.000E+00	0.000E+00	1.241E-08	2.142E+04	3.149E-04	6.816E+03
4	6	0.000E+00	0.000E+00	1.241E-08	2.142E+04	3.149E-04	6.815E+03
4	7	0.000E+00	0.000E+00	1.037E-08	2.142E+04	2.902E-04	8.299E+03
4	8	0.000E+00	0.000E+00	6.623E-09	2.142E+04	2.453E-04	1.169E+04
4	9	0.000E+00	0.000E+00	1.847E-09	2.142E+04	1.907E-04	2.488E+04
4	10	-7.537E-01	1.361E+00	0.000E+00	0.000E+00	0.000E+00	4.959E+04
5	1	0.000E+00	7.535E-01	0.000E+00	0.000E+00	0.000E+00	3.221E+04
5	2	9.256E-01	1.188E+00	0.000E+00	0.000E+00	0.000E+00	1.597E+04
5	3	0.000E+00	0.000E+00	9.422E-09	2.390E+04	2.662E-04	9.184E+03
5	4	0.000E+00	0.000E+00	1.304E-08	2.390E+04	3.137E-04	5.295E+03
5	5	0.000E+00	0.000E+00	1.605E-08	2.390E+04	3.398E-04	4.294E+03
5	6	0.000E+00	0.000E+00	1.605E-08	2.390E+04	3.398E-04	4.294E+03
5	7	0.000E+00	0.000E+00	1.306E-08	2.390E+04	3.137E-04	5.278E+03
5	8	0.000E+00	0.000E+00	8.451E-09	2.390E+04	2.662E-04	9.156E+03
5	9	0.000E+00	0.000E+00	4.329E-09	2.390E+04	2.091E-04	1.592E+04
5	10	-9.256E-01	1.188E+00	0.000E+00	0.000E+00	0.000E+00	3.220E+04
6	1	0.000E+00	5.924E-01	0.000E+00	0.000E+00	0.000E+00	4.017E+04
6	2	1.002E+00	1.085E+00	0.000E+00	0.000E+00	0.000E+00	2.376E+04
6	3	0.000E+00	0.000E+00	5.280E-09	1.236E+04	4.076E-04	1.357E+04
6	4	0.000E+00	0.000E+00	7.338E-09	1.236E+04	4.763E-04	9.392E+03
6	5	0.000E+00	0.000E+00	8.725E-09	1.236E+04	5.143E-04	7.899E+03
6	6	0.000E+00	0.000E+00	8.725E-09	1.236E+04	5.143E-04	7.899E+03
6	7	0.000E+00	0.000E+00	7.344E-09	1.236E+04	4.763E-04	9.394E+03
6	8	0.000E+00	0.000E+00	5.093E-09	1.236E+04	4.076E-04	1.353E+04
6	9	0.000E+00	0.000E+00	2.909E-09	1.236E+04	3.259E-04	2.370E+04
6	10	-1.002E+00	1.085E+00	0.000E+00	0.000E+00	0.000E+00	4.016E+04
7	1	0.000E+00	3.946E-01	0.000E+00	0.000E+00	0.000E+00	1.797E+04
7	2	1.162E+00	9.680E-01	0.000E+00	0.000E+00	0.000E+00	1.133E+04
7	3	0.000E+00	0.000E+00	9.163E-09	5.520E+00	6.657E-01	6.687E+03
7	4	0.000E+00	0.000E+00	1.322E-08	5.520E+00	7.699E-01	4.634E+03
7	5	0.000E+00	0.000E+00	1.580E-08	5.520E+00	8.280E-01	3.877E+03
7	6	0.000E+00	0.000E+00	1.581E-08	5.520E+00	8.280E-01	3.877E+03
7	7	0.000E+00	0.000E+00	1.324E-08	5.520E+00	7.699E-01	4.629E+03
7	8	0.000E+00	0.000E+00	9.196E-09	5.520E+00	6.657E-01	6.663E+03
7	9	0.000E+00	0.000E+00	5.428E-09	5.520E+00	5.437E-01	1.129E+04
7	10	-1.162E+00	9.680E-01	0.000E+00	0.000E+00	0.000E+00	1.797E+04
8	1	0.000E+00	2.935E-01	0.000E+00	0.000E+00	0.000E+00	9.159E+03
8	2	1.240E+00	9.108E-01	0.000E+00	0.000E+00	0.000E+00	6.198E+03
8	3	0.000E+00	0.000E+00	1.544E-08	2.822E+00	1.144E+00	3.965E+03
8	4	0.000E+00	0.000E+00	2.105E-08	2.822E+00	1.314E+00	2.909E+03
8	5	0.000E+00	0.000E+00	2.445E-08	2.822E+00	1.409E+00	2.505E+03
8	6	0.000E+00	0.000E+00	2.445E-08	2.822E+00	1.409E+00	2.505E+03
8	7	0.000E+00	0.000E+00	2.105E-08	2.822E+00	1.314E+00	2.909E+03
8	8	0.000E+00	0.000E+00	1.545E-08	2.822E+00	1.144E+00	3.963E+03
8	9	0.000E+00	0.000E+00	9.986E-09	2.822E+00	9.470E-01	6.194E+03
8	10	-1.240E+00	9.108E-01	0.000E+00	0.000E+00	0.000E+00	9.159E+03
9	1	0.000E+00	2.470E-01	0.000E+00	0.000E+00	0.000E+00	1.652E+04
9	2	1.287E+00	9.984E-01	0.000E+00	0.000E+00	0.000E+00	1.167E+04
9	3	0.000E+00	0.000E+00	2.487E-08	4.154E+00	1.999E+00	7.389E+03
9	4	0.000E+00	0.000E+00	3.576E-08	4.154E+00	2.270E+00	5.139E+03
9	5	0.000E+00	0.000E+00	4.332E-08	4.154E+00	2.423E+00	4.242E+03
9	6	0.000E+00	0.000E+00	4.334E-08	4.154E+00	2.423E+00	4.241E+03
9	7	0.000E+00	0.000E+00	3.598E-08	4.154E+00	2.270E+00	5.107E+03

9	8	0.000E+00	0.000E+00	2.528E-08	4.154E+00	1.999E+00	7.269E+03
9	9	0.000E+00	0.000E+00	1.598E-08	4.154E+00	1.689E+00	1.150E+04
9	10	-1.287E+00	8.884E-01	0.000E+00	0.000E+00	0.000E+00	1.650E+04
10	1	0.000E+00	1.637E-01	0.000E+00	0.000E+00	0.000E+00	1.827E+04
10	2	1.370E+00	8.197E-01	0.000E+00	0.000E+00	0.000E+00	1.472E+04
10	3	1.445E+00	1.508E+00	0.000E+00	0.000E+00	0.000E+00	1.078E+04
10	4	0.000E+00	0.000E+00	2.226E-08	2.204E+00	3.427E+00	8.253E+03
10	5	0.000E+00	0.000E+00	2.575E-08	2.204E+00	3.619E+00	7.135E+03
10	6	0.000E+00	0.000E+00	2.576E-08	2.204E+00	3.619E+00	7.133E+03
10	7	0.000E+00	0.000E+00	2.241E-08	2.204E+00	3.427E+00	8.201E+03
10	8	0.000E+00	0.000E+00	1.733E-08	2.204E+00	3.093E+00	1.060E+04
10	9	-1.445E+00	1.508E+00	0.000E+00	0.000E+00	0.000E+00	1.451E+04
10	10	-1.370E+00	8.197E-01	0.000E+00	0.000E+00	0.000E+00	1.825E+04
11	1	0.000E+00	7.381E-02	0.000E+00	0.000E+00	0.000E+00	0.000E+00
11	2	1.488E+00	7.486E-01	0.000E+00	0.000E+00	0.000E+00	0.000E+00
11	3	1.519E+00	1.429E+00	0.000E+00	0.000E+00	0.000E+00	0.000E+00
11	4	0.000E+00	0.000E+00	0.000E+00	0.000E+00	0.000E+00	0.000E+00
11	5	0.000E+00	0.000E+00	0.000E+00	0.000E+00	0.000E+00	0.000E+00
11	6	0.000E+00	0.000E+00	0.000E+00	0.000E+00	0.000E+00	0.000E+00
11	7	0.000E+00	0.000E+00	0.000E+00	0.000E+00	0.000E+00	0.000E+00
11	8	0.000E+00	0.000E+00	0.000E+00	0.000E+00	0.000E+00	0.000E+00
11	9	-1.519E+00	1.429E+00	0.000E+00	0.000E+00	0.000E+00	0.000E+00
11	10	-1.488E+00	7.486E-01	0.000E+00	0.000E+00	0.000E+00	0.000E+00

CONCLUSIONS

Hohlraum:

- No-yield shots above 1.0 MJ are likely to have vaporized hohlraum debris, and possibly micron-size droplets.
- The most Au and Cu deposition occurs along hohlraum axis and normal to axis.

Cryo Tubes:

- The number and sizes of larger solid shrapnel pieces generated by neutron deposition is roughly independent of yield.
- Total velocities of fragments do not vary greatly with yield.

Projection of Shrapnel/Debris to First Wall:

- Mass coming from different sections and sectors of cryo tubes will overlap on wall; but mass densities are low.

Appendix VI

NIF CHAMBER FIRST WALL, DEBRIS SHIELD, AND BEAM DUMP HARDENING ISSUES

NIF CHAMBER FIRST WALL, DEBRIS SHIELD, AND BEAM DUMP HARDENING ISSUES

R. E. Tokheim, D. R. Curran, M. Tobin

Presented at Oak Ridge, 5-6 December 1995

OUTLINE OF BRIEFING

- Chamber wall radius issue

- First wall hardening material issues
  - Candidate materials
  - Configuration
  - X-ray ablation
  - Response to x-ray-induced stress waves (e.g. spall or delamination)
  - Response to shrapnel and debris
  - Mounting configurations
  - Effect of deposited debris and embedded shrapnel on subsequent exposures
  - Response to $1\omega/2\omega$

- Debris shield and beam dump hardening issues
  - Same as above, except minus candidate materials, and plus
  - Efficacy of plastic coating

- Minimum thicknesses of hardening materials required for survival under multiple exposures

- Qualification testing issues
  - Worst case threat definition
  - Proposed tests

CHAMBER WALL RADIUS ISSUE

- Decision: 5 meters
- Assumes we will solve the above issues
- Discussed in separate briefing

FIRST WALL MATERIAL HARDENING ISSUES

- Candidate materials: B4C, B, SiC, AL2O3

- Assumed configuration: The hardening material is sprayed or glued to a thicker metal substrate plate (see later discussion)

- X-ray ablation
  - B4C and B are expected to have removal depths < 0.5 μm, and provide adequate protection for the aluminum chamber wall for yields up to 45 MJ.

- Response to x-ray-induced stress waves (e.g. delamination, spall).

  - Earlier analyses for 0.5 mm plasma sprayed boron with an aluminum nitride bond to an aluminum substrate suggested that stresses at the rear of the boron were less than 0.01 kbars for fluences up to 3.5 J/cm^2. Bond strengths of 0.15 kbars are attainable. Thus, debonding is probably avoidable. (Although higher stresses can be expected for HIP material, we can also use a strong epoxy bond in that case).

  - Above estimates used a equation of state that needs more data for validation.

  - More calculations and tests are needed.

• Response to shrapnel and debris (20 MJ threat)

Material	Ave. size of fragments	Total no. of fragments in the chamber	Approximate speed at first wall
Gold from Hohlraum	Vapor	Vapor	10 km/s
Copper from shine shields (but probably not present in 20 MJ shots)	Vapor plus micron-sized droplets	$> 10^{11}$ droplets	10 km/s
Small steel shrapnel	≈ 1 μm	10^{7}-10^{8}	≤ 10 km/s
Large steel shrapnel	≈ 150 μm	≈ 150	400 m/s

- Worst case: 150 μm steel particles impacting at 400 m/s

- Expected damage from above worst case: Each 150 μm particle produces only a small crater, but a roughly hemispherical, heavily fractured region beneath the impact site with a radius ≈ 1 mm.

- Expected damage from the small, hypervelocity fragments: a 1 μm particle produces a hemispherical crater about 5 μm deep.

• Mounting configurations

- Unbacked ceramic plates are susceptable to bending-induced fracture.

- Standard ceramic armor design practise is to bond the ceramic to a relatively thick, ductile metal backing plate to prevent bending, and provide "confinement". The overall goal is to keep the ceramic in compression during the attack.

- The above recommended practise can be met by plasma spraying directly on an aluminum substrate plate or on an interface material, or by epoxy bonding a sintered material to the substrate plate.

• Effect of deposited debris and imbedded shrapnel on subsequent x-ray and 1ω/2ω exposures

- Transfer of shrapnel material to debris shields

- Damage from "hot spot" stress waves

- Needs analyses and tests

DEBRIS SHIELD AND BEAM DUMP HARDENING ISSUES

- Response to shrapnel and debris: Uncoated silica response will be similar to that of B4C and B because silica is also a high compressive strength, brittle material.

- Efficacy of plastic coating
  - Data exist for glass beads impacting teflon at 1-7 km/s.

  - These data can be extrapolated to steel fragments.

  - The worst case steel fragment (150 μm particle at 400 m/s) is expected to penetrate to a depth of 1-2 mm in plastic.

MINIMUM THICKNESSES REQUIRED FOR SURVIVAL UNDER MULTIPLE EXPOSURES FOR FIRST WALL HARDENING MATERIAL AND DEBRIS SHIELD/BEAM DUMP MATERIALS

Material	Minimum thickness (mm)	Comments
Fully dense B4C, B, or SiC for first wall protection	5	Criterion is that the layer thickness be five times the damage radius. The craters are shallow, but a large sub-crater fractured zone is probable. A thinner layer may be possible if the fractured material remains bonded to the substrate.
85% dense B4C, B, or SiC for first wall protection	4 - 6	"
Debris shield coating plastic	2-4	Criterion is that the layer thickness be twice the damage radius. Lack of large sub-crater fracture zone allows a thinner layer than for the first wall ceramics.

QUALIFICATION TESTING ISSUES

- Worst case threat definition: 150 μm diameter steel shrapnel fragments impacting at 400 m/s

- Proposed test goals

  -Verify that the manufactured material has the specified density, composition, and thermo-mechanical properties.

  - Subject the samples to representative impacts.

  - Quick turn-around time.

  - Cost effective.

RELEVANT HISTORY

- Work in 1970s and 80s on erosion-resistant IR windows and ceramic turbine components.

- Work since the 1960s on x-ray hardening of space assests.

- Work since the 1960s on ceramic armor.

APPLICATIONS OF PAST HISTORY TO FIRST WALL AND DEBRIS SHIELD/BEAM DUMP MATERIAL TESTING

- The ceramics should be bonded to a metal (e.g. aluminum) backer plate that has a thickness significantly greater than that of the ceramic (to prevent bending).

- Cratering can be prevented or minimized if the ceramic or fused silica has a Hugoniot Elastic Limit (HEL) much higher than that of the shrapnel material. (e.g. this requirement is met for fully dense B4C or SiO2 against steel shrapnel).

- Ring, conical, and radial cracks are formed at relatively low impact velocities, and may penetrate through the ceramic to the metal backing plate. Therefore, the ceramic must be well-bonded to the backing plate in order to hold the fractured ceramic together.

- B4C is a high performance armor material, but the much cheaper SiC is also good. We should calculate the expected ablation from SiC before settling on B4C or B.

- Dynamic impact tests are necessary because in quasistatic indentation tests, the shrapnel materials used as the indentor fail too early. Also, for plastic coatings, the 400 m/s impact velocity for steel shrapnel is in the grey area between rigid body penetration and hydrodynamic penetration.

CURRENTLY AVAILABLE IMPACT TEST FACILITIES

- SRI has a simple, small launcher that can shoot sub-mm spheres at velocities up to ≈ 500 m/s. Such launchers probably exist (or could easily be constructed) at other facilities as well.

- NASA has a facility that can shoot mm-sized spheres at velocities up to ≈ 7 km/s.

PROPOSED TESTS

- Particle impact tests at several particle sizes and impact velocities chosen to span the range expected for the shrapnel (from dud shots to over 20 MJ).
  - Particle sizes from 0.1 to 1.0 mm.
  - Impact velocities from 10 m/s to 10 km/s.
  - Simple gas gun for velocities up to 500m/s.
  - NASA facility for higher velocities.

- Standard mechanical and chemical analyses to verify the material's density and composition.
  - SEM scans.
  - Density measurements, porosimeter tests
  - Hardness, tensile strength, fracture toughness.
  - Thermal properties (e.g. incipient vaporization energy, sublimation energy, thermal diffusivity, thermal expansion coefficient).
  - Chemical composition tests.

RECOMMENDATIONS FOR QUALIFICATION TESTING

- Promising first wall coating materials should be first tested in particle impact tests at the lower impact velocities (below 500 m/s).

- If the material still looks promising, then higher velocity impact testing and thorough laboratory characterization can proceed in parallel.

Appendix VII

UPDATE ON RECENT HOHLRAUM AND SHRAPNEL RESULTS

UPDATE ON RECENT HOHLRAUM AND SHRAPNEL RESULTS

R. E. Tokheim and D. R. Curran
SRI INTERNATIONAL

31 January 1996

OUTLINE

- NO-YIELD HOHLRAUM DEBRIS COMPUTATIONS
- CRYO TUBE SHRAPNEL COMPUTATIONS
- RESULTS AND CONCLUSIONS

NO-YIELD HOHLRAUM DEBRIS COMPUTATIONS

- 1.8 MJ with shine shields
  - Without material phase boundaries
  - With material phase boundaries
- 1.0 MJ with shine shields
  - Without material phase boundaries

Configuration for Hohlraum with Shine Shields:

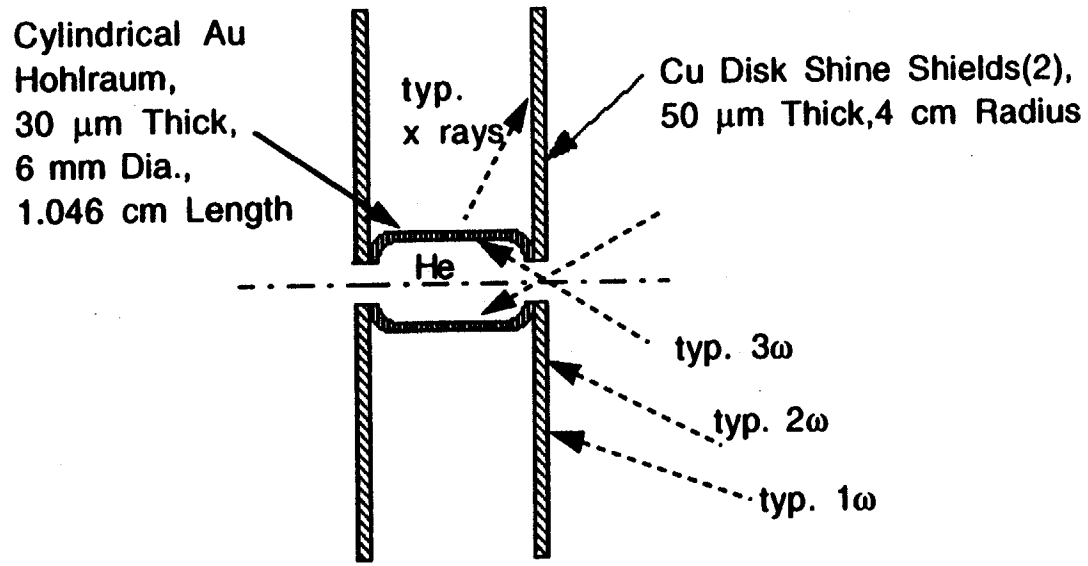

Approach:

- LLNL computations of 1ω/2ω intensity onto Cu shine shields
- Plot of typical intensity variation on shine shields
- Use of HYADES runs at certain locations for initialization of shine-shield L2D computations
- Modified use of previous L2D Au hohlraum computations
- Energy deposition of mixed-blackbody x rays through hohlraum to inside of shine shields during L2D run

- 1.8 MJ with shine shields
  - Without material phase boundaries

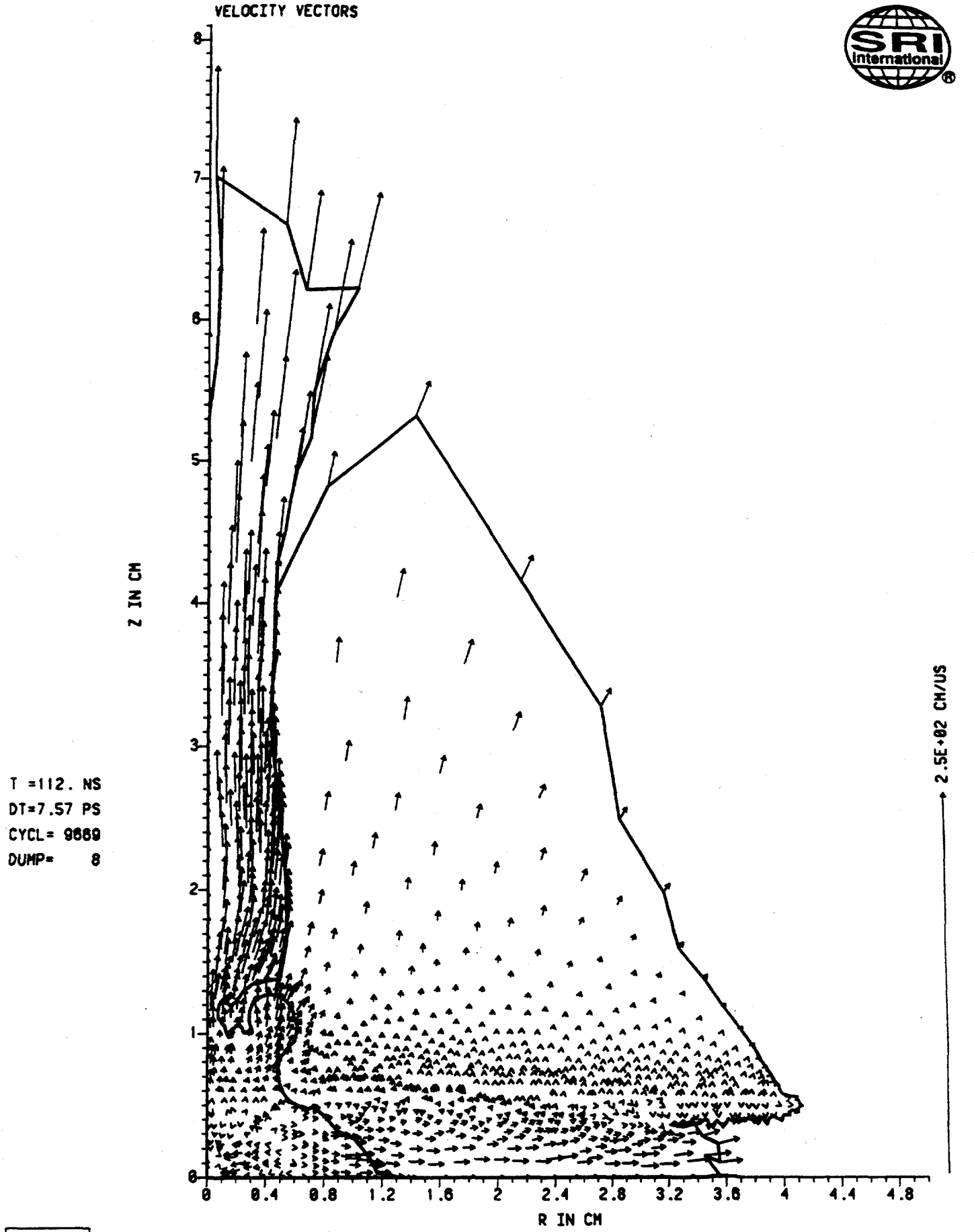
VELOCITY VECTORS
Z IN CM
R IN CM
2.5E+02 CM/US
T =112. NS
DT=7.57 PS
CYCL= 9869
DUMP= 8
0
1
2
3
4
5
6
7
8
0
0.4
0.8
1.2
1.6
2
2.4
2.8
3.2
3.6
4
4.4
4.8

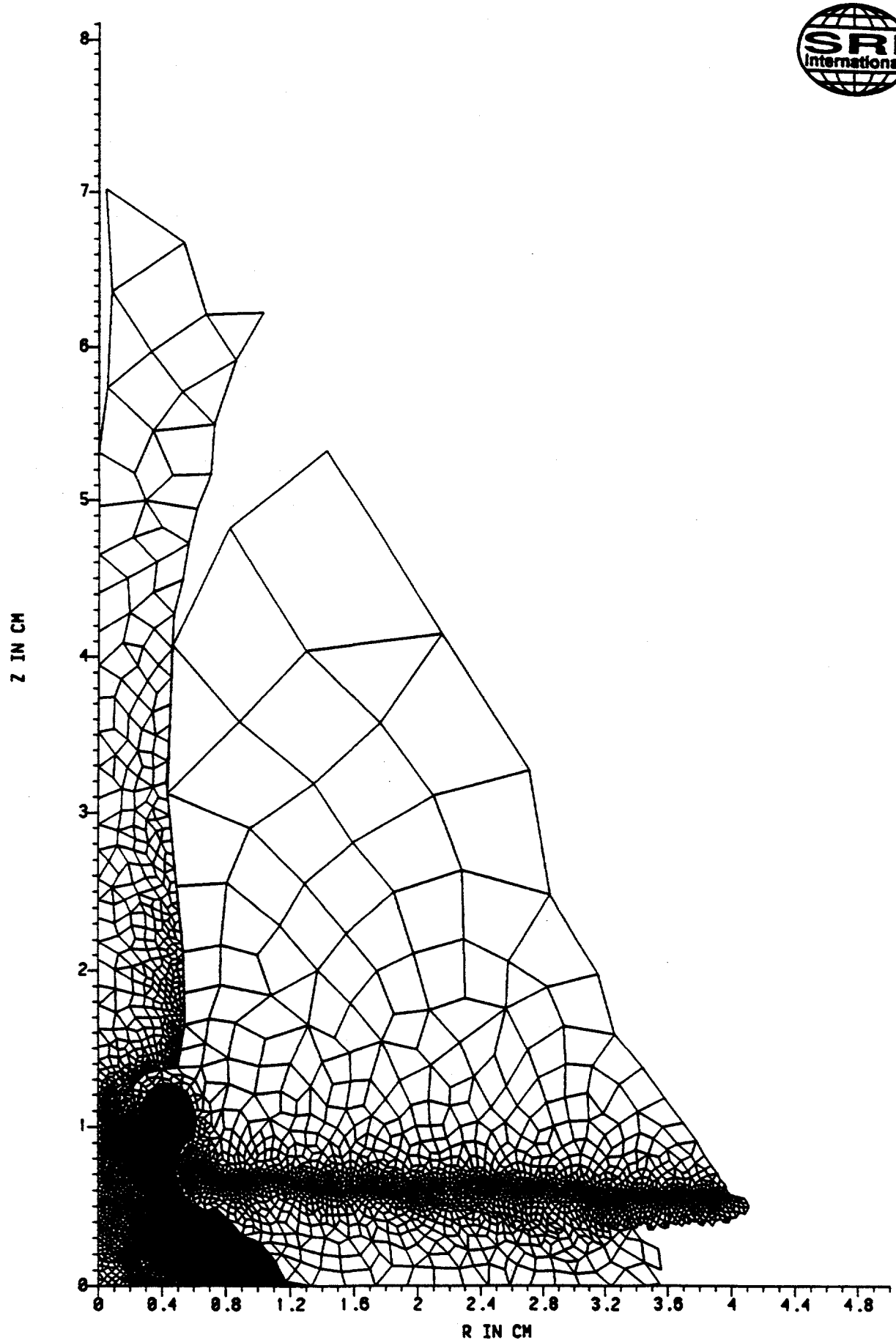

T =112. NS
DT=7.57 PS
CYCL= 9669
DUMP= 8

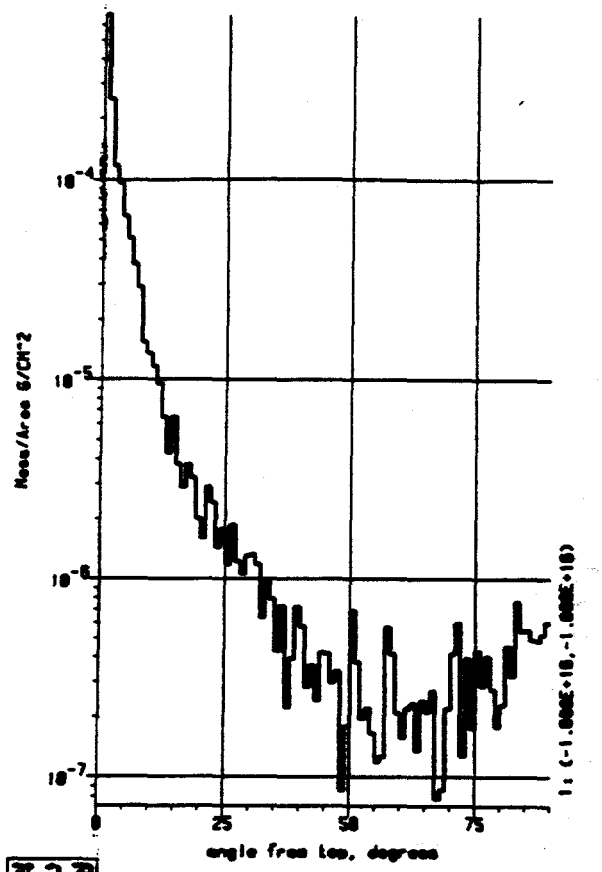

図2-3 15-Sep-95 20:50:50 N:f,1.8MJ,nph,500 cm 001

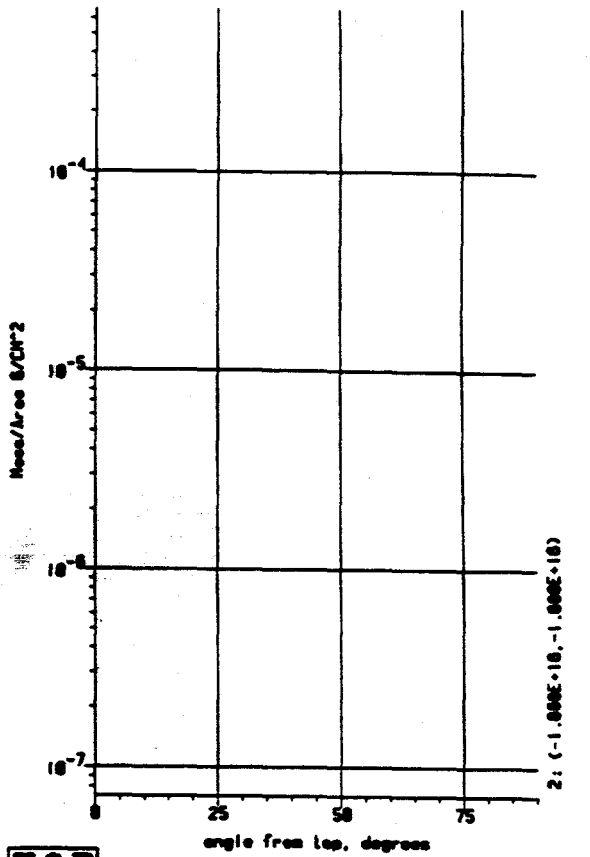

図2-3 15-Sep-95 20:50:50 N:f,1.8MJ,nph,500 cm, solid GOLD 002

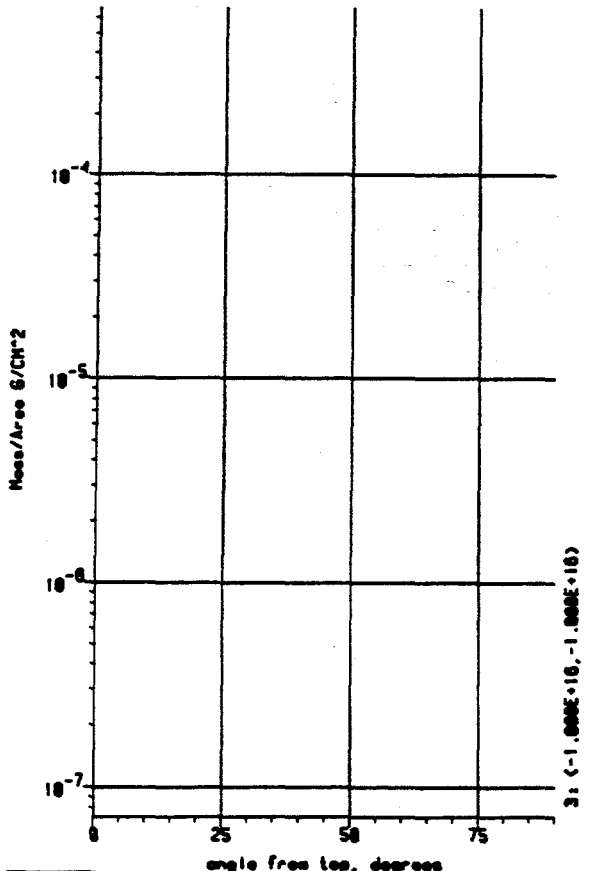

図2-3 15-Sep-95 20:50:50 N:f,1.8MJ,nph,500 cm, rolled GOLD 003

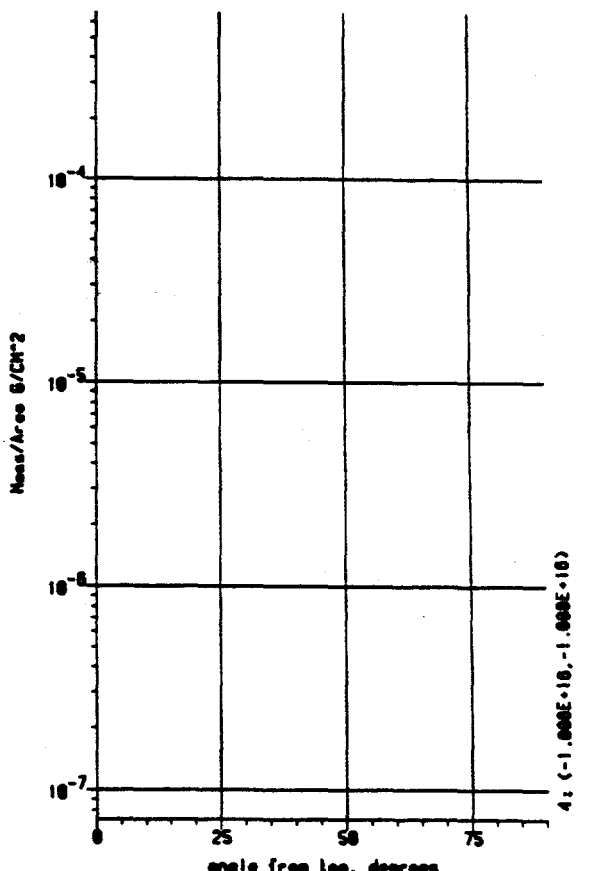

図2-3 15-Sep-95 20:50:50 N:f,1.8MJ,nph,500 cm, vaporized GOL 004

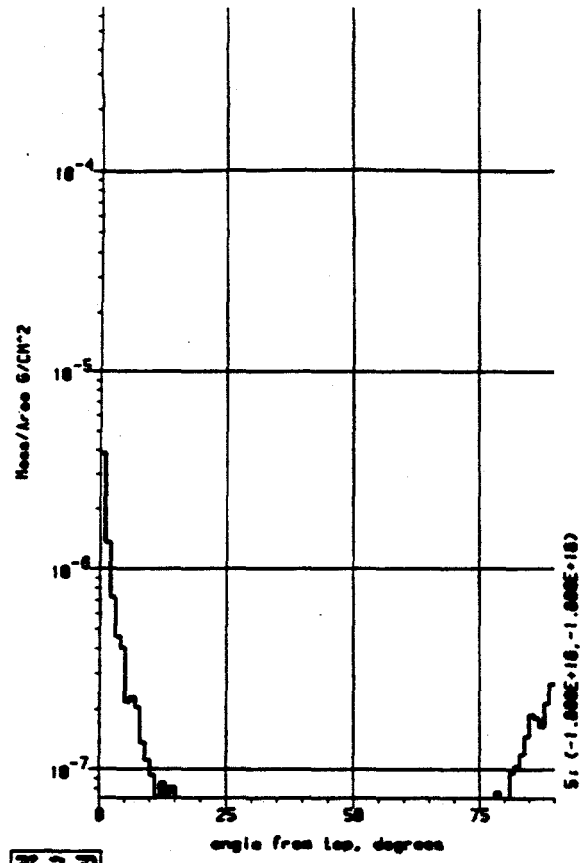

그림 5 15-Sep-95 20:58:58 N:f,1.0MJ,mph,500 cm, ionized GOLD 005

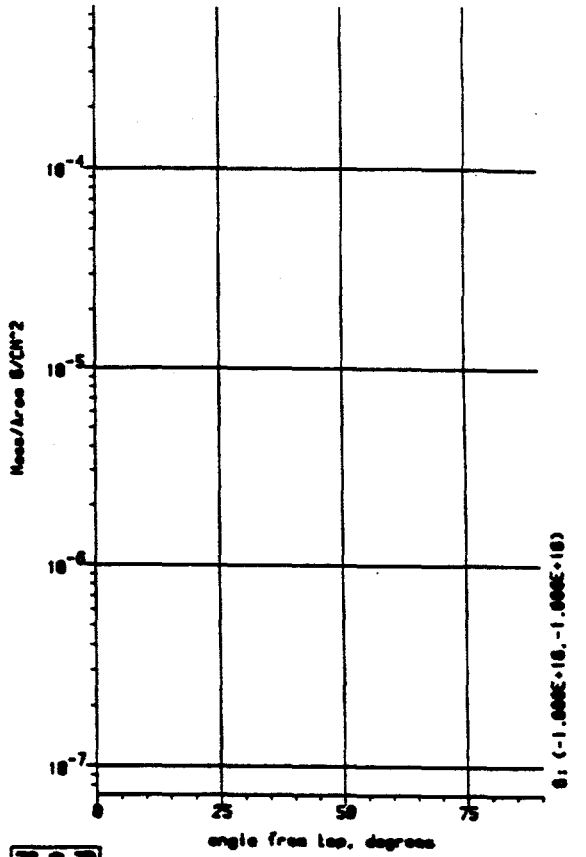

그림 6 15-Sep-95 20:58:58 N:f,1.0MJ,mph,500 cm, solid CU 006

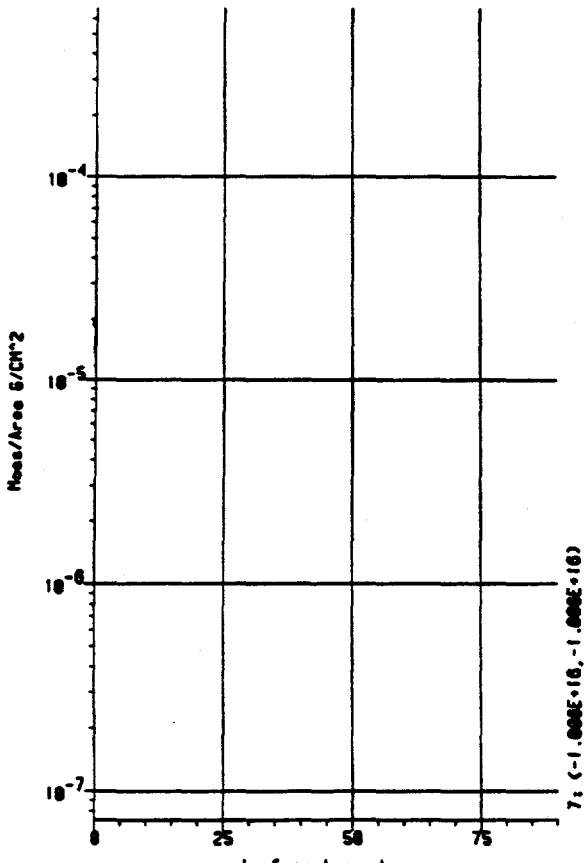

그림 7 15-Sep-95 20:58:58 N:f,1.0MJ,mph,500 cm, melted CU 007

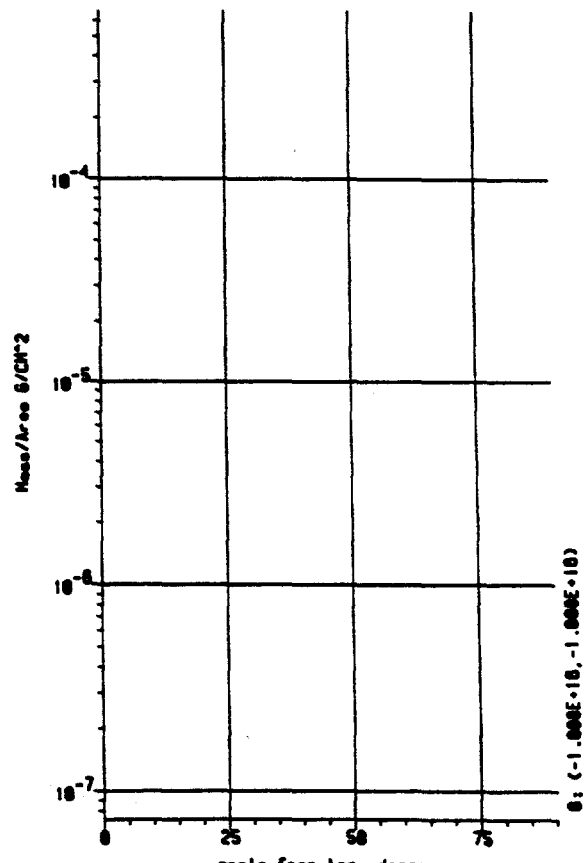

그림 8 15-Sep-95 20:58:58 N:f,1.0MJ,mph,500 cm, vaporized CU 008

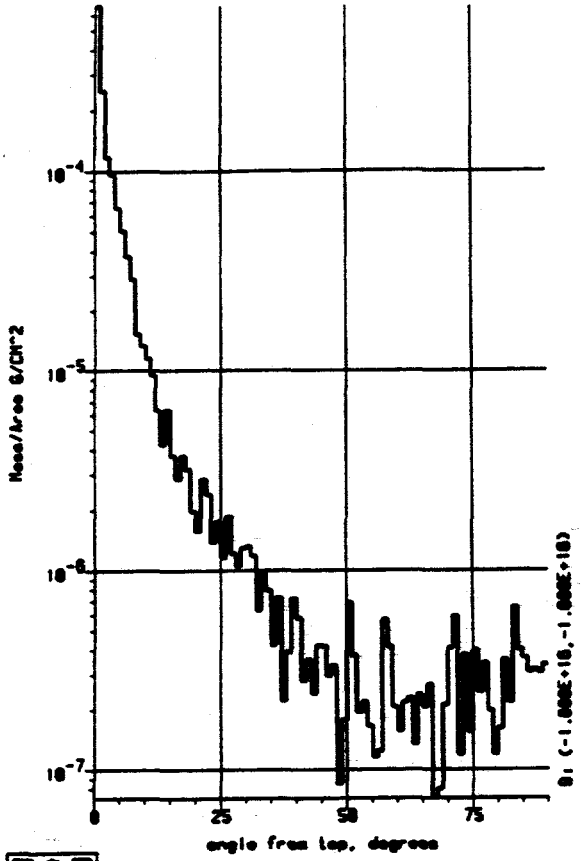

図2.3 15-Sep-95 20:58:58 N:f,1.0MJ,mph,500 cm, ionized CU 006

- 1.8 MJ with shine shields
  - With material phase boundaries

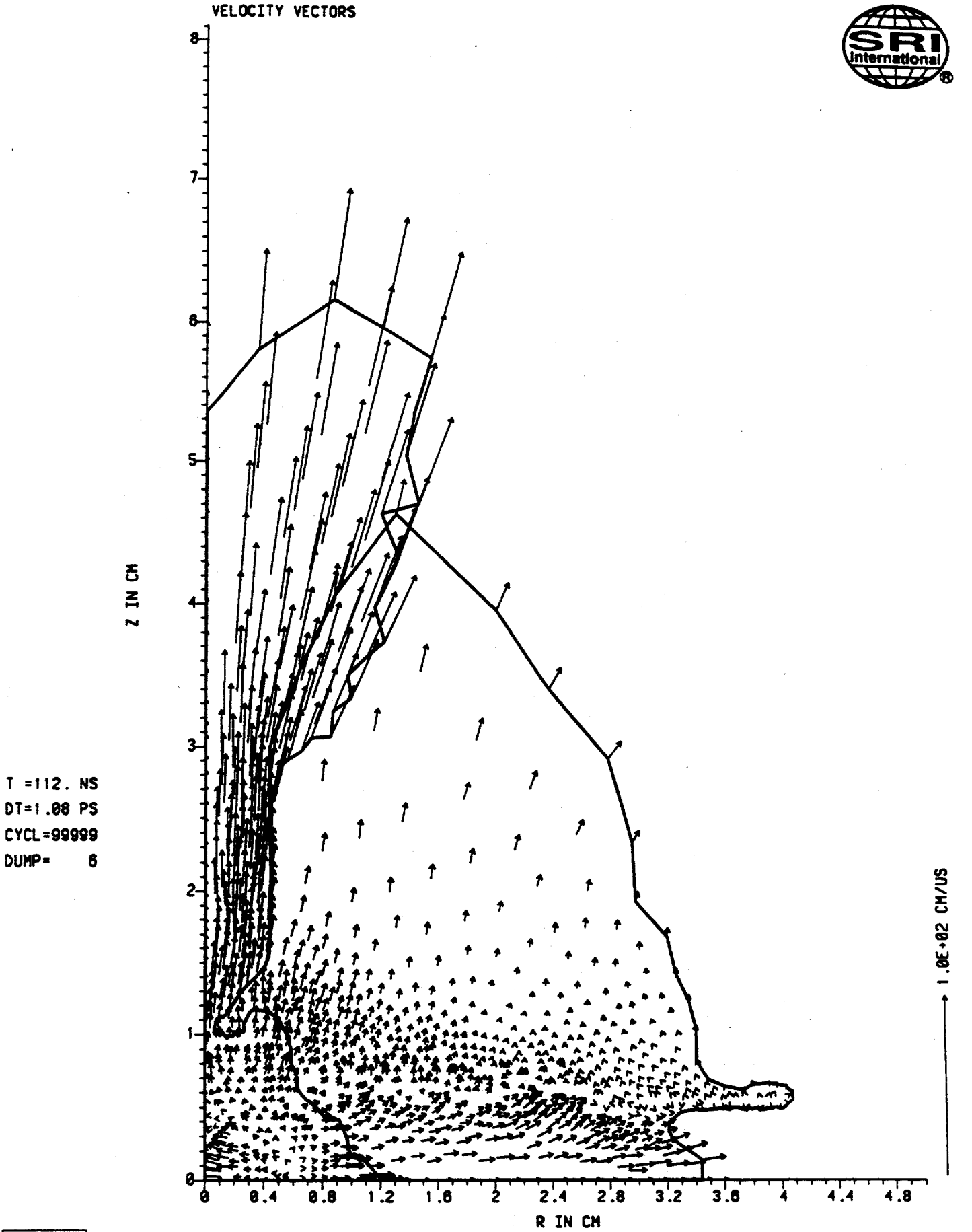

I 2 D

27-Sep-95 13:59:07 Nif,1.8MJ,ph

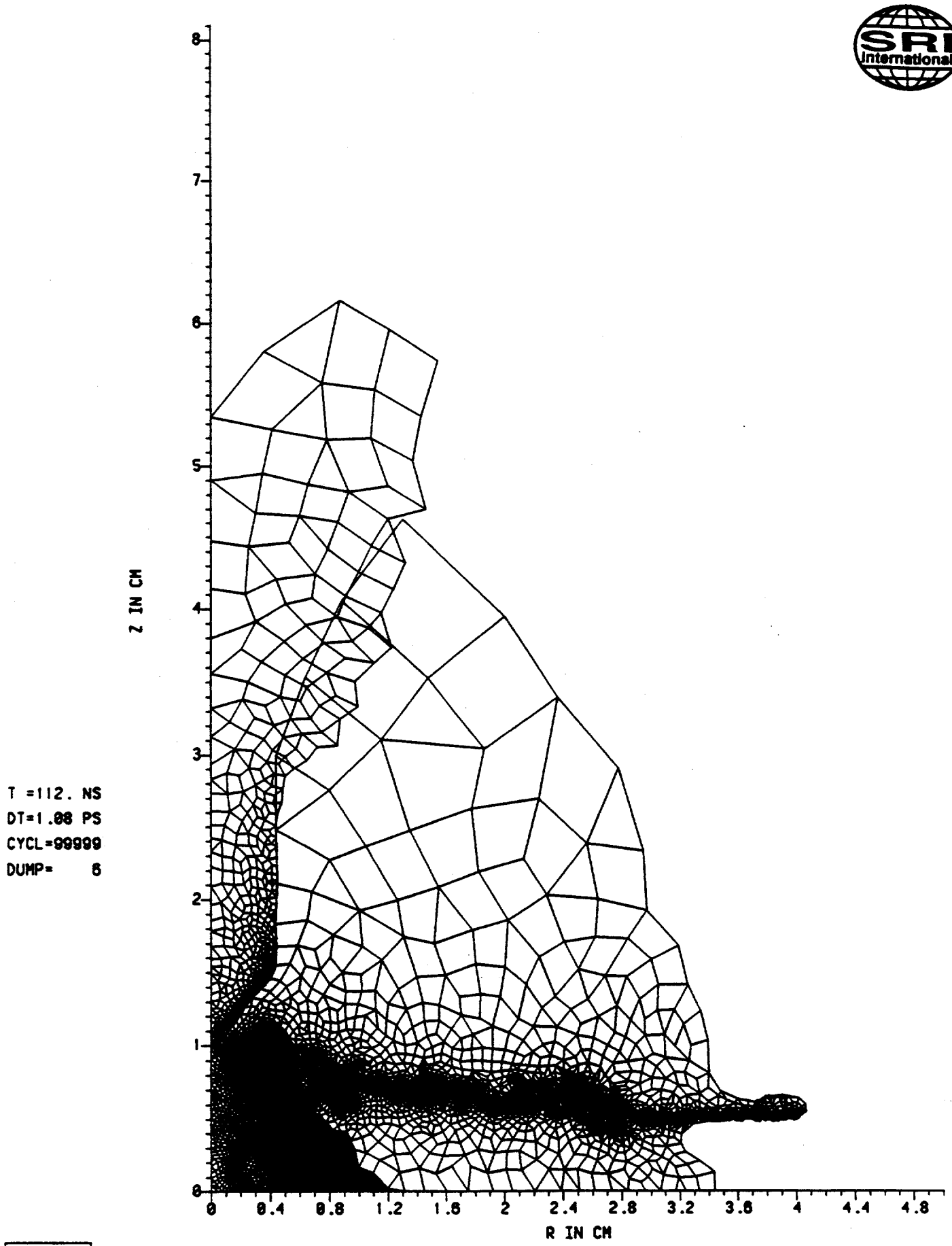
Z IN CM
R IN CM
0
1
2
3
4
5
6
7
8
0
0.4
0.8
1.2
1.6
2
2.4
2.8
3.2
3.6
4
4.4
4.8
T =112. NS
DT=1.08 PS
CYCL=99999
DUMP= 6
27-Sep-95 13:59:07 N:f,1.8MJ,ph

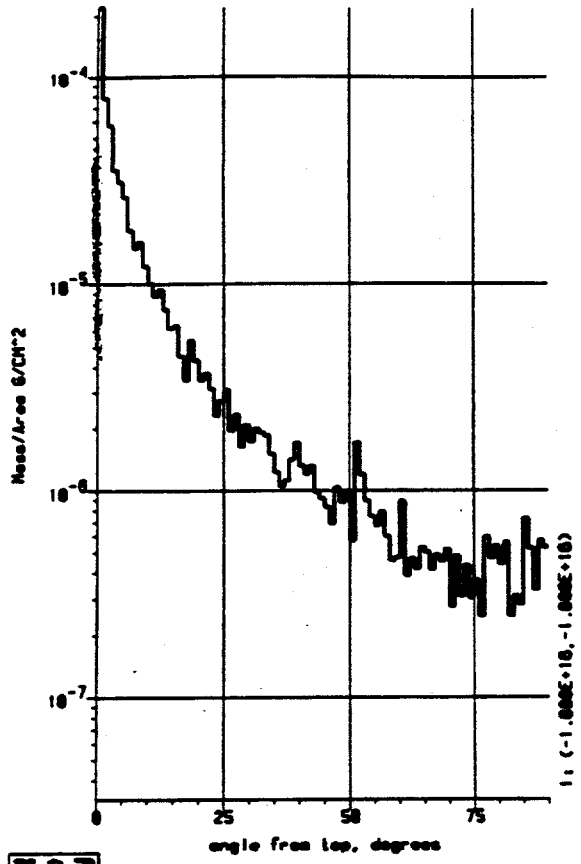

図2種 27-Sep-95 13:58:07 Nif,1.8MJ,ph,500 cm 001

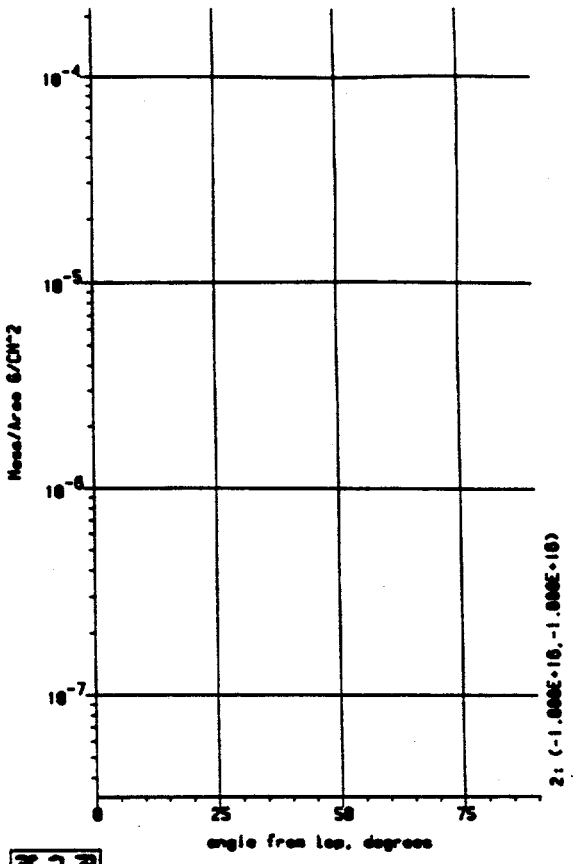

図2種 27-Sep-95 13:58:07 Nif,1.8MJ,ph,500 cm, solid GOLD 002

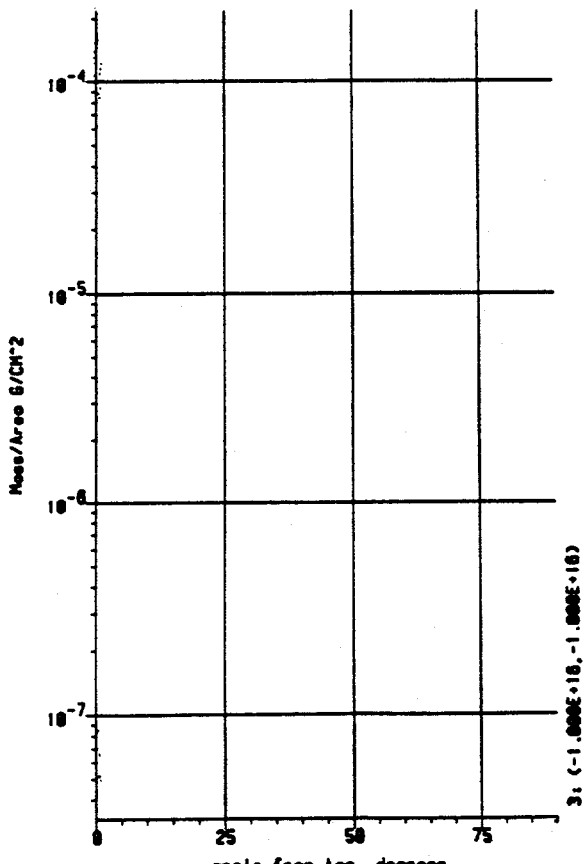

図2種 27-Sep-95 13:59:07 Nif,1.8MJ,ph,500 cm, melted GOLD 003

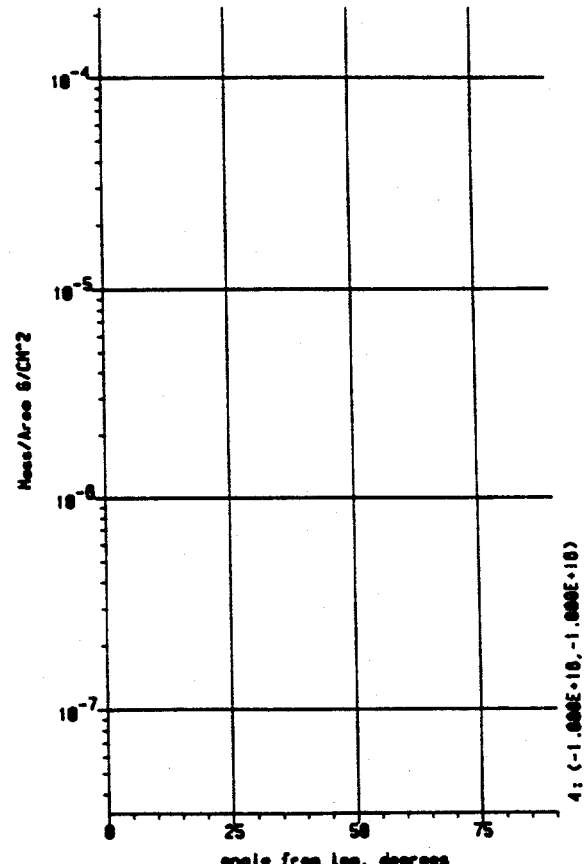

図2種 27-Sep-95 13:58:07 Nif,1.8MJ,ph,500 cm, vaporized GOLD 004

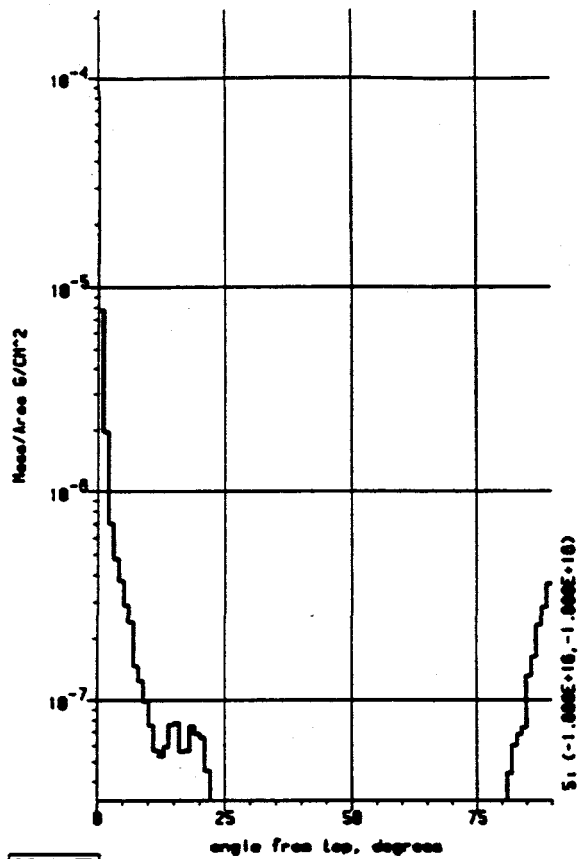

図2.3 27-Sep-95 13:58:07 Nif,1.8MJ,ph,500 cm, ionized GOLD 005

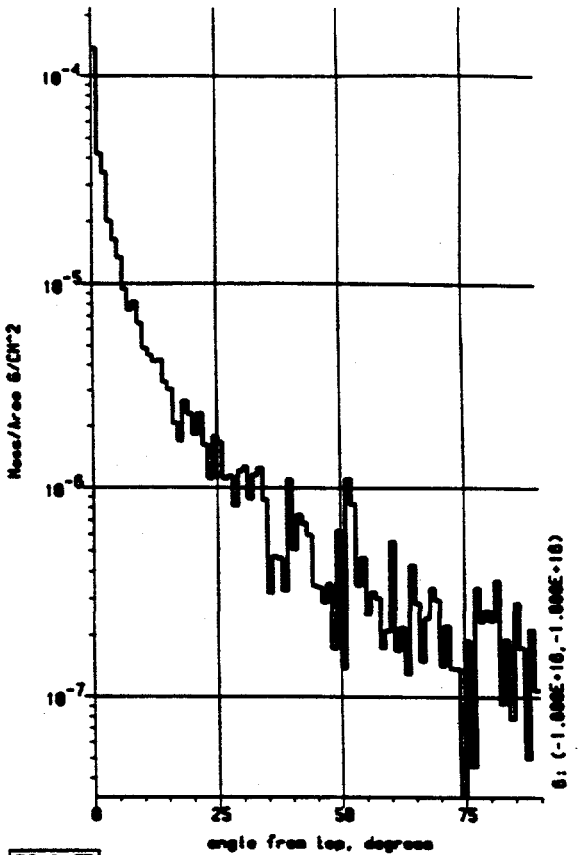

図2.3 27-Sep-95 13:58:07 Nif,1.8MJ,ph,500 cm, solid CU 006

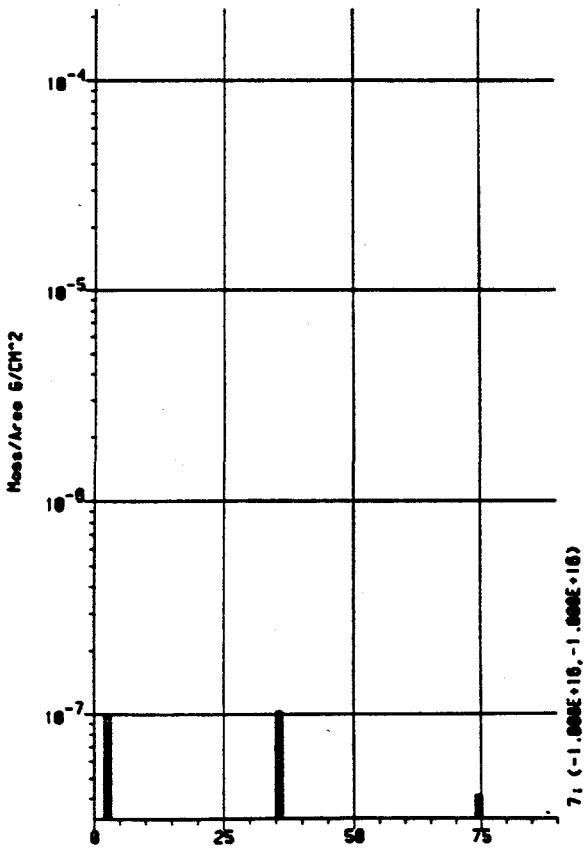

図2.3 27-Sep-95 13:58:07 Nif,1.8MJ,ph,500 cm, melted CU 007

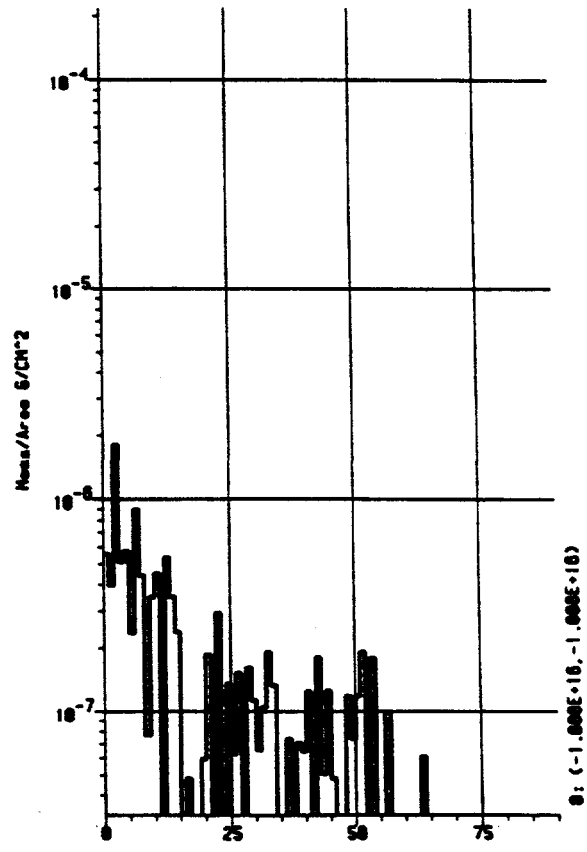

図2.3 27-Sep-95 13:58:07 Nif,1.8MJ,ph,500 cm, vaporized CU 0

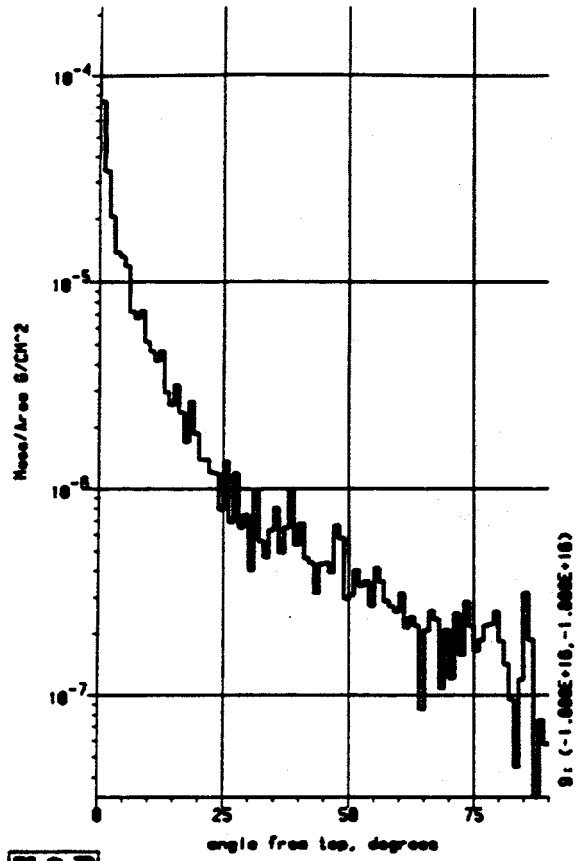

図2 27-Sep-95 13:50:07 N:f,1.8MJ,ph,500 cm, ionized CU 888

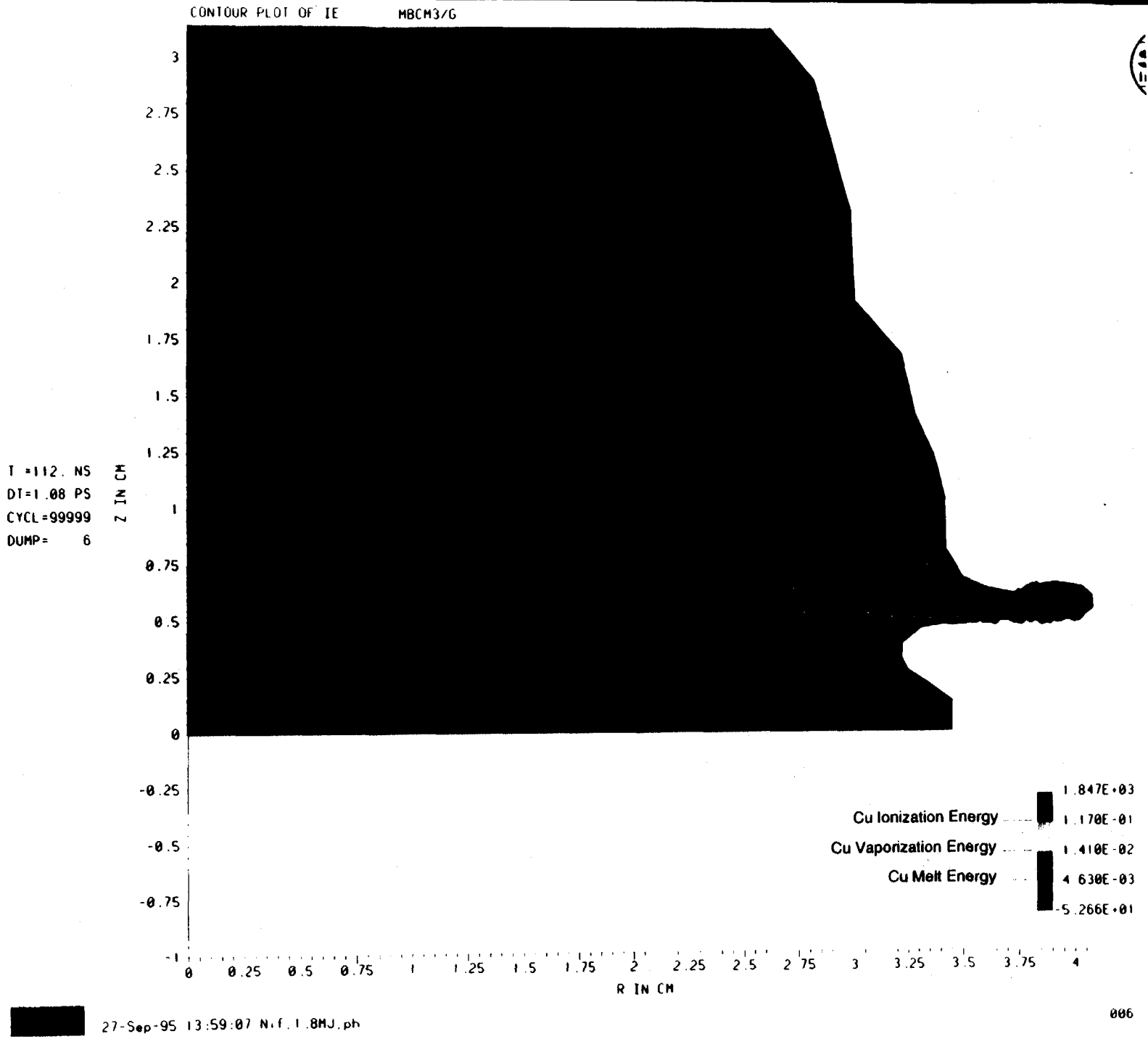
CONTOUR PLOT OF IE
MBCM3/G
T =112. NS
DT=1.08 PS
CYCL=99999
DUMP= 6
Z IN CM
3
2.75
2.5
2.25
2
1.75
1.5
1.25
1
0.75
0.5
0.25
0
-0.25
-0.5
-0.75
-1
0 0.25 0.5 0.75 1 1.25 1.5 1.75 2 2.25 2.5 2.75 3 3.25 3.5 3.75 4
R IN CM
Cu Ionization Energy
Cu Vaporization Energy
Cu Melt Energy
1.847E+03
1.170E-01
1.410E-02
4.630E-03
-5.266E+01
27-Sep-95 13:59:07 Nif.1.8MJ.ph
006

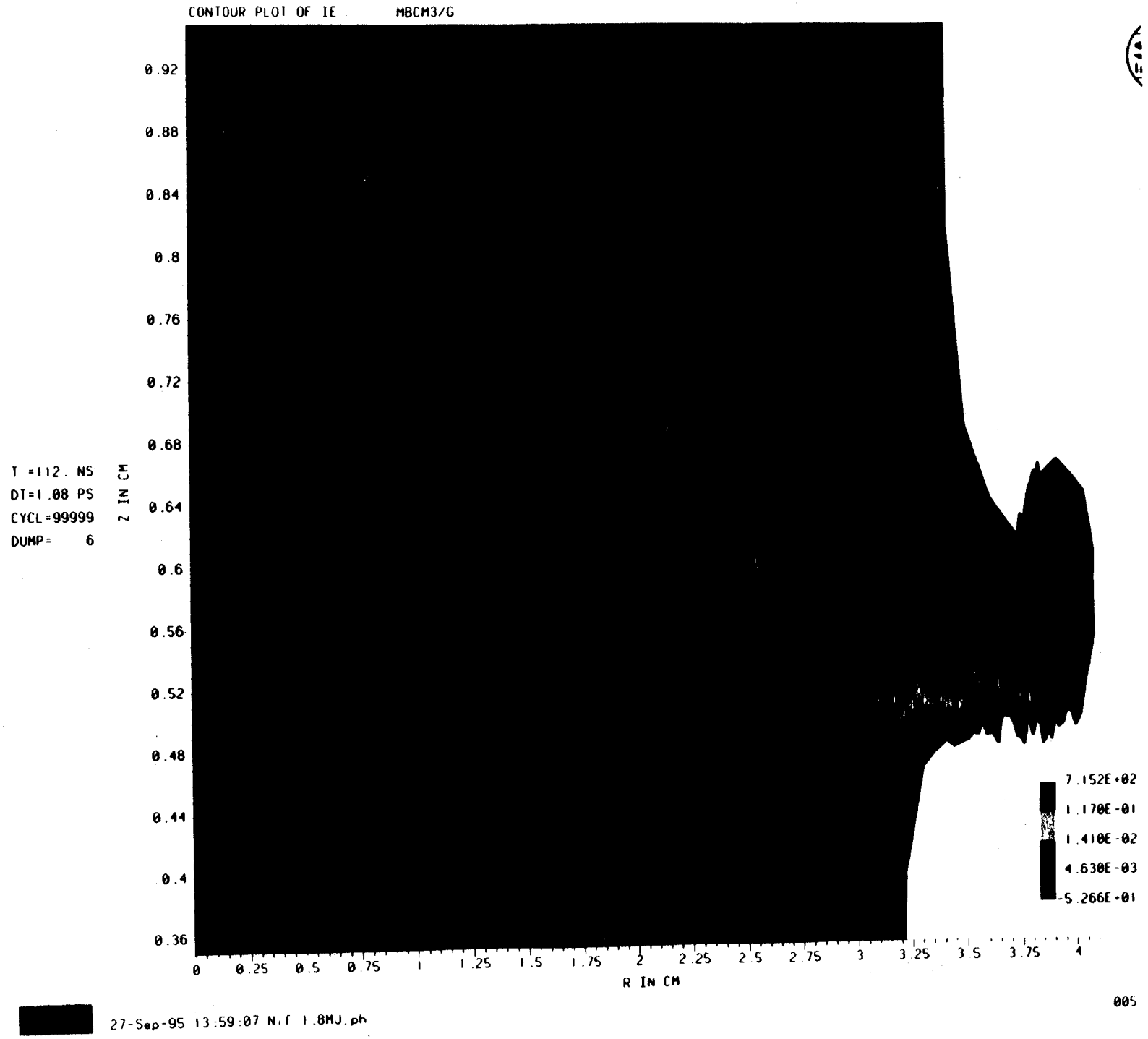
CONTOUR PLOT OF IE MBCM3/G
0.92
0.88
0.84
0.8
0.76
0.72
0.68
0.64
0.6
0.56
0.52
0.48
0.44
0.4
0.36
Z IN CM
T =112. NS
DT=1.08 PS
CYCL=99999
DUMP= 6
0 0.25 0.5 0.75 1 1.25 1.5 1.75 2 2.25 2.5 2.75 3 3.25 3.5 3.75 4
R IN CM
7.152E+02
1.170E-01
1.410E-02
4.630E-03
-5.266E+01
005
27-Sep-95 13:59:07 N:f 1.8MJ.ph

- 1.0 MJ with shine shields
  - Without material phase boundaries

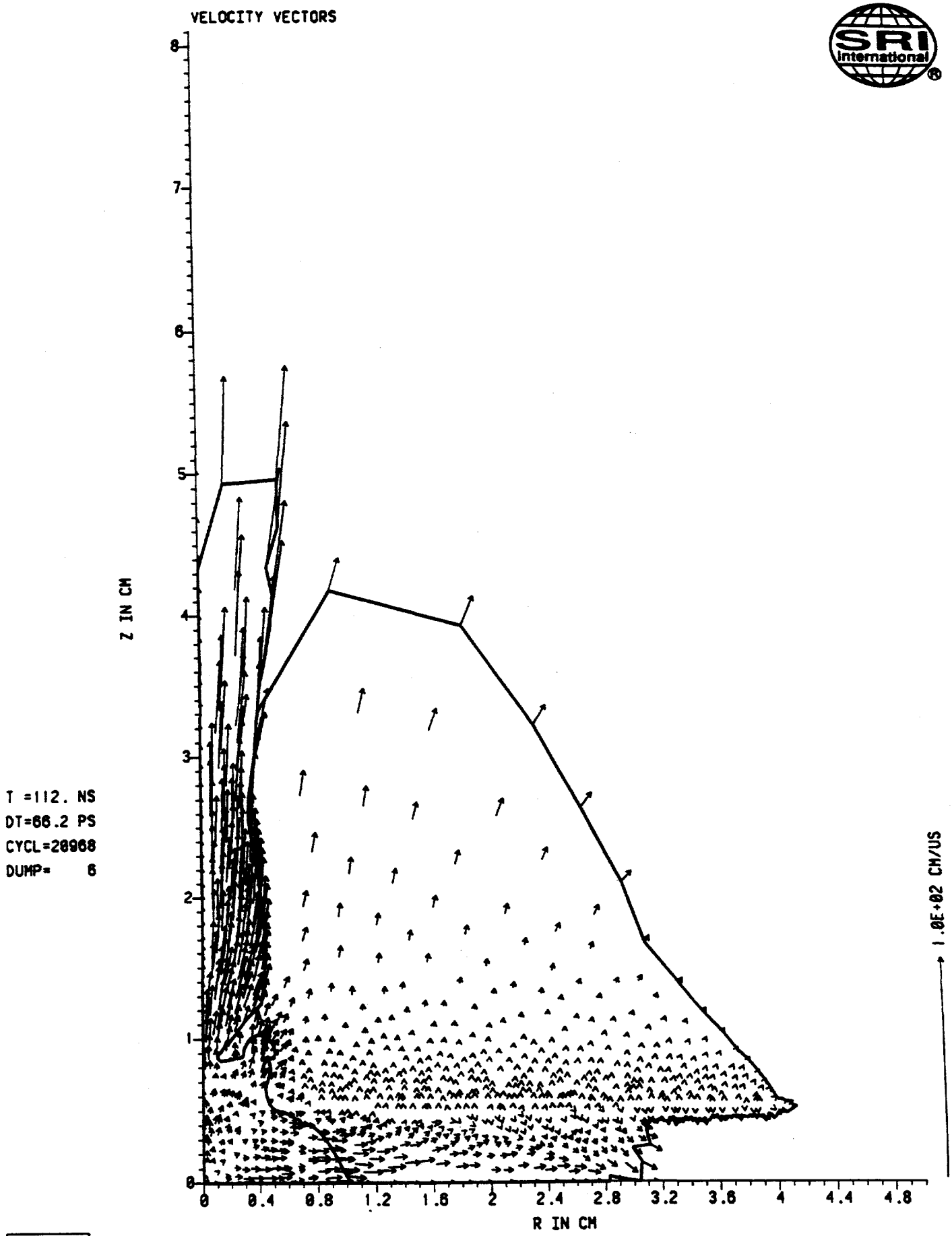

I 2 B

6-Nov-95 15:59:05 N:f,1.MJ,nph

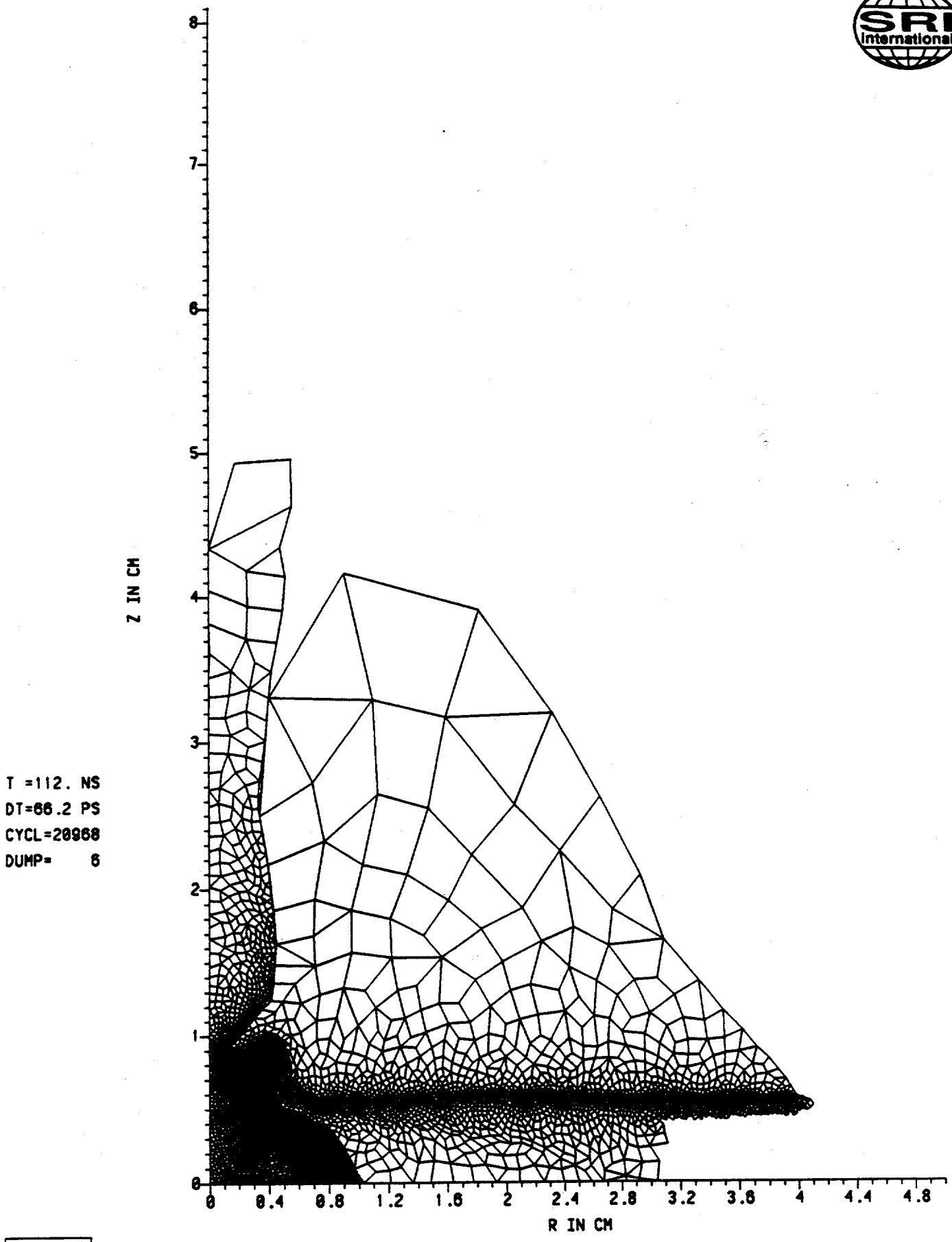

I 2 B

6-Nov-95 15:59:05 N:f,1.MJ,nph

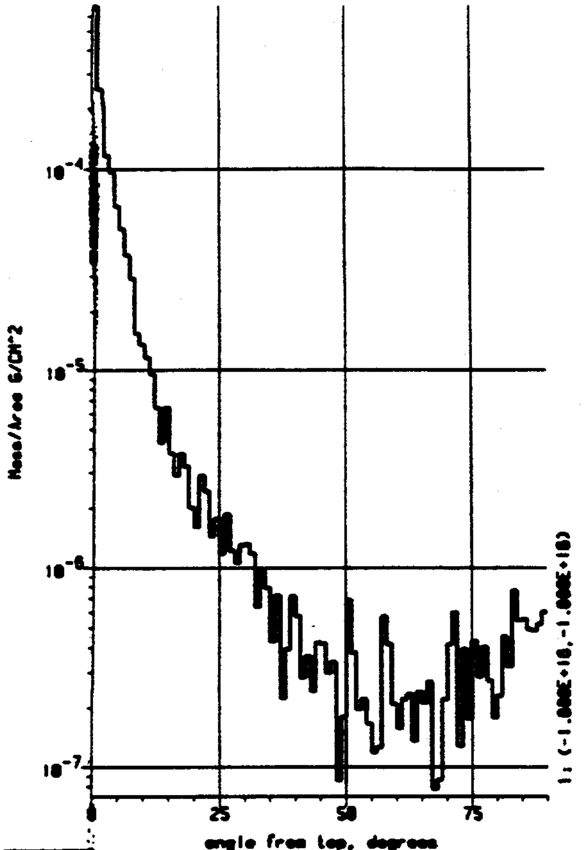

図23 6-Nov-95 15:50:05 N:f,1MJ,nph,500 cm 001

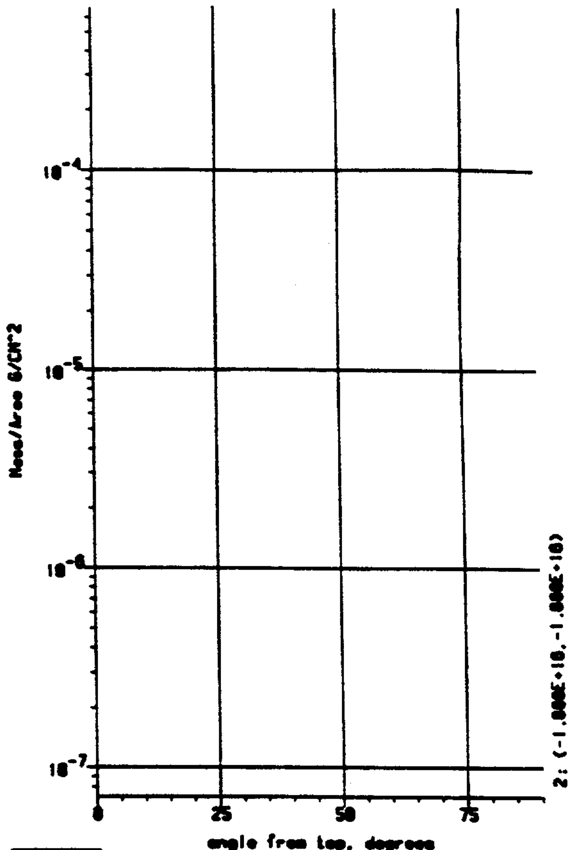

図23 6-Nov-95 15:50:05 N:f,1MJ,nph,500 cm, solid GOLD 002

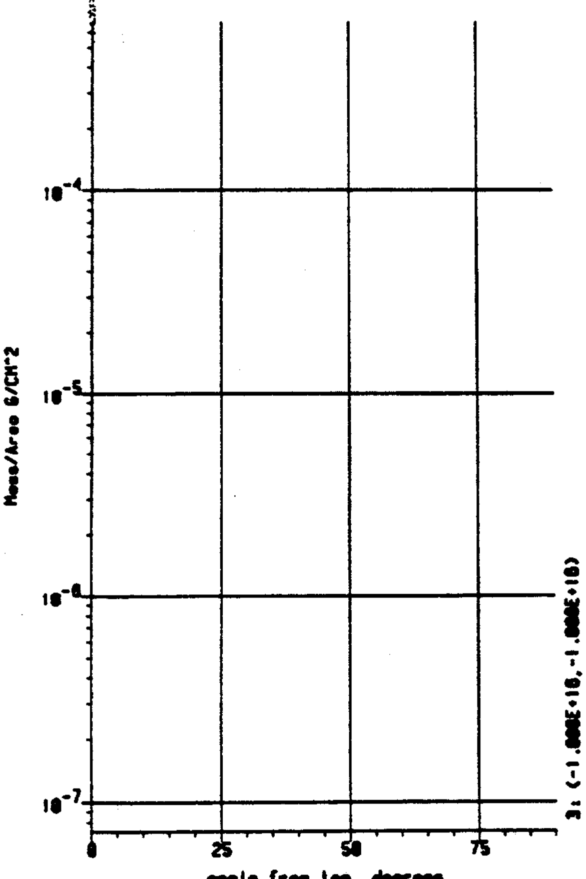

図23 6-Nov-95 15:50:05 N:f,1MJ,nph,500 cm, melted GOLD 003

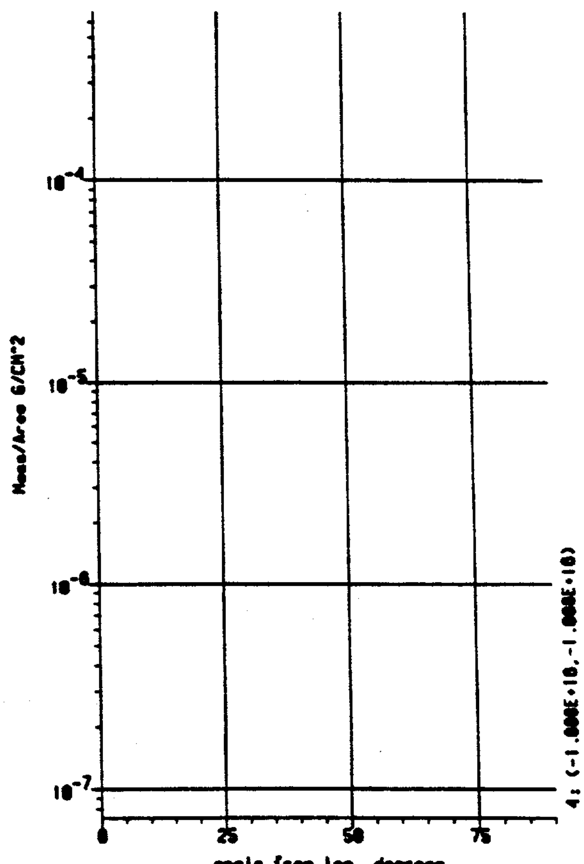

図23 6-Nov-95 15:50:05 N:f,1MJ,nph,500 cm, vaporized GOLD 00

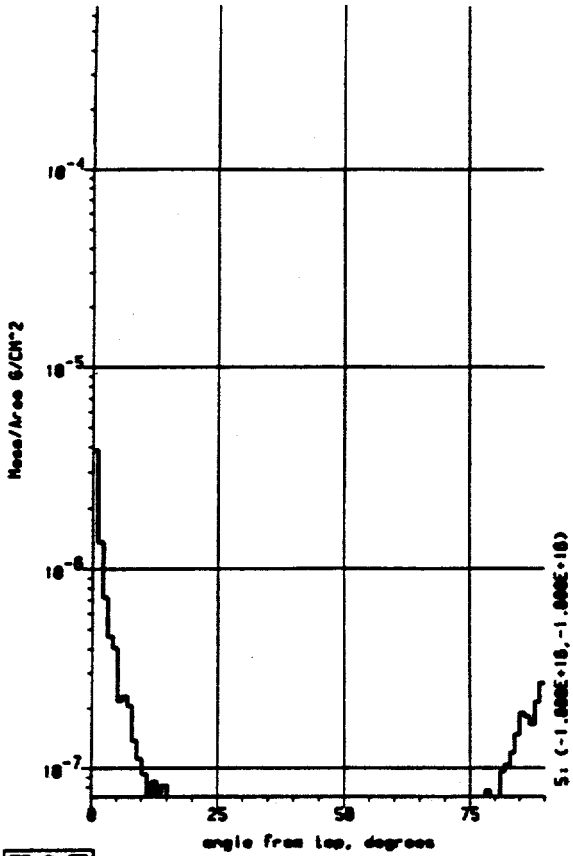

第2表 6-Nov-95 15:58:05 N:f,1MJ,nph,500 cm, ionized GOLD 005

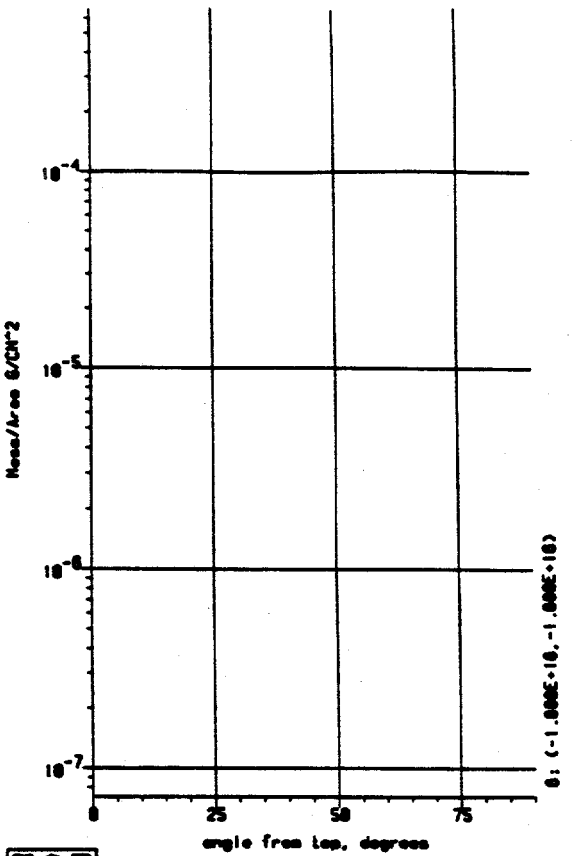

第2表 6-Nov-95 15:58:05 N:f,1MJ,nph,500 cm, solid CU 006

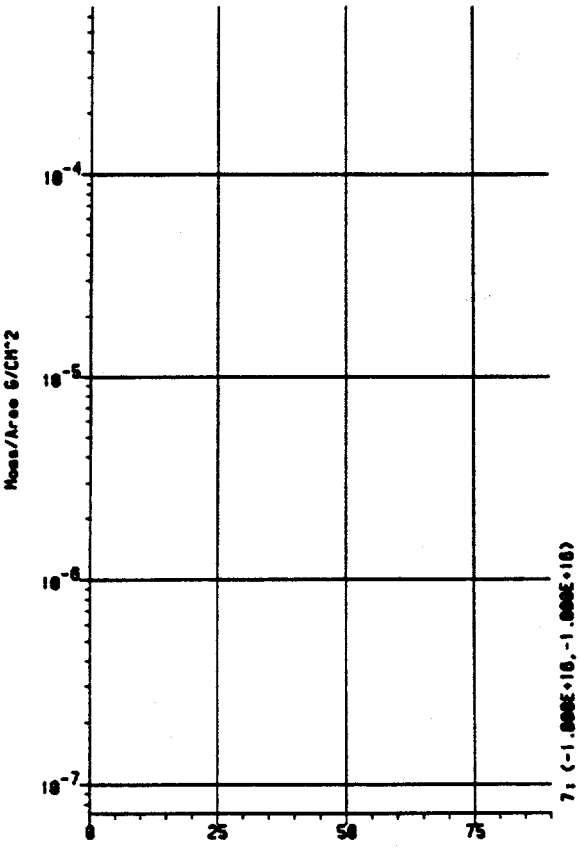

第2表 6-Nov-95 15:58:05 N:f,1MJ,nph,500 cm, melted CU 007

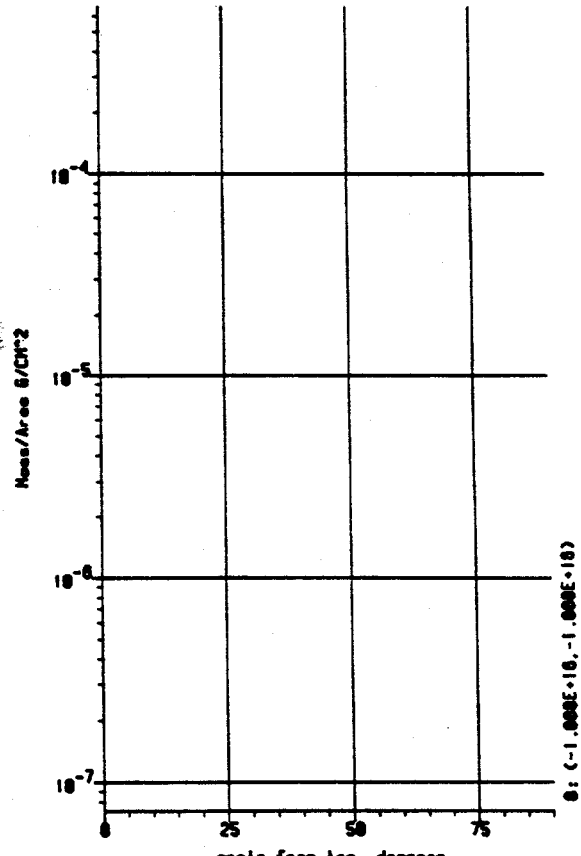

第2表 6-Nov-95 15:58:05 N:f,1MJ,nph,500 cm, vaporized CU 008

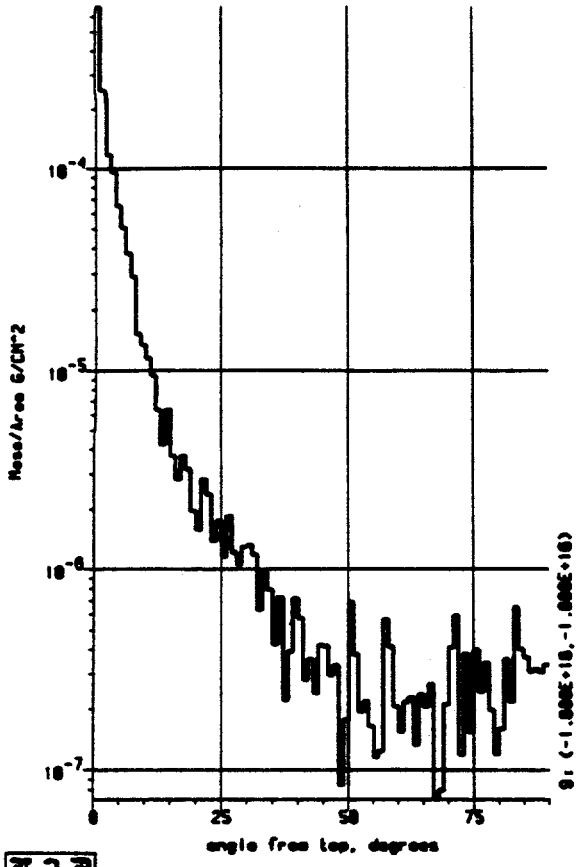

실2형

6-Nov-95 15:58:05 N.f, INJ, nph, 500 cm, ·en·zed CU 000

CRYO TUBE SHRAPNEL COMPUTATIONS

Previous Work (see 5-6 Dec 95 presentation)

- 20 MJ yield case (16 MJ neutrons)
- Previously computed shrapnel and associated neutron, x-ray, and debris velocity contributions are included.
- Shrapnel regions traced to first wall

Recent Work

- Representation of shrapnel mass and particle densities at first wall in spherical polar-coordinate space (for convenience of comparison with laser hole/debris shield locations)

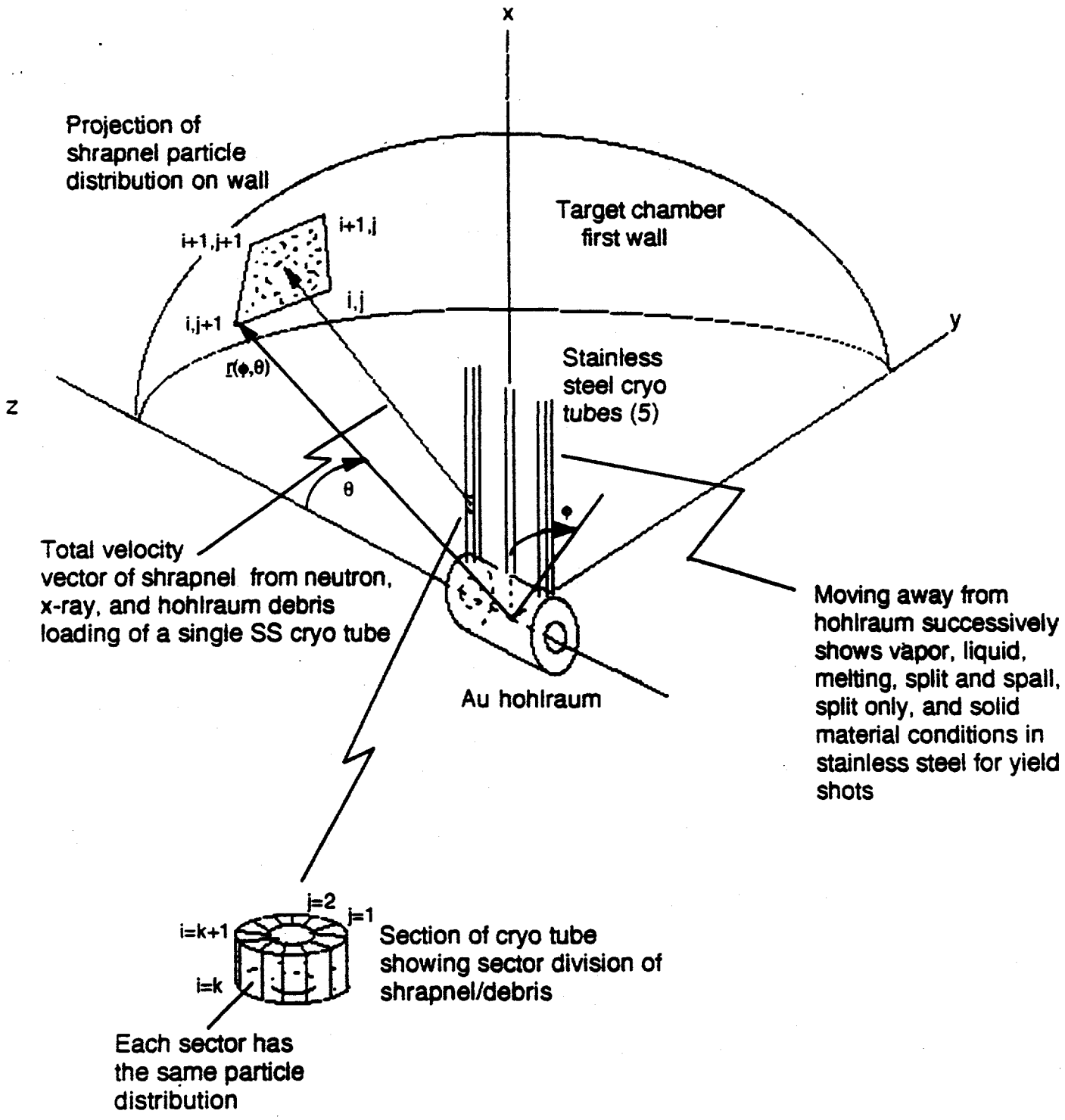

Figure--Configuration for NIF yield shot showing treatment of cryogenic tube break-up and shrapnel/debris projection onto target chamber first wall

Mass Density of Shrapnel in θ-ϕ Space for Single Cryo Tube Pair

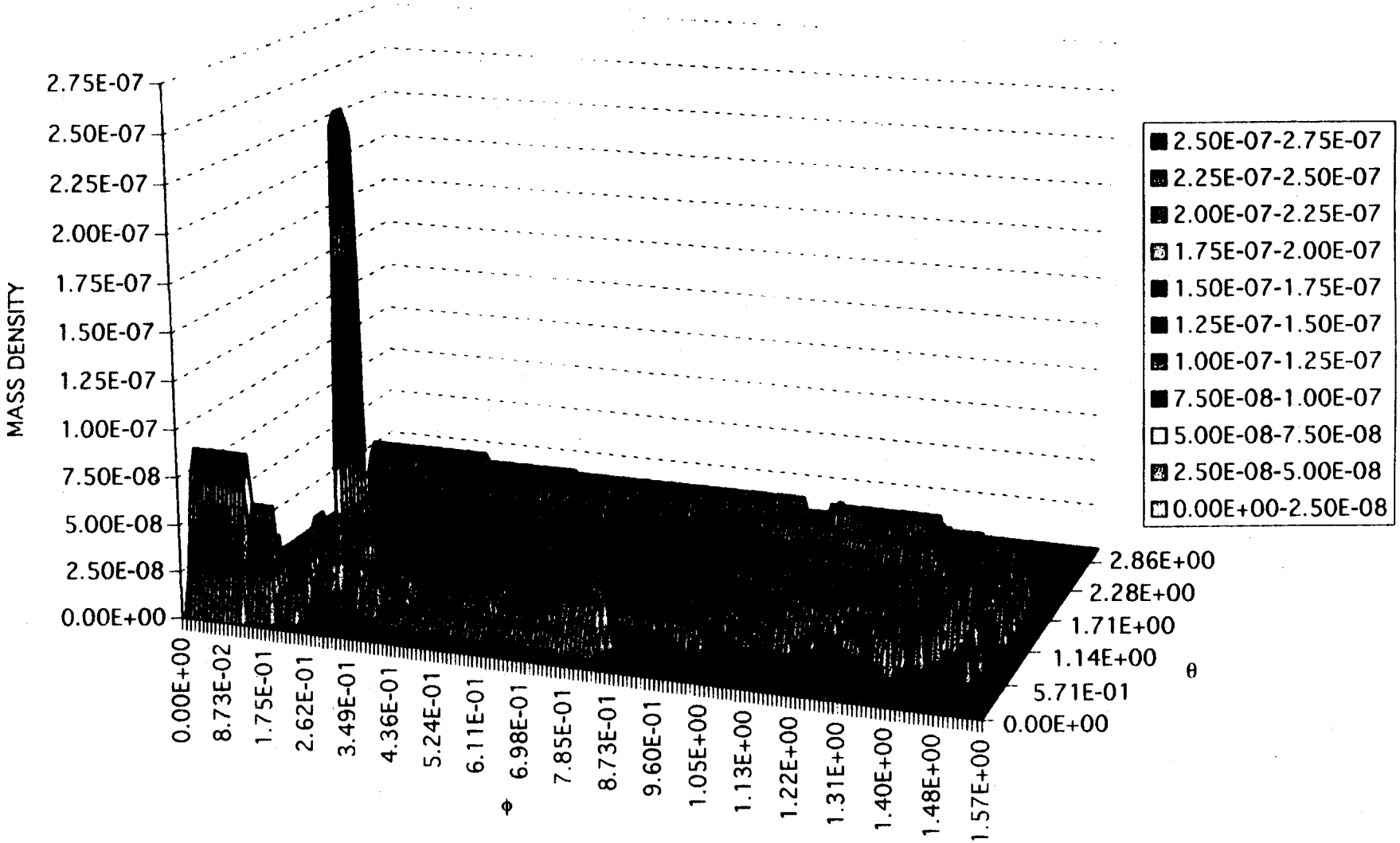

Mass Density (Expanded Scale) of Shrapnel in θ-ϕ Space for Single Cryo Tube Pair

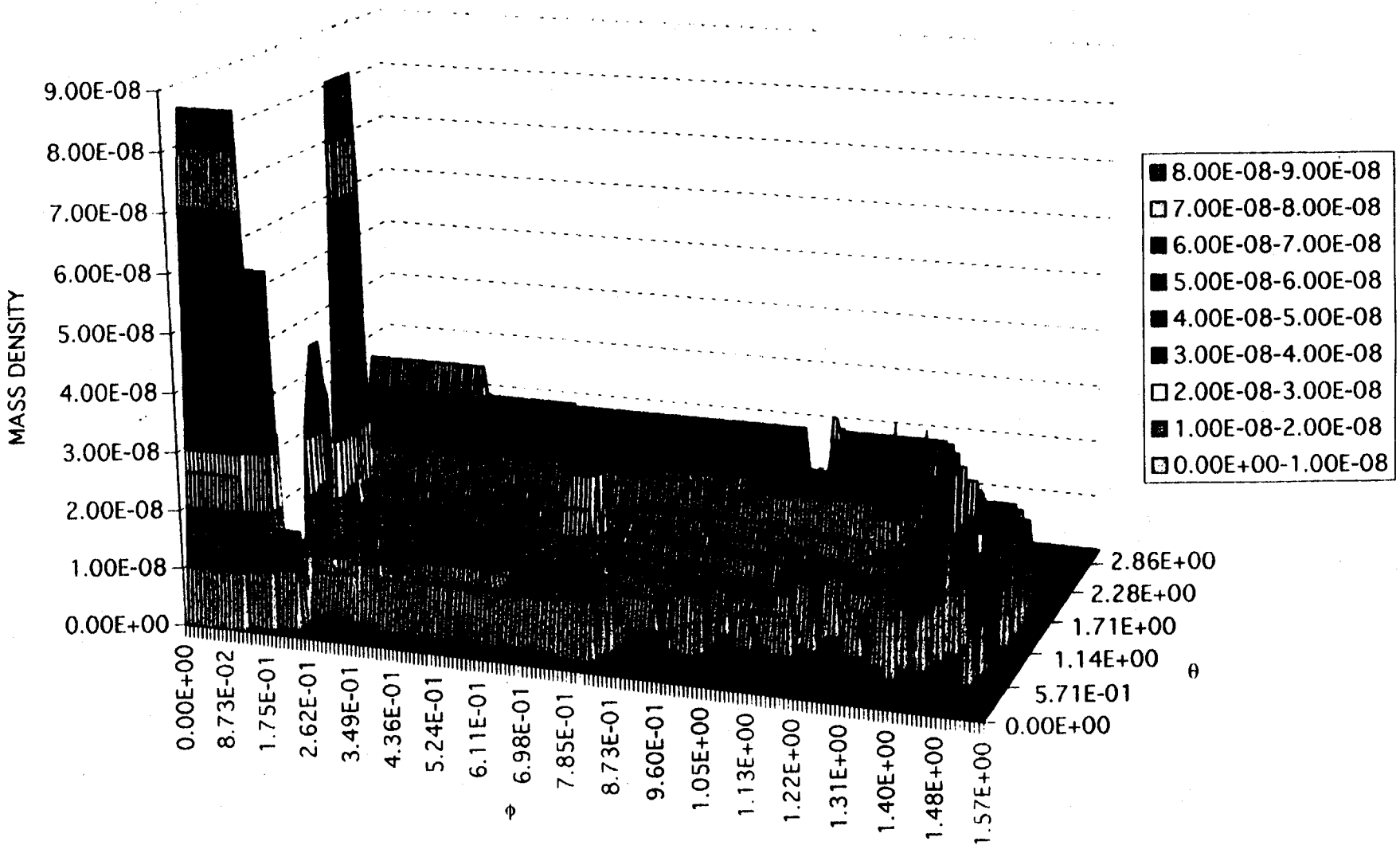

Number of Shrapnel Particles in θ-ϕ Space for Single Cryo Tube Pair

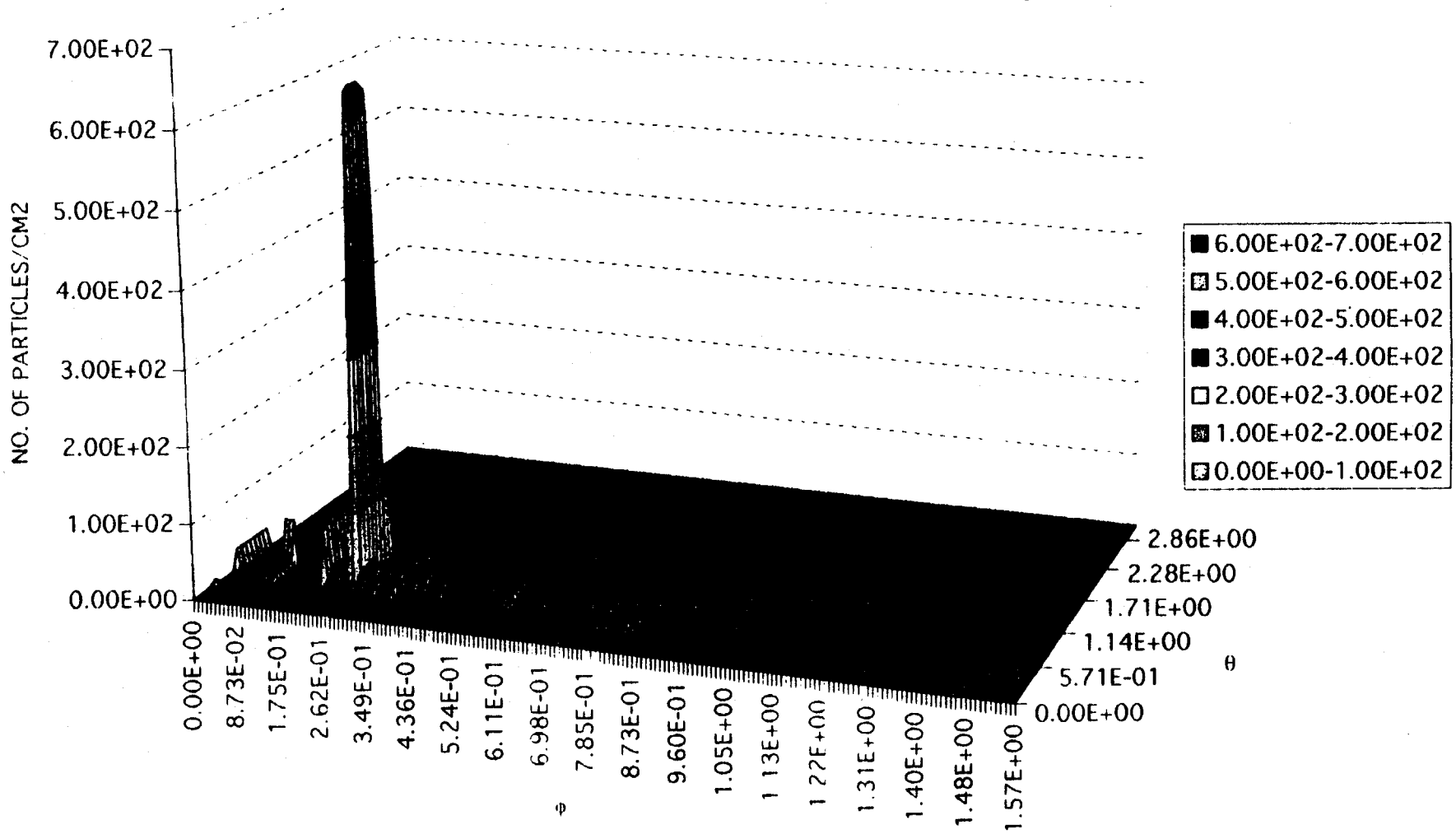

Number of Shrapnel Particles (Expanded Scale) in θ-ϕ Space for Single Cryo Tube Pair

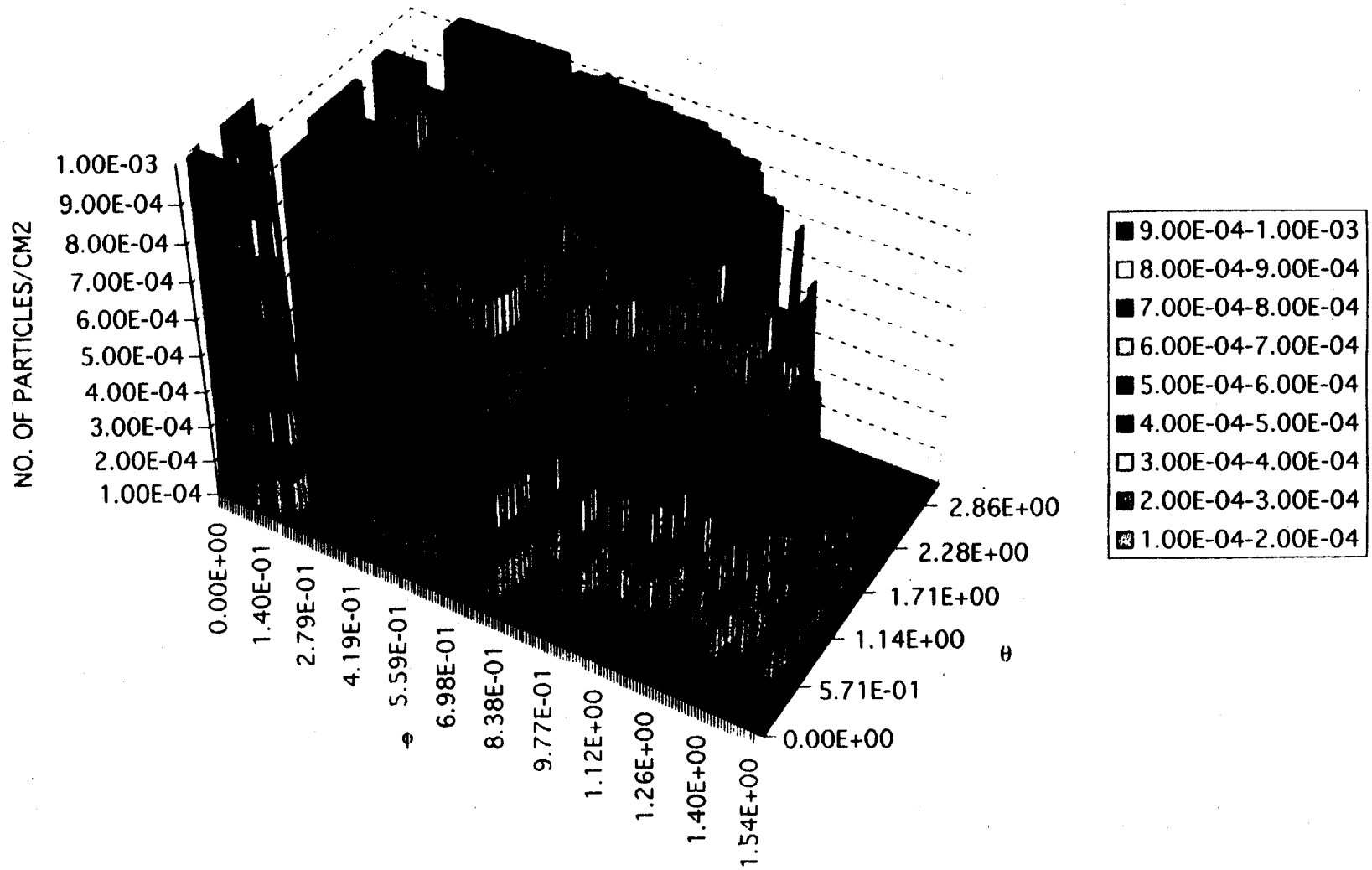

RESULTS AND CONCLUSIONS

Hohlraum:

- The most Au and Cu deposition on the first wall occurs along the hohlraum axis and normal to axis.
- No-yield shots at 1.8 MJ and 1.0 MJ with no cell material phase boundaries give only ionized Au and Cu debris. Maintaining material phase boundaries for the 1.8 MJ shot gives only ionized Au, but equal masses of ionized and solid Cu, with a considerably lesser amount of vaporized Cu, and no appreciable melted Cu.

Shrapnel from Cryo Tubes: (preliminary results are shown for a single tube pair)

- Mass coming from different sections and sectors of cryo tubes overlap at the first wall in a complicated array.
- Melt and vapor material are somewhat directional, whereas solid shrapnel tends to be more uniformly dispersed.
- Further work is needed to verify the results obtained and to compute more selected mass and particle size distributions at the first wall and debris shields; also, then damage can be computed based on algorithms we have and expect to improve based on beebee gun experiments.